POLY-SI FILMS ON ZnO:Al COATED GLASS PREPARED BY THE ALIMINIUM-INDUCED LAYER EXCHANGE PROCESS

von
Master of Engineering
KYU YOUL LEE

geboren in Seoul/Südkorea

der Fakultät IV - Elektrotechnik und Informatik
der Technischen Universität Berlin
zur Erlangung des akademischen Grades
Doktor der Ingenieurwissenschaften (Dr. -Ing.)
genehmigte Dissertation

Promotionsausschuss:

Vorsitzender: Herr Professor Dr. Karlheinz Bock
Gutachter: Herr Professor Dr. Bernd Rech
Herr Professor Dr. Jürgen Müller (TU Hamburg-Harburg)

Tag der wissenschaftlichen Aussprache: 17.5.2010

Berlin 2010

D83

CONTENT

ABSTRACT

The formation of large-grained polycrystalline silicon (poly-Si) films on transparent conductive oxide (TCO) coated glass opens up new possibilities for the fabrication of photovoltaic devices. This work addresses the growth of large-grained poly-Si films on Al doped ZnO (ZnO:Al). A fundamental prerequisite was the realization of temperature stable Al doped ZnO and the successful formation of poly-Si layers on the ZnO:Al layer. The investigated key aspects have been (i) the temperature stability of the ZnO:Al films which are capped with a poly-Si layer, (ii) the study of poly-Si thin films formed on ZnO:Al coated glass and on bare glass (for comparison) by the aluminium-induced layer exchange (ALILE) process, and (iii) the fabrication of poly-Si thin film solar cells on ZnO:Al coated glass.

While uncoated ZnO:Al films show a strong increase of resistivity upon heat treatment, Si coating of the ZnO:Al layers used in this study resulted in electrical properties that were not only stable but considerably improved in their electrical properties. The kinetics of Si crystallization on ZnO:Al coated glass and on bare glass by the ALILE process was studied. Although the activation energy for the nucleation and the grain growth on ZnO:Al coated glass showed no significant difference as compared to the activation energy for the nucleation and the grain growth on bare glass, it was found that the ALILE process time on ZnO:Al coated glass is shorter than the ALILE process time on bare glass. Structural properties of poly-Si thin films on ZnO:Al coated glass and on bare glass were studied by Raman spectra, EBSD, and XRD measurements. The preferential (100) orientation of poly-Si films on ZnO:Al coated glass and on bare glass had a similar value of 60% and did not depend on annealing temperatures. The grain size of poly-Si films on ZnO:Al coated glass was slightly smaller than the grain size of poly-Si films on bare glass. The underlying ZnO:Al film did not influence the defect density of thickened poly-Si films as determined by Secco etching. Finally, poly-Si films formed on ZnO:Al coated glass using the ALILE process have been successfully introduced as seed layers in poly-Si thin film solar cells, showing an efficiency and open-circuit voltage of 2% and 389 mV, respectively.

CHAPTER 1
INTRODUCTION

The European photovoltaic industry association (EPIA) announced that world's future is bright with solar electricity [EPIA]. As EPIA said, the photovoltaic (PV) market is booming and dramatically growing. The cumulative installed capacity of PV systems around the world had reached more than 9,200 megawatts (MW) by the end of 2007. The yearly installed capacity of PV around the world in 2007 reached a record of 2,826 MW, representing growth of 62% compared to the previous year [Sol08]. Installations of PV cells and modules around the world have been growing at an average annual rate of more than 35% since 1998 [EPI08]. The lowest price for a PV module, excluding installation and other system costs, has dropped from almost $100 per watt in 1975 to less than $4 per watt at the end of 2008. Average PV prices are projected to drop to $2 per watt in 2010 with expanding polysilicon supplies and production costs of thin film PV are expected to reach $1 per watt in 2010. According to Earth Policy Institute solar electricity is poised to take a prominent position in the global energy economy with concerns about rising oil prices and climate change spawning political momentum for renewable energy [Ear07].

PV cells are generally fabricated either from crystalline silicon, sliced from ingots or from grown ribbons, or from thin films on a low-cost substrate. The crystalline silicon PV cell (mono and multi silicon wafer) has monopolized 87% of PV cell production in 2007. Meanwhile, thin film production more than doubled from 181 MW in 2006 to 400 MW in 2007, accounting for 12% of total PV production [Sol08].

Crystalline silicon wafer is still the mainstay of most PV modules in despite of the highest price. Efficiencies of more than 20% have been obtained with silicon cells already in mass production [Tan03]. The thickness of wafers is also an important factor as well as the efficiency of the solar cells. Thinner wafers mean less silicon needed per solar cell and therefore lower cost. The average thickness of wafers has been reduced

from 0.32 mm in 2003 to 0.17 mm in 2008 [EPI08]. Over the same period, the average efficiency has increased from 14% to 16%. Nevertheless, the thickness of wafers is limited by the mechanical stability during wafer handling. The problem has to be solved to reduce the thickness of wafers for reducing PV prices.

Thin film PV modules are produced by depositing extremely thin films by either silicon or other materials onto a low-cost substrate such as glass, stainless steel or plastic. These have a benefit compared to the crystalline silicon PV technology in lower production costs. Several new companies are working on the development of thin film production. The successful implementation of such thin film technologies will offer opportunities for significantly higher throughput in the factory and lower costs. EPIA expects a growth in the thin film market share to reach about 20% of the total production of PV modules by 2010 [EPI08]. Mainly, three types of thin film modules are commercially available at the moment. These are manufactured from copper indium diselenide (CIS) or copper indium gallium diselenide (CIGS), hydrogenated amorphous silicon (a-Si:H) and/or microcrystalline silicon (μc-Si:H), and cadmium telluride (CdTe). All of these have active layers in the thickness range of less than a few micrometers. This allows higher automation once a certain production volume is reached, while a more integrated approach is possible in module construction. The process is less labor-intensive compared to the assembly of crystalline modules, where individual cells have to be interconnected. In order to collect all the current, the thin film device is sandwiched between two contact layers. The front contact ought to be conductive and transparent. Therefore transparent conducting oxides (TCOs) like ZnO:Al, SnO_2:F or In_2O_3:SnO_2 (ITO) are used.

On a-Si:H/μc-Si:H tandem solar modules of sizes up to 5.7 m^2 remarkable initial efficiencies of 11.6% were obtained by Applied Materials in 2008 [She08]. Even though the result is quite impressive, it is believed that a-Si:H/μc-Si:H tandem structures are limited compared to multi-crystalline silicon wafer due to the recombination at grain boundaries and the light-induced degradation of a-Si:H caused by the Staebler-Wronski effect [Sta77]. A large grain size is desirable in order to minimize recombination at grain boundaries.

Large-grained polycrystalline silicon (poly-Si) thin-film solar cells feature the potential to combine the advantages of both crystalline silicon wafers (high material quality) and thin-film technologies (low costs). Recent theoretical calculations show that it is possible to achieve 17% efficiency in 2 µm thick silicon films if the grain size is larger than 10 µm and the dislocation density is less than 10^6 cm^{-2} [Deb00]. Ideally a large grained silicon thin film should be formed on a foreign inexpensive substrate, like glass. Large grained can be defined as laterally larger than the layer thickness. In this case the efficiency is limited by the recombination at the front and back contacts. Thin poly-Si films on glass for solar cells can be prepared for example by (i) solid phase crystallization (SPC) [Mat90, Gre04], where amorphous Si (a-Si) is transformed into poly-Si by annealing at about 600 °C, (ii) laser crystallization (LC), where amorphous Si is melted by laser pulses [Im93] and subsequently into solidified poly-Si, or (iii) the 'seed layer approach' [Fuh04], where in a first step a very thin large-grained poly-Si film (seed layer) is formed and in a second step this seed layer is thickened homo-epitaxially [Rau04, Ges06].

So far the most successful way to prepare poly-Si thin-film solar cells is based on SPC of amorphous silicon. Poly-Si thin film solar cells based on the SPC process are fabricated by CSG Solar. The Mini-module efficiencies of up to 10.4% have already been obtained [Kee07]. However, the SPC process requires long crystallization times. In case of LC technique, the achievable Si grain sizes of the crystallized material are in the range of hundred micrometers [Vou03] and of good crystallographic quality [And06]. The major disadvantage of LC, based on excimer laser technology, is its low throughput due to small laser spot size, which is not suitable for large area devices such as solar cells.

Another attractive method to prepare such large-grained seed layers is the aluminum-induced layer exchange (ALILE) [Nas98, Mat01, Sch05] which is used in this work. The ALILE process has a shorter process time compared to SPC. Commercial deposition techniques can be used such as sputtering or e-beam evaporation which is not expensive. The ALILE process is a special form of aluminum-induced crystallization (AIC). During the ALILE process the initial glass/Al/oxide/a-Si layer stack is

transformed into a glass/poly-Si/oxide/Al(+Si) layer stack by a simple annealing step below the eutectic temperature of the Al/Si system (577 °C).

The resulting poly-Si layer is continuous and features large grains (over 10 µm) with a preferential (100) orientation [Kim02]. The process temperature and time of the ALILE process are more cost effective compared to a process temperature and time of SPC. Even though the films feature a large grain size, the poly-Si films are not suitable for absorber layers due to the very low thickness and the very high doping level of Al. But due to the large grain sizes such layers are used as templates for subsequent epitaxial thickening. Although the poly-Si seed layer is highly doped with Al (doping concentration of 1×10^{19} cm^2 [Nas00]) the sheet resistance is too high for high-efficiency solar cells. An additional contacting scheme is requested to improve a lateral conductance.

An appealing option for an additional contacting scheme is the seed layer formation on a transparent conductive oxide (TCO) coated substrate because TCOs show a high transparency in the spectral region where the solar cell is operating and they provide a high electrical conductivity. TCOs are well established for thin-film solar cells based on amorphous Si (a-Si:H) or microcrystalline Si (µc-Si:H) [Mul04, Klu03, Rec06] but are not used so far for poly-Si thin-film solar cells. The formation of poly-Si seed layers on Al doped ZnO (ZnO:Al) coated glass using the ALILE process has been introduced recently [Dim07].

The formation of poly-Si films on ZnO:Al coated glass substrates using the ALILE process is the topic of this work. The thesis is divided into following chapters:

Chapter 2: ‘State of the art’ provides the background and the current status of the aluminum-induced layer exchange (ALILE) process and the Aluminium-doped ZnO (ZnO:Al).

Chapter 3: ‘Experimental’ lists the sample preparation steps from the preparation of substrates to chemical mechanical polishing to produce a flat surface of the resulting thin films and to remove the Al layer on top. The characterization methods are

explained.

Chapter 4: ‘Temperature stability of ZnO:Al’ shows the electrical and optical properties of ZnO:Al/poly-Si stacks. In particular, the properties of ZnO:Al layer covered with poly-Si film fabricated using the ALILE process are studied.

Chapter 5: ‘Poly-Si films on ZnO:Al coated glass’ addresses the influence of the two main parameters on the poly-Si properties. First, the influence of ALILE process temperature is investigated as it is crucial for the layer exchange process. Second, the properties of poly-Si films on ZnO:Al coated glass are compared with the properties of poly-Si films on glass.

Chapter 6: ‘Solar cells’ shows poly-Si thin film solar cells fabricated on ZnO:Al coated glass. Sample structure and solar cell performance are characterized in detail and the suitability of the applied ZnO:Al coated glass substrates is evaluated.

Chapter 7: ‘Conclusion’ summarizes the most important results and closes with an outlook on future perspectives of the ALILE process.

CHAPTER 2
STATE OF THE ART

2.1 ALUMINIUM-INDUCED LAYER EXCHANGE (ALILE) PROCESS

In this chapter the history of the aluminum-induced layer exchange (ALILE) process is summarized. The ALILE process is a special form of aluminium-induced crystallization (AIC) where a substrate/Al/a-Si stack is transformed into a substrate/poly-Si/oxide/Al(+ Si islands) stack by a simple annealing step below the eutectic temperature of the Al/oxide/Si system (577 °C). The ALILE process is well explained by O. Nast [Nas00] and illustrated schematically in Fig 2.1.

The crystallization of a-Si with Al was used in a type of layer exchange process already by Boatright et al. and Greene et al. [Boa76, Gre76]. The experiment investigated by Boatright et al. is shown schematically in Fig. 2.2. A hole was made by photolithographic means in a Si oxide layer covering a silicon wafer. After deposition of Al on top of the oxide covered wafer and annealing at 550 °C for 5...25 min, the Al dissolved the Si beneath the hole. Amorphous silicon was evaporated onto the Al layer (Fig. 2.2(a)) and this stack was annealed again at 475...525 °C for another 10...20 min. It was found that the hole is refilled with crystalline silicon (Fig. 2.2(b)). At that time many researcher investigated the phenomena for understanding the crystallization of a-Si in contact with Al. Majni et al. [Maj77, Maj78, Maj79] investigated the growth kinetics of the crystallization of a-Si by deposition of Al (700 nm)/a-Si (650 nm) double layers on differently orientated Si wafers and actually mentioned for the first time that Si and Al exchange their position during heat treatment at lower temperatures. Tsaur et al. [Tsa81] used the crystallization of a-Si through an Al layer to form highly p-doped emitters on n-doped c-Si wafers. The separated Al layer was removed and the resulting solar cells reached an efficiency of 10.4 %. The Al inclusions in crystalline silicon films were mentioned by Scranton et al. [Scr78]. They concluded that fast growth rates can

cover defects, such as Al inclusions, in the epitaxial film but the epitaxial films prepared with slower growth rates by Majni et al. [Maj77] also contained Al inclusions. QingHeng et al. [Qin82] investigated the diffusivity and growth rate of silicon in Al and revealed that the activation energy is almost identical to that of the Al-Si system but the change of diffusivity is caused by different experimental conditions. They also mentioned that the existence of a thin oxide layer at the Al/a-Si interface reduces the diffusion process significantly and the growth time usually should be longer to produce higher quality growth layers.

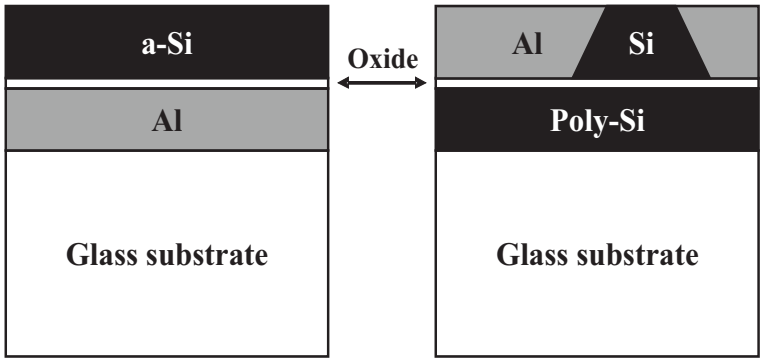

Figure 2.1: Schematic of the ALILE process. The layer stack before (left) and after (right) the layer exchange are shown [Nas00]. The oxide interface layer remains in position during the process.

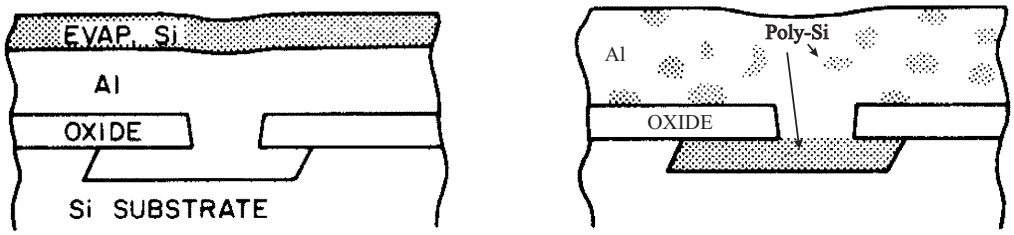

(a) (b)

Figure 2.2: Schematic illustration of a layer exchange phenomenon by Boatright et al. [Boa76]: (a) Evaporating amorphous Si (~200 nm) on thick Al layer and (b) after heat treatment at 475-525 °C for 10 or 20 min Si fill the dissolution pit.

Researchers investigated Al-induced crystallization (AIC) process on oxidized silicon wafer or on silicon wafer at that time. Nast et al. [Nas98] started to investigate the AIC process on glass substrate at the University of New South Wales (UNSW) in Sydney, Australia. And then many other institutions started research in this field.

2.1.1 THE GROWTH MODELING OF THE ALILE PROCESS

Konno et al. [Kon92, Kon93, Kon94] studied the crystallization mechanism of a-Si in an a-Si/Al multilayer system using transmission electron microscopy (TEM). They found that the Si atoms diffuse through the Al grain from amorphous to crystalline phases and suggested that the fastest reaction path occur to reduce the excess free energy for crystallization of a-Si. Nast et al. [Nas00S] developed a model for the ALILE process dividing the overall process into four steps. This model was extended by Widenborg et al. [Wid02] as shown in Fig 2.3. They found that the formation of Si islands in the top layer is completed after the crystallization process in the bottom layer. Step 1 involves the interaction of amorphous silicon with the Al and the dissociation of the amorphous phase across the oxidized Al/Si interface. Once Si is dissolved in the metal, the Si atoms diffuse within the Al layer (step 2). The Si nucleates within the Al layer (step 3). While process steps 1, 2 and 3 correspond to the steps suggested by Nast, here step 4 describes the diffusion of Al into the top layer. Al is displaced by Si grains and forced to diffuse into the a-Si top layer (step 4a). The a-Si crystallizes in presence of the Al and small Si crystallites form in the Al top layer. The Al in this mixed phase dissolves further a-Si and grows (step 4b) competing with the Si growth in the bottom layer in this model. While the poly-Si in the bottom layer grows supplied by step 5, silicon is also crystallized in the top layer. Small nanocrystalline Si (nc-Si) crystallites will agglomerate at the more compact central Si islands, even when the actual layer exchange is completed (step 6).

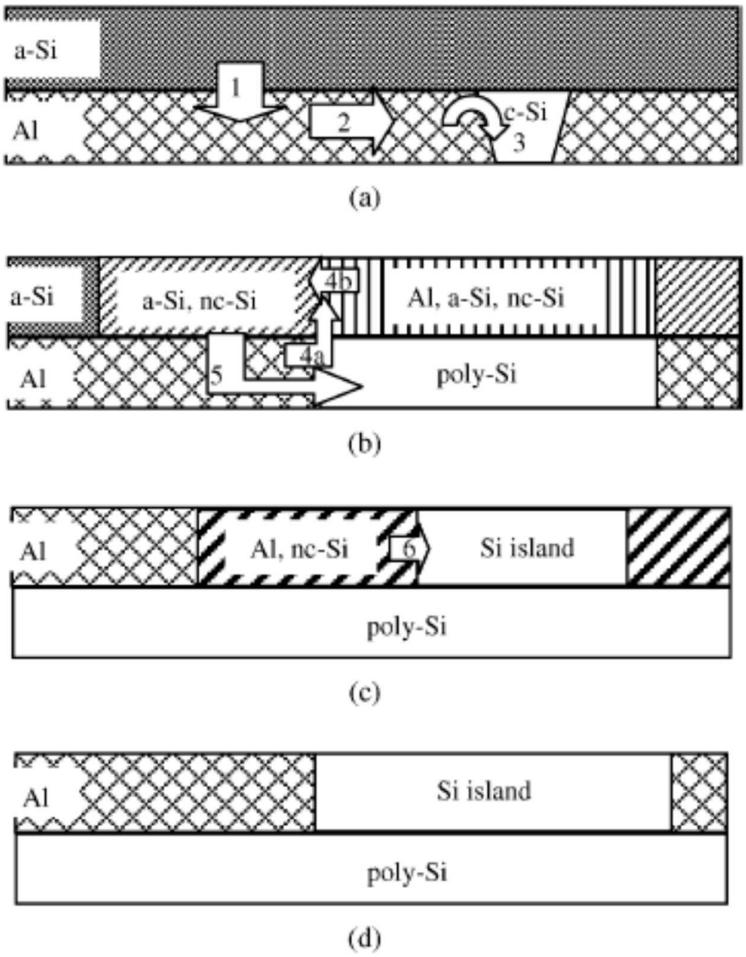

Figure 2.3: ALILE growth model by Widenborg et al. [Wid02]. Details are explained in the text.

Various deposition methods and processing parameters are known to influence the layer exchange process. In the following these factors are highlighted for the ALILE process.

2.1.2 THE INFLUENCE OF THE THICKNESS RATIO OF a-Si/Al

The relevance of the thickness ratio of Al and a-Si layer was recognized by Harris et al. [Har77]. However, they did not succeed in producing continuous poly-Si films. Nast et al. [Nas00S] investigated the influence of the thickness ratio of Al and a-Si layer and found that the a-Si layer must be at least as thick as the Al layer for obtaining a

continuous layer of poly-Si. Sugimoto et al. [Sug05] found that the crystal direction was strongly influenced by the thicknesses of Al and Si and showed preferred orientation with Si (111) with decreasing thicknesses. Hsu et al. [Hsu03] found that the Al has compressive stress and the a-Si layer has tensile stress and there is a compressive/tensile stress turning point at a thickness ratio of 4/1 for the a-Si/Al stacked structure.

2.1.3 THE INFLUENCE OF THE INTERLAYER BETWEEN Al AND a-Si LAYER

The ALILE process requires a thin permeable membrane between the Al and the a-Si layer which controls the diffusion of Al and Si [Gal02a]. This membrane does not participate in the layer exchange process and therefore remains in position throughout the annealing process. The interlayer between the initial Al and a-Si layer plays a crucial role because it influences grain size, preferential orientation and crystallization time.

The influence of an Al oxide layer formed at an Al/a-Si interface was studied by Ottaviani et al. and Cai et al. [Ott79, Cai92]. Ottaviani et al. suggested that the oxide layer act as a diffusion barrier for the Al atoms, but allows Si atoms to diffuse into the metal layer with subsequent crystallization. However, Cai et al. concluded that a gradual Al/Si interface reduces the crystallization temperature even further. However, the presence of oxygen at the Al/a-Si interfaces inhibits the Al-induced crystallization.

The role of the Al/a-Si interface on the overall crystallization process was also investigated by Nast et al. [Nas00] and by Sieber et al. [Sie03]. According to the report by Sieber et al., an oxide layer introduced at the a-Si/Al interface is very important from the viewpoint of a diffusion of Si into Al film and the local nucleation of Si in the Al film, which lead to ALILE of the a-Si/Al bilayer and poly-Si formation of large grain size. The influence of the aluminium oxide interlayer produced by different oxidation processes was investigated by Schneider et al. [Sch05] and Pihan et al. [Pih04]. Usually a native Al oxide layer is formed on top of the Al prior to a-Si deposition. This oxide

layer remains in position and separates top and bottom layer throughout the layer exchange process. Schneider et al. [Sch05] investigated the effect of aluminium oxide layers formed by air and by thermal oxidation. Pihan et al. [Pih04] fabricated the aluminium oxide using HNO_3 solution. Both aluminium oxides produced by thermal oxidation and using HNO_3 solution can increase the grain size of poly-Si films compared to the aluminium oxides formed by air. The influence of oxygen present within Al layers was investigated by Klein et al. [Kle04]. They found that the increasing oxygen content within Al layers leads to faster crystallization.

Kim et al. [Kim96] studied glass/a-Si/SiO_2/Al structures to analyze the process mechanism at an oxidized interface between Al and a-Si layer during aluminium-induced crystallization. They presented that the silicon oxide acts as a membrane that allows the local interaction of the Al and the amorphous silicon due to the reduction of the oxide and the formation of Al spikes.

Schneider investigated the influence of molybdenum (Mo) as an interlayer and it was found that the grain size of poly-Si film is much bigger (up to 40 µm), but Mo reacts with Al and Si during the ALILE process [Sch05].

2.1.4 THE INFLUENCE OF THE PROCESS TEMPERATURE

The process temperature is one of the most important parameters which influence the grain size and the preferential orientation. It was shown that the grain size decreases and the preferential (100) orientation increases with decreasing annealing temperature [Kim02, Gal06].

2.1.5 THE INFLUENCE OF HYDROGEN IN a-Si LAYER

Amorphous silicon (a-Si) layers can be deposited by either physical vapor deposition (PVD) or plasma enhanced chemical vapor deposition (PECVD) methods. Amorphous

silicon layers deposited by PECVD method using Silane (SiH_4) as source gas contain hydrogen. The influence of hydrogenated a-Si (a-Si:H) was investigated by Kishore et al. [Kis03]. It was found by in-situ XRD measurements that the crystallization of a-Si:H occurs faster than crystallization of a-Si without hydrogen at a process temperature of 150 °C. The influence of different annealing atmospheres and hydrogen concentration in a-Si on the layer exchange process was investigated by Dimova-Malinovska and Grigorov [Dim06, Gri06]. They showed that the use of hydrogen in the annealing atmosphere leads to improved structural properties of the resulting poly-Si film when the a-Si:H precursor layers contain 9 at.% hydrogen. Zou et al. [Zou05] concluded that tensile stress in a-Si:H can have a significant effect on AIC of a-Si:H. The crystallization of intrinsic and boron-doped a-Si:H was studied by Al-Dhafiri et al. [Al05]. They noticed that crystallization was further enhanced in the p-type a-Si:H.

2.1.6 THE REMOVAL OF Si ISLANDS

Si islands present on the surface of ALILE poly-Si seed layers have a negative effect on the epitaxy [Dog08]. The removal of these islands could therefore lead to an increased absorber layer quality and solar cell performance. To remove the residual Si islands on top of poly-Si films various treatments are used. A wet chemical lift-off process for the Si islands within the Al layer has been developed in order to produce a smooth and flat surface on the ALILE layer [Wid03]. A chemical mechanical polishing (CMP) method was used to remove Si islands [Sch05]. Plasma selective etching process with SF_6 gas was used by Van Gestel et al. [Ges08a].

2.1.7 THE EFFECT OF HYDROGEN PASSIVATION

Walter Schottky Institute in Germany investigated the influence of hydrogen passivation on the electronic properties of ultra-thin poly-Si films prepared by ALILE [Jae08]. They found a drastic increase of the resistivity for very thin hydrogenated

samples, which is attributed to a combination of two effects: (1) the reduction of free holes due to acceptor passivation and (2) compensation of free holes remaining after H-passivation by interface states.

2.1.8 THE FORMATION OF N-TYPE POLY-Si LAYER

Recently, the formation of n-type ALILE seed layers was investigated by Tüzün et al. [Tuz08]. It was found that p-type poly-Si layers obtained by ALILE of amorphous silicon can be successfully converted into n^+-type by phosphorus diffusion from a highly doped solid source in a furnace at 950 °C for 1hour.

2.1.9 THE USE OF A SUBSTRATE COATED WITH A CONDUCTING LAYER

Although the poly-Si films formed using ALILE process feature a high Al concentration of 10^{19} cm^{-3}, the lateral conductivity of poly-Si film itself is not sufficient for solar cell applications. Glass substrates coated with a conductive material coated were investigated in order to increase the lateral conductivity. Widenborg et al. [Wid02] investigated the formation of poly-Si films on molybdenum (Mo) and on titanium nitride (TiN) coated substrate. It was found that although Mo is not compatible due to the reaction with Si during the AIC process TiN has a medium to high resistivity (120–500 μΩ cm) and an estimated low back reflectance at the near-infrared wavelengths critical for light trapping. But TiN is the only possible choice for process temperatures above 540 °C.

Dimova-Malinovska et al. [Dim07] produced poly-Si films on ZnO:Al coated glass by Aluminium-Induced Crystallisation (AIC) in different annealing atmospheres (air, N_2, and N_2+H_2) and analyzed only the structural properties of poly-Si thin films on ZnO:Al coated glass substrates using Raman spectra and XRD method. It was found that an

annealing in forming gas (N_2+H_2) led to a better structural quality of the poly-Si films, compared to annealing in air or nitrogen. The (111) preferential orientation was observed by XRD.

2.1.10 FURTHER APPLICATIONS OF THE ALILE PROCESS

Zou et al. [Zou07] investigated the formation of silicon nanowires (SiNWs) using ALILE process. They asserted that both aluminum thickness and native silicon oxide between Al and a-Si play critical roles in the formation of the nanostructures. The results suggest that the rapid in-plane growth of these SiNWs can be attributed to self-assembly of nanosilicon islands, which is different from traditional SiNWs growth mechanisms such as vapor-liquid-solid.

Some research groups investigate the formation of poly-SiGe layers using aluminium-induced layer exchange process. The use of the ALILE process for crystallization of amorphous SiGe is investigated by Gjukic et al. [Gju04, Gju05]. Here, it was found that ALILE is suitable for crystallizing binary amorphous material without segregating different phases [Gju04]. The optical and electrical properties of the resulting polycrystalline films were found to be comparable with high quality crystalline SiGe films [Gju05]. Low-temperature Al-induced crystallization of hydrogenated amorphous silicon–germanium thin films has been investigated by Peng et al. [Pen08]. They found that the increase of the Ge fraction and annealing temperature yields an enhancement in film crystallinity and grain size.

2.2 THE ABSORBER LAYER GROWTH

ALILE poly-Si layers are not suitable as absorber layers due to the high hole density of 2×10^{18} cm^{-3} [Nas01] which is inherent due to the remaining Al dopant content in the line. Several institutes have investigated the epitaxial thickning of ALILE poly-Si films

by using various silicon deposition methods. There are two types of approaches: One is the low temperature approach where poly-Si films are thickened at temperatures upto 700 °C, and the other is the high temperature approach where poly-Si films are thickened at a temperature above 1000 °C. The UNSW and HZB focus on the low temperature approach which promises a higher potential for cost reduction than the high temperature approach. The low temperature approach allows for the use of cheap substrates like a glass. The ALILE seed layers prepared on glass substrates were successfully thickened epitaxially for the first time by ion assisted deposition (IAD) [Har00]. Different cell concepts have been developed involving IAD and solid phase epitaxy (SPE) from a-Si layers deposited on the seed layer [Abe05]. Widenborg et al. [Wid07] announced an open-circuit voltage (Voc) of 480 mV for poly-Si solar cells. ALILE poly-Si seed layers have been also thickened epitaxially using pulsed sputter deposition system (SPUTTER) [Rei02], electron cyclotron resonance chemical vapor deposition (ECRCVD) [Rau04, Ree06] or electron beam (e-beam) evaporation [Dog08]. So far, the best crystal qualities have been achieved by the later method. A Voc of 346 mV was measured for a solar cell fabricated by epitaxially thickening of poly-Si film by e-beam evaporation. Ito et al. [Ito03] explored the use of the crystallization of a-Si deposited on ALILE seed layers for solar cell applications. Some simulations were done to extrapolate the future goals for solar cells involving ALILE seed layers which claimed that efficiencies of about 13% could be achieved when various solar cell parameters are improved [Ito04]. A low temperature epitaxy using ECRCVD on an inverse ALILE seed layer structures (glass/a-Si/Al) has been studied by Ekanayake et al. [Eka03, Eka04]. The structural quality of the films was analyzed using electron back scatter diffraction (EBSD) and X-ray diffraction (XRD) analysis. Some researchers [Sla06, Gor07] focus on the high temperature approach to thicken ALILE poly-Si films. ALILE seed layers on ceramics substrates are studied using atmospheric pressure chemical vapor deposition (APCVD), Gordon et al. have recently achieved solar cell efficiencies of 8% [Gor07].

2.3 ALUMINIUM DOPED ZINC OXIDES

In this section the basic properties and the current status of ZnO are reviewed. The deposition methods for ZnO are summarized. Nowadays ZnO:Al films are widely applied as a front contact layer in order to fabricate thin film solar cells, because ZnO:Al films are highly transparent in the active range of the absorber layer (400 – 1100 nm in case of μc-Si:H) and also highly conductive to avoid ohmic losses. In the p-i-n structure, the front contact additionally has to possess a rough surface to provide efficient light scattering. Furthermore, the ZnO:Al film features favourable physico-chemical properties for the growth of silicon. In general, the TCO/p-contact plays an important role for cell performance [Kub96, Boh96, Mul01].

Obvious parameters of the front contact for thin film solar cells are electrical conductivity and transparency. An improved transparency of the TCO results in a higher short circuit current density, while an improved conductivity allows a higher fill factor of an otherwise optimized solar cells. A low sheet resistance is most important for thin film solar cells due to the high short circuit currents. ZnO:Al is a suitable material.

2.3.1 BASIC PROPERTIES OF ZnO

ZnO is a II-VI compound semiconductor whose ionicity resides at the borderline between the covalent and ionic semiconductors. It crystallizes in the hexagonal Wurtzite structure. The wurtzite structure has a hexagonal unit cell with two lattice parameters *a* and *c* in the ratio of $c/a = \sqrt{8/3} = 1.633$ (in an ideal wurtzite structure) and belongs to the space group C_{6v}^4 in the Schoenflies notation and $P6_3mc$ in the Hermann–Mauguin notation [Mor09]. A schematic representation of the wurtzitic ZnO structure is shown in Fig 2.4. The structure consists of two pervasive grids together. One of the grids is filled with Zinc atoms, the other with oxygen atoms. The two hexagonal densest lattices packing lie along the anisotropy c-axis a fraction of the lattice parameter offset. Each atom is fourfold coordinated, with the nearest neighbors of each atom by the other

atomic sites originate. The lattice parameters are a_0 = 0.325 nm and c_0 = 0.52066 nm at room temperature [Ell01]. The melting temperature is 1975 °C and the density is 5.67 g·cm^{-3} at room temperature [Ell01]. The direct band gap of Zinc oxide is 3.2 eV to 3.4 eV [Ell01, Iba03]. The thermal expansion coefficient of ZnO is given as $\alpha_a = 4.31\times10^{-6}$ K^{-1} and $\alpha_c = 2.49\times10^{-6}$ K^{-1} at 300K [Hel82, Ada05].

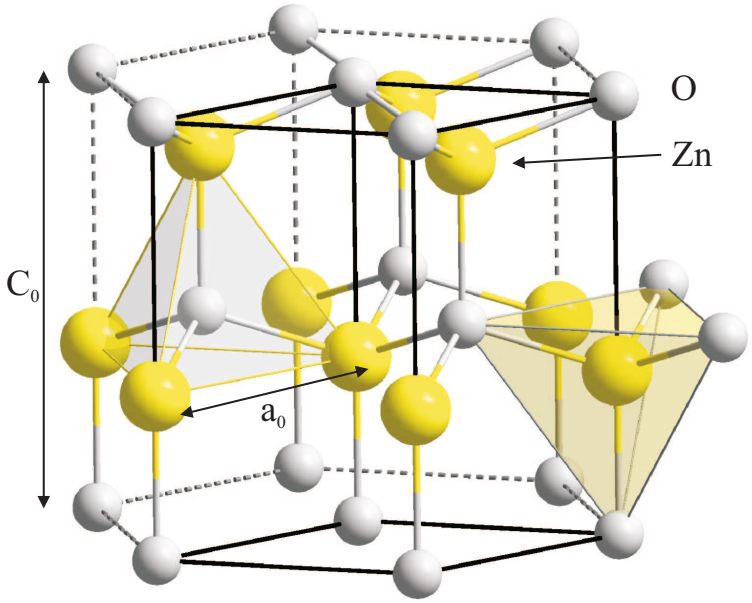

Figure 2. 4: Schematic representation of a wurtzitic ZnO structure. The c-axis is the anisotropy axis.

2.3.2 DEPOSITION OF ZINC OXIDE THIN FILMS

Different deposition methods are introduced for the production of ZnO (for review see [Cho83, Hel82, Man81, Vos76, Cha80, Gro01, Pul84,]). These are, for example, the sputtering [Szy99], chemical vapor deposition (CVD) [Fay00], the pulsed laser deposition (PLD) [Lor03], electrochemical deposition from aqueous solution [Iza96], the spray pyrolysis [Par99] and evaporation method (thermally or through electron) [Wu00]. The sputtering method allows a large area deposition making ZnO films the industrially most advanced deposition technique for ZnO [Gla00].

First sputtering processes for ZnO deposition were developed in the late 1960's for manufacturing surface acoustic wave devices [Hic73]. Large-area sputtering of ZnO was established in the field of energy-efficient glazing in the early 1980's. ZnO was chosen as dielectric material because of its high sputtering rate and its suitability for reactive DC sputtering. Transparent and conductive, sputtered ZnO-based films with resistivity below 1,000 μΩ were first reported by Brett et al. [Bre83]. Breakthroughs such as high-rate magnetron sputtering of ZnO:Al [Ell94] guided the developments towards large-area manufacturing technology, with main emphasize on thin-film photovoltaics [Men98, Mul03].

Many attempts have been made to deposit ZnO:Al-based films by magnetron sputtering. Table 2.1 summerizes a literature survey on sputtered ZnO:Al film. The classification criteria are: plasma excitation used (DC/MF/RF), reactive or ceramic deposition; material deposited and film properties relevant for TCO applications.

Some important deposition parameters to control ZnO:Al film properties are deposition pressure, substrate temperature and amount of oxygen in the sputter gas mixture [Hup06, Klu03, Min84, Szy99]. Doping concentration in ZnO films plays another important role for opto-electronic properties [Aga04, Min84, Ell01].

TABLE 2.1. Literatures survey on magnetron sputtering of ZnO:Al-based TCO films

Ref.	Scope	Growth conditions	Layer properties
	Process Material Year	Coater and magnetron Process mode and control Target Substrate, T_s (°C) P/A (W cm^{-2}) a_s(nm s^{-1})/a_d(nm s^{-1})	d (nm), c_d (at.%), ρ (Ωcm), n_e (cm^{-3}), μ ($cm^2V^{-1}s^{-1}$)
[Bre99]	RDCMS ZnO:Al 1999	Batch, 90 mm planar Low power Zn:2 wt% Al Glass, RT 1.6 W cm^{-2},0.8-2 nm s^{-1}	170-400 nm, 1.4 – 1.8 at.% 6×10^{-4} Ωcm 1.0×10^{21} cm^{-3} 10 $cm^2V^{-1}s^{-1}$
[Har91]	RDCMS ZnO:Al ZnO:In 1991	Batch Low power Zn target, Al or In pieces Glass, 180 – 220 °C < 2 nm s^{-1}	700 nm 2 at.% (Al), ~11 at.% (In) 5×10^{-4} Ωcm (Al) 1.4×10^{-3} Ωcm (In)
[Ell94]	RDCMS ZnO:Al 1994	Batch, 3inch planar Low power Zn:2 wt% Al Glass, < 150 °C 2.2 W cm^{-2} < 2 nm s^{-1}	~ 500 nm 1.8 – 2.2 at.% 4.5×10^{-4} Ωcm 8×10^{20} cm^{-3} 17 $cm^2V^{-1}s^{-1}$
[Wal03]	RDCMS RMFMS ZnO:Al 2003	In-line, dual magnetron tm, q(O_2) = f(PEM) 1400 ×100 mm^2 each Zn:2 wt% Al Glass, RT < 5 W cm^{-2} 125 nm m min^{-1}	1040 nm 9.1×10^{-4} Ωcm
[Min90]	DCMS ZnO:Al 1990	Batch, 120 mm planar Zn:2-3 wt% Al_2O_3 Glass, 250 °C	300-600 nm 2.7×10^{-4} Ωcm
[Mal00]	RMFMS ZnO:Al 2001	Batch, dual magnetron tm, q(O_2) = f(U) 500 ×88 mm^2 Zn:1.5 wt% Al Glass, RT, 250 °C ~ 6 W cm^{-2} 7 nm s^{-1}	500 nm 7.5×10^{-4} Ωcm 2.5×10^{-4} Ωcm
[Szy99]	RMFMS ZnO:Al 1999	Batch, 500 ×88 mm^2 DMS Met. mode, Zn deposition Zn:0.9-1.5 wt% Al (segmented) 100 °C, 250 °C ~ 10 W cm^{-2} 8.2, 8.8 nm s^{-1}	~ 500 nm 3.6 at.%, 2.2 at.% 4.8, 3.0×10^{-4} Ωcm 8.6, 8.5×10^{20} cm^{-3} 15, 25 $cm^2V^{-1}s^{-1}$

Ref.	Scope	Growth conditions	Layer properties
[Kon03]	RMFMS ZnO:Al 2003	In-line, 400 ×120 mm^2 DMS tm, $q(O_2)$ = f(PEM) Zn:1.5 wt% Al RT, 300 °C 2.9 W cm^{-2}	~ 10, 4.4×10^{-4} Ωcm 5.8×10^{20} cm^{-3} 24 $cm^2V^{-1}s^{-1}$
[Iga88]	RMFMS ZnO:Al 1988	Batch, 125 mm planar Zn, Al wires Glass, 100 °C 0.01 nm s^{-1}	540 nm 4.9×10^{-4} Ωcm 4.3×10^{20} cm^{-3} 24 $cm^2V^{-1}s^{-1}$
[Iga91]	RFMS ZnO:Al 1991	Batch, 125 mm magnetron Zn:2.0 wt% Al_2O_3 Sapphire, 230 °C < 1.4 W cm^{-2} 0.5 nm s^{-1} Hetero epitaxial growth	380-670 nm 2 at.% 1.2 nm min-1: 140 μΩcm 1.3×10^{21} cm^{-3} 34 $cm^2V^{-1}s^{-1}$ 22.3 nm min-1: 300 μΩcm
[Bos96]	RFMS ZnO:Al 1996	Batch, 4 inch planar Zn:2.0 wt% Al_2O_3, sintered Glass, 150 °C	~ 700 nm 6.9×10^{-4} Ωcm
[Par97]	RFMS ZnO:Al 1997	Batch, 4 inch planar Zn:0.5 wt% Al_2O_3, sintered Glass, 150 °C	140 nm 4.7×10^{-4} Ωcm 7.5×10^{20} cm^{-3} 15 $cm^2V^{-1}s^{-1}$
[Add99]	RFMS ZnO:(Al, H) 1999	Batch Zn:2.0 wt% Al_2O_3, sintered RT 2 W cm^{-2}	500 nm 4×10^{-4} Ωcm 6×10^{20} cm^{-3} 27 $cm^2V^{-1}s^{-1}$
[Hau01]	RFMS ZnO:Al CIS 2001	Batch, 100 mm magnetron ZnO:2.0 wt% Al_2O_3 200-250 °C 3.2 W cm^{-2} 0.5 nm s^{-1}	~ 10^{-3} Ωcm
[Ceb98]	RFDCMS M: ZnO:Al 1998	Batch, 3 inch magnetron ZnO:2.0 wt% Al_2O_3 RT 0.5 W cm^{-2} < 0.5 nm s^{-1} dev CIS	10-370 nm 3.3-4.0 at.% ~ 7×10^{-4} Ωcm $5\text{-}7\times10^{20}$ cm^{-3} ~ 15 $cm^2V^{-1}s^{-1}$
[Jin88]	Co-deposition ZnO:Al 1988	Batch Zn:2 wt% Al Glass, < 100 °C 0.2 nm s^{-1}	~ 300 nm 2.14 at.% 5.4×10^{-4} Ωcm 4.5×10^{20} cm^{-3} 26 $cm^2V^{-1}s^{-1}$

(DCMS: DC magnetron sputtering; RDCMS: reactive DC magnetron sputtering; RMFMS: reactive MF magnetron sputtering; RFMS: RF magnetron sputtering; tm: Transition mode; Met. mode: Metallic mode)

CHAPTER 3
EXPERIMENTAL

In the first part of this chapter the sample preparation is described in detail. The second part of this chapter describes the measurement methods for characterizing structural, electrical, and optical properties of polycrystalline silicon (poly-Si) films and ZnO:Al/poly-Si stacks.

3.1 PREPARATION

The ALILE process on ZnO:Al coated glass is shown schematically in Fig. 3.1. The layer stacks before (left) and after (center) the layer exchange and after chemical mechanical polishing (right) are shown.

The substrates and their cleaning procedure are described in section 3.1.1. The conditions for the deposition of ZnO:Al, Al, and a-Si layers are described in section 3.1.2. The oxide interface layer was formed by simple oxidation method as described in section 3.1.3. The layer stacks have been annealed either within a furnace or a heating stage of an optical microscope (section 3.1.4). After the layer exchange the Al (+Si) top layer has to be removed in order to uncover the poly-Si layer. Chemical mechanical polishing was used to produce a smooth surface as described in section 3.1.5. The last step is of importance because the poly-Si layer is used as template for epitaxial thickening in order to form the absorber layer of the thin film solar cell.

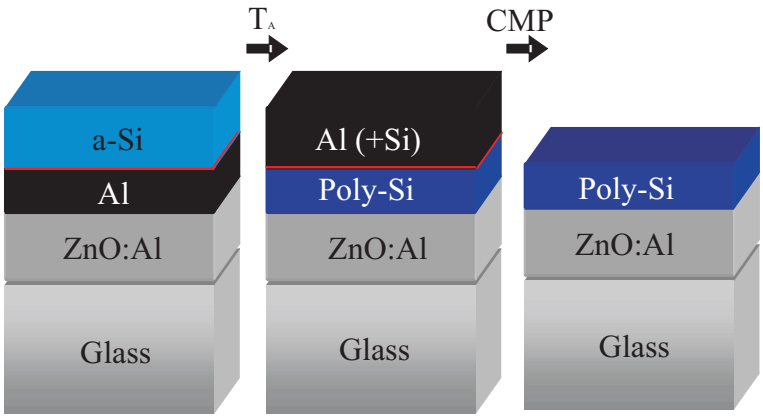

Figure 3. 1: Schematic of ALILE process: The layer stacks before (left) and after (center) the layer exchange and after CMP (right) are shown. The oxide interface layer (red layer) remains in position during the ALILE process and is removed by chemical-mechanical polishing (CMP) process.

3.1.1 SUBSTRATES

Borofloat33 glasses from Schott were used as substrates in this study. The chemical composition of this glass is shown in table 3.1. The strain point lies at 518 °C, which is lower than the strain point (666 °C) of Corning1737 glass. The coefficient of linear thermal expansion (C.T.E) of Borofloat33 glass is 3.25×10^{-6} K^{-1} in the range of 20 to 300 °C. This value is lower than the value (3.76×10^{-6} K^{-1}) of Corning1737. The C.T.E of silicon is 2.6×10^{-6} K^{-1} at 25 °C and 3.25 - 3.6×10^{-6} K^{-1} in the range of 400 - 500 °C [Hul99, Wat04]. This means that the C.T.E of Borofloat33 glass has a better match to the C.T.E of silicon than that of Corning1737 glass. The better match should lead to less stress and cracking.

The glass substrates were cleaned with a normal glass cleaning solution (Mucasol). The temperature of the cleaning solution was 80 - 90 °C and the cleaning time was 10 min. After that the samples were rinsed in de-ionized (DI) water and dried by N_2. Square 1×1 inch samples with a thickness of 0.7 mm were used. For some experiments silicon

nitride (SiN_X) coated Borofloat33 glasses supplied by CSG Solar were used. The thickness of the SiN_X layer and the glass is about 80 nm and 3 mm, respectively.

TABLE 3.1: Chemical composition of Borofloat33 glass [Schott].

	SiO_2	Al_2O_3	B_2O_3	Na_2O/K_2O
Chemical composition	81%	2%	13%	4%

3.1.2 LAYER DEPOSITION

ZnO:Al films used in this work were obtained by Forschung Zentrum Jülich (FZJ). They were deposited in an in-line sputtering system in dynamic mode using non-reactive RF-sputtering from ceramic targets containing 1 wt.% Al_2O_3. A constant deposition pressure of 0.1 Pa and a substrate temperature of 300 °C were used. Details of the sputtering procedure can be found in [Aga04]. The thickness of the ZnO:Al films used in this thesis, determined by fitting optical transmission and reflection spectra, was between 690 and 770 nm. The ZnO:Al coated glasses were cleaned by a 10 minute immersion in an ultrasonic bath filled with DI water heated at 80 ~ 90 °C and dried with nitrogen gas.

The initial layer stacks for the ALILE process (Al and a-Si) were deposited onto the ZnO:Al coated glass and on Borofloat33 glass (for comparison) by DC magnetron sputtering. The base pressure in the sputter chamber was 7×10^{-7} mbar. The initial layer stacks were deposited at room temperature with an Ar pressure of 6.5×10^{-3} mbar. For Al deposition the purity of the Al target was 4N. A sputtering power of 500 W, resulting in a deposition rate of 160 nm/min, was used to deposit a 300 nm thin film. For a-Si deposition a Si target with a boron concentration of 1×10^{16} atoms/cm^{3}was used. Here a sputtering power of 300 W was used and a film of 375 nm was grown using a deposition rate of 66 nm/min.

3.1.3 OXIDATION

An Al oxide layer was formed by exposure to air of the Al-coated substrate prior to the a-Si deposition in order to obtain continuous poly-Si films. Al oxide layers are formed rapidly upon exposure to an oxygen containing atmosphere such as air. The oxidation of aluminium is self-limited. This means that upon reaching a certain oxide thickness, no further oxidation takes place. It has been shown that the thickness of the native Al oxide formed on aluminium in dry air at room temperature is in the range 1-2 nm [Mar93, Nyl94]. In this work the samples were oxidized by exposure to air for 2 hours.

3.1.4 ANNEALING

In order to fabricate poly-Si films on ZnO:Al coated glass and on bare glass the stacked Al and a-Si layers were annealed in a tube furnace at an annealing temperature between 425 °C and 525 °C in nitrogen ambient. The samples annealed at 425 °C and 450 °C were annealed for 16 hours and the samples annealed between 475 °C and 525 °C were annealed for 4 hours. In addition to the annealing experiments in the tube furnace, annealing experiments were carried out in a heating stage of an optical microscope (see section 3.2.1.1). These experiments enable the in-situ observation of crystallization (nucleation and subsequent growth) during the ALILE process.

3.1.5 CHEMICAL MECHANICAL POLISHING (CMP)

Chemical Mechanical Polishing (CMP) is a process that uses abrasive, corrosive slurry to physically grind flat and chemically remove the microscopic topographic features on a substrate so that subsequent processes can begin from a flat surface. The oxide interface layer is also removed by CMP process as shown in Fig 3.1.

In the CMP process the sample is put into a carrier head which is pressed onto a pad covering the main plate. Both carrier and main plate rotate while a defined amount of slurry is poured onto the pad. The slurry is a liquid including colloidal particles. Between sample and pad a small film of slurry is formed. While the chemical component modifies the surface at a homogeneous depth the combined mechanical polishing effect of colloids and pad take off the most protruding parts. This combined effect results in a very smooth surface.

A Logitech CDP machine and silicic acid based slurry (Syton® HT-50 colloidal silica slurry from DuPont Air Product NanoMaterials L.L.C) were used to polish the samples. After the CMP process the samples were cleaned using hot DI water (~ 80 °C) in an ultrasonic bath. The standard parameters for the main plate and carrier rotation velocities, the download pressure on the sample and the flow of slurry are shown in table 3.2. The polishing process takes about 2 min and four samples in size of 1×1 inch can be polished at once.

TABLE 3.2: Main CMP parameters.

Main plate	Carrier	Download pressure	Slurry
60 RPM	40 RPM	0.5 ... 0.7 mbar	50 ml/min

3.2 CHARACTERIZATION

A number of characterization techniques are used to assess the quality of the poly-Si films and solar cells fabricated in this thesis. The characterization methods used in this study can be divided roughly into four categories: structural, electrical, and optical characterization and solar cell performance analysis (see chapter 6). In this section, the measurement methods and analytical procedures are described.

In-situ optical microscopy, Raman spectroscopy, electron backscatter diffraction (EBSD), and X-ray diffraction (XRD) were used to characterize structural properties. In-situ optical microscopy (section 3.2.1) was used to analyze the kinetics of the crystallization and to calculate an average estimated grain size of poly-Si films. Raman spectra (section 3.2.2) were performed to characterize the crystalline quality of the resulting poly-Si films. Electron backscatter diffraction (EBSD) was used to analyze the crystallographic surface orientation and the grain size (section 3.2.3). X-ray diffraction (XRD) was measured to investigate the crystallographic orientation (section 3.2.4). In order to characterize the electrical properties of the ZnO:Al/poly-Si stacks formed using the ALILE process 4-point probe and Hall measurements were used (section 3.2.5 and 3.2.6). UV-VIS spectroscopy (section 3.2.7) measurements were used to characterize the optical and structural properties of poly-Si films on ZnO:Al films coated glass. For the extended defect analysis, poly-Si films have been Secco-etched and then investigated by Scanning Electron Microscopy (SEM) using a Hitachi S4100 (25 keV) SEM equipped with a cold field emission cathode. The concentration of impurities within the poly-Si layers was measured by secondary ion mass spectrometry (SIMS).

3.2.1 IN-SITU OPTICAL MICROSCOPY

Samples were annealed in the optical microscope to determine the process time, an average estimated grain size and the kinetics of the crystallization of the ALILE process. In-situ images were recorded within time intervals of 1 sec to 10 min, depending on the

process temperature, through the glass substrates. The interface of the ZnO:Al layer and the Al layer was investigated. The spatial resolution limit of the in-situ optical microscopy is about 0.5 µm. Due to the high reflectivity of the Al the micrographs appear bright at the beginning of the process. As soon as the size of the Si grains exceeds the resolution limit of the microscope, the crystallized Si becomes visible as small dark spots at the ZnO:Al/Al interface due to the lower reflectivity of Si compared to Al. The black fraction of the images recorded is used as crystallized fraction. The crystallized fraction curves are evaluated as function of the annealing time. The crystallized fraction is 0% at the beginning of the process and corresponds to all Al at the interface. The time when first dark areas are detected is defined as the nucleation time. The process time is defined as the time required reaching a crystallized fraction of 99%. Counting the number *n* of black objects in the black and white image of area A_0 determines the nucleation density N_G in each image ($N_G = n/A_0$). The maximum of the nucleation density was used to evaluate the final average estimated grain size d_G of grains which are assumed to be square shaped:

$$d_G = \sqrt{1/N_G} \tag{3.1}$$

The setup of the in-situ optical microscopy and the evaluation methods of the obtained images are described in detail in the doctoral thesis of J. Schneider [Sch05]. Five assumptions are established to estimate the average grain size: (i) the maximum number of grains is detected when no new grains are formed, (ii) at this point no grains have coalesced, i.e. all grains are separated and counted, (iii) all grains are averaged in size, (iv) a square shape of the grains is assumed, (v) the areas grown from one nucleus correspond to one grain.

3.2.2 RAMAN SPECTROSCOPY

Raman is a powerful light scattering technique for characterizing the structural properties such as the crystal quality of thin films [Sch90] or any stress present in thin films [Nic00]. Light of a known frequency and polarization is scattered from a sample.

The scattered light is then analyzed for frequency and polarization. Raman scattered light is frequency-shifted with respect to the excitation frequency, but the magnitude of the shift is independent of the excitation frequency. This "Raman shift" is therefore an intrinsic property of the sample. Because Raman scattered light changes in frequency, the rule of conservation of energy dictates that some energy is deposited in the sample. A definite Raman shift corresponds to excitation energy of the sample (such as the energy of a free vibration of a molecule). In general, only some excitations of a given sample are "Raman active," that means, only some may take part in the Raman scattering process. Hence the frequency spectrum of the Raman scattered light maps out part of the excitation spectrum. For solids phonon excitation and crystal structure can be identified. As can be seen in Fig 3.2, the normalized Raman peak of crystalline silicon (c-Si) and amorphous silicon (a-Si) is 520 and 480 cm^{-1}, respectively. Details about Raman spectrum for thin Si films are descriebed in [Wu96, Bo02, Owe03].

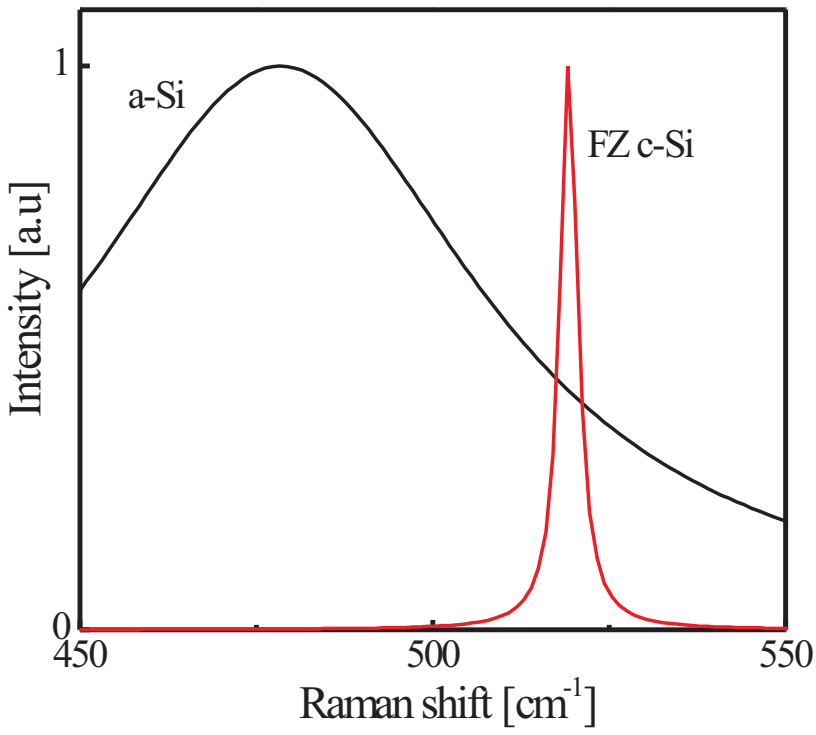

Figure 3. 2: Normalized Raman spectra of a-Si layer (2 µm) and FZ c-Si (320 µm).

In this thesis Raman Spectroscopy (set-up: LABRAM from Jobin Yvon Horiba) with a HeNe-Laser at wavelength of 632.8 nm was used as a standard measurement for the crystallographic quality of poly-Si layer formed by the ALILE process. The resolution of Raman spectroscopy is 1 cm^{-1}. Lorentzian line shape is fitted to the Raman spectra of poly-Si films formed using the ALILE process and FZ c-Si as a reference to get the peak position and full width half maximum (FWHM). It was separately tested that the laser beam did not induce any crystallization in a-Si films on glass even after extended periods of exposure (over 1 hour).

3.2.3 ELECTRON BACKSCATTER DIFFRACTION (EBSD)

Electron Back Scatter Diffraction (EBSD) method was used to investigate the crystallographic structure of the samples. The EBSD measurements are performed with an SEM tool equipped with a phosphor screen detector. EBSD provides quantitative microstructural information about the crystallographic nature of materials. It reveals grain size, grain boundary character, and grain orientation of the sample under the beam. EBSD operates by arranging a flat sample at a shallow angle, usually 20°, to the incident electron beam (since the SEM stage is often used to tilt the plane of the sample to this shallow angle, the value of stage tilt is often referred to and is typically 70°). Fig 3.3 shows the electron interaction with crystalline silicon. Electron diffraction occurs from the incident beam point on the sample surface. With the beam stationary, an EBSD pattern emanates spherically from this point. This EBSD pattern is the Kikuchi pattern. The Kikuchi pattern contains the angular relationship between the planes, the symmetry of the crystal and orientation information. Bright Kikuchi bands correspond to planes in the crystal lattice. The width of bands depends upon the electron wavelength and the lattice plane spacing. Relationship is given by the Bragg's equation ($n\lambda = 2d\sin\theta$) [Tro93]. The variable λ is the wavelength of the incident beam, θ is a certain angles of the incidence beam, the variable *d* is the distance between atomic layers in a crystal, and n is an integer determined by the order given.

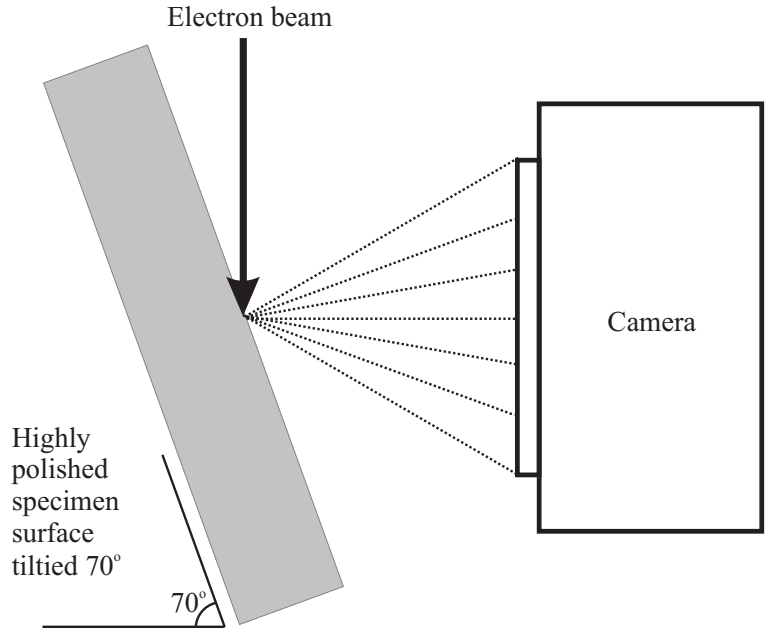

Figure 3. 3: Electron interaction with crystalline silicon [Day01].

The EBSD conditions used in this thesis are an acceleration voltage of 20 kV, a spot size of 5.4 µm and a step size of 0.2 µm. A matrix of 400×400 points was measured for all samples corresponding to an area of 80×80 μm^2. For determining the grain sizes of samples, only grains with a size of at least 0.6 µm (3 times the step size) were taken into account. EBSD measurements were in cooperation with IMEC in the framework of the European project ATHLET.

3.2.4 X-RAY DIFFRACTION SPECTROSCOPY

X-ray diffraction measurements were carried out to investigate the orientation of the Si grains of the polycrystalline material. X-ray diffraction (XRD) is a powerful non-destructive diagnostic technique analyzing the crystalline phases of thin-films and determining the structural properties of these phases such as the preferred orientation and average grain size [Klu74, Sch90]. X-ray diffractograms of the poly-Si films were measured in symmetric θ-2θ geometry. These X-rays are generated by a cathode ray tube, filtered to produce monochromatic radiation, collimated to concentrate, and

directed toward the sample. The interaction of the incident rays with the sample produces constructive interference (and a diffracted ray) when conditions satisfy Bragg's Law ($n\lambda=2d \sin \theta$). Here d is the spacing between diffracting planes in a crystalline sample, θ is the incident angle, *n* is any integer, and λ is the wavelength of the beam. Fig 3.4 illustrates schematically the interference between waves scattered from two adjacent rows of atoms in a crystal. This law relates the wavelength (λ) of electromagnetic radiation to the diffraction angle (θ) and the lattice spacing (d) in a crystalline sample. h is a half of the path difference between the two reflected rays. These diffracted X-rays are then detected and counted.

For the thin film silicon samples the angle 2θ is scanned through a range of 20 - 100°. The lattice spacing in the films can be determined from the position of the detected peaks. By comparison of the relative peak intensities with the spectrum of a powder sample in which a random orientation should be present, preferred orientation of crystal grains can be determined.

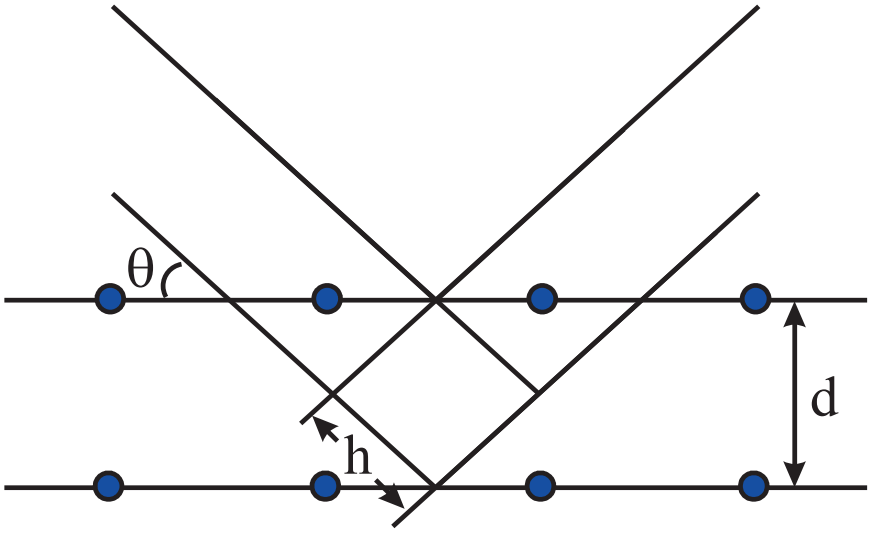

Figure 3. 4: Schematic diagram for determining Bragg's law.

3.2.5 4-POINT PROBE MEASUREMENT

The 4-point probe is a simple technique used to measure the resistivity of a thin film on an insulating material. By forcing a current through two outer probes and measuring the voltage between the inner probes the substrate resistivity can be measured. While simple in principle, there are experimental issues to take into account when using a 4-point probe. Very high or very low resistivity samples require adjustment of the current to obtain a reliable measurement.

3.2.6 HALL MEASUREMENT

The conductivity, the free carrier concentration and the mobility of samples were determined with Hall measurements. The measurements (magnetic flux of 0.64 T) were performed on 5×5 mm^2 samples and in the Van der Pauw geometry. In order to form ohmic contacts gold contacts with a thickness of 20 nm were deposited at room-temperature by thermal evaporation. An overview of the measuring principle and experimental details are given in [Blo92]. The Van der Pauw technique can be used to measure resistivity of a thin, arbitrary-shaped sample with 4 ohmic contacts placed on the periphery. Van der Pauw demonstrated that there are two characteristic resistances associated with the four terminals.

The measurement is performed as follows:

First the sheet resistance R_S is calculated. This is related to the resistivity ρ by the film thickness t,

$$R_s = \frac{\rho}{t} \ [\Omega / sq] \tag{3.2}$$

Next, a current I is applied between two contacts and a perpendicular magnetic field B is applied. The Hall voltage V_H is measured across the two remaining contacts. The schematic of the Hall measurement is illustrated in Fig 3.5.

From this the sheet carrier density N_S can be calculated:

$$N_s = \frac{10^{-4} I \cdot B}{q|V_H|} \quad [cm^{-2}] \tag{3.3}$$

where the sheet carrier density N_S is given by $N_e \times t$, N_e is the carrier density [cm^{-3}], and q is the charge. Once R_S and N_S are known the Hall mobility can be calculated,

$$\mu_H = \frac{1}{qN_sR_s} \quad [cm^2V^{-1}s^{-1}] \tag{3.4}$$

Further details on this Hall measurement can be taken from [Pau58].

There are practical aspects which must be considered when carrying out Hall and resistivity measurements. Primary concerns are (1) ohmic contact quality and size, (2) sample uniformity and accurate thickness determination, (3) thermo-magnetic effects due to non-uniform temperature, and (4) photoconductance and photovoltaic effects which can be excluded by measuring in a dark environment. Also, the sample lateral dimensions must be large compared to the size of the contacts and the sample thickness.

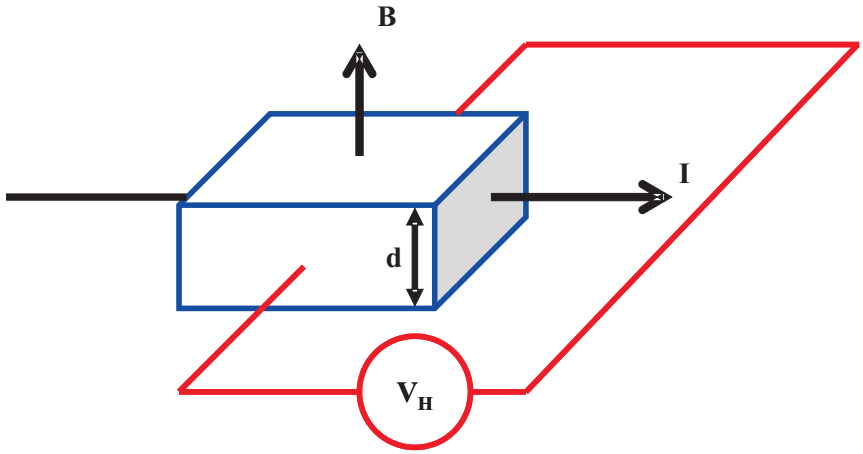

Figure 3. 5: The Hall effect measurement.

3.2.7 UV-VIS SPECTROSCOPY

UV-VIS-IR spectroscopy (Lamba19 from Perkin-Elmer, spectral range: 250 ~ 2000 nm, double-beam spectrophotometer with an integrating sphere) was used in order to investigate the following: (i) the quality of poly-Si film formed using the ALILE process and (ii) the properties of the ZnO:Al layer.

The characteristic peaks in the ultraviolet (UV) reflectance at ~ 360 and ~ 275 nm (e1 and e2, respectively) are related to direct optical transitions at the critical points in c-Si and hence are a measure of the crystalline quality of the silicon material investigated (note that defects in the material lead to a decrease and broadening of the peaks [Kam88]).

The absorption in near infrared (NIR) is related to the free carriers of ZnO:Al. Near-infrared (NIR) spectroscopy offers the characterization of the free carrier properties since this spectral domain is well described by the Drude theory of free electrons, allowing the determination of the free carrier density and local conductivity [Cou00].

CHAPTER 4
TEMPERATURE STABILITY OF ZnO:Al/POLY-Si STACKS

This chapter investigates the sputtered ZnO:Al films on glass which are capped with a poly-Si layer formed during a thermal treatment. Two types of glass/ZnO:Al/poly-Si samples were investigated: The poly-Si thin film was formed by either (i) the ALILE process or (ii) the SPC process. The sample preparation for the ALILE process is explained in chapter 3.1. For SPC process the sample preparation will be described later. The most important finding of this chapter is that the capped ZnO:Al film can withstand the high temperature treatments while its electrical properties even improve.

4.1 MOTIVATION

In the case of the aluminium-induced layer exchange (ALILE) process, an annealing step is necessary so that only temperature-stable substrates can be used. The formation of poly-Si films on transparent conductive oxides (TCOs), however, would be an appealing option, especially for the preparation of thin-film solar cells because they allow for a simple contacting scheme and light trapping [Mue04, Rec06]. Among the available TCO materials, SnO_2:F and ZnO:Al films are commonly used as front contact material in a-Si:H solar cells and are considered here. The ALILE process is processed in nitrogen ambient and at higher temperature compared to amorphous silicon (a-Si) and/or microcrystalline silicon (μc-Si) solar cells. Studies on the stability of ZnO:Al upon treatment at temperatures above the deposition temperature, as used for the crystallization of Si, have so far concentrated on annealing of ZnO:Al films on glass under various ambient conditions. Usually a strong decrease of electrical conductivity is observed during annealing in air at temperatures between 300 and 400 °C [Min90, Cha01], while much higher temperatures can be applied in vacuum [Iga88] or, in the

case of rapid thermal annealing, nitrogen [Kim05]. As the films do not show structural degradation but rather an improved crystallinity, Minami et al. [Min99] suggested oxygen to be responsible for both the decreased carrier density and mobility upon annealing in air.

Recently the formation of poly-Si layers on ZnO:Al coated glass using the ALILE process has been introduced [Dim07], but no comments on the evolution of ZnO:Al properties were given. The formation of poly-SiGe layers on ZnO:Al coated glass using the ALILE process has been introduced by Lechner [Lec03]. He concluded that Zinc oxide proved to be thermally stable in the pertaining temperature region (550 °C), but the removal of aluminium residuals after the ALILE process turned out to be problematic.

4.2 PROPERTIES OF ZnO:Al LAYERS

First of all, in order to study the influence of the annealing temperature (425 ~ 525 °C) on the properties of the ZnO:Al films used for this study, the electrical properties of ZnO:Al films deposited on glass without Si on top before and after annealing were measured. The sheet resistance of ZnO:Al films on bare glass as a function of annealing time and annealing temperature is shown in Fig 4.1. The sheet resistances were measured by 4-point probe. The sheet resistance of as-deposited ZnO:Al films was 6.3 Ω/sq. The ZnO:Al films on glass were annealed in a tube furnace with nitrogen ambient for 0 to 16 hours. After one hour annealing the sheet resistance increased by about one order of magnitude. The influence of the annealing temperature is relatively small. For long annealing times the sheet resistance depends strongly on the annealing temperature. The sheet resistances of the samples annealed at 450 °C have similar values as the samples annealed at 425 °C. But if the annealing temperature is higher than 450 °C, the sheet resistances of the annealed ZnO:Al films are significantly increased with increasing annealing temperature. The sheet resistance of the ZnO:Al film annealed at

525 °C for 16 hours increased to ~ 10^4 Ω/sq (degradation of more than 3 orders of magnitude).

Compared to results obtained for annealing in vacuum [Yu05, Ber06] the annealing in nitrogen atmosphere used in this work leads to a faster degradation. Hamad et al. [Ham05] concluded that the changes of the electrical properties upon annealing in nitrogen ambient are due to both, the reduction of the free carrier density and the reduction of carrier mobility. One possible reason is a chemical reaction with residual oxygen within the nitrogen gas which is used in order to prevent a contamination of oxygen from outside [Ber08].

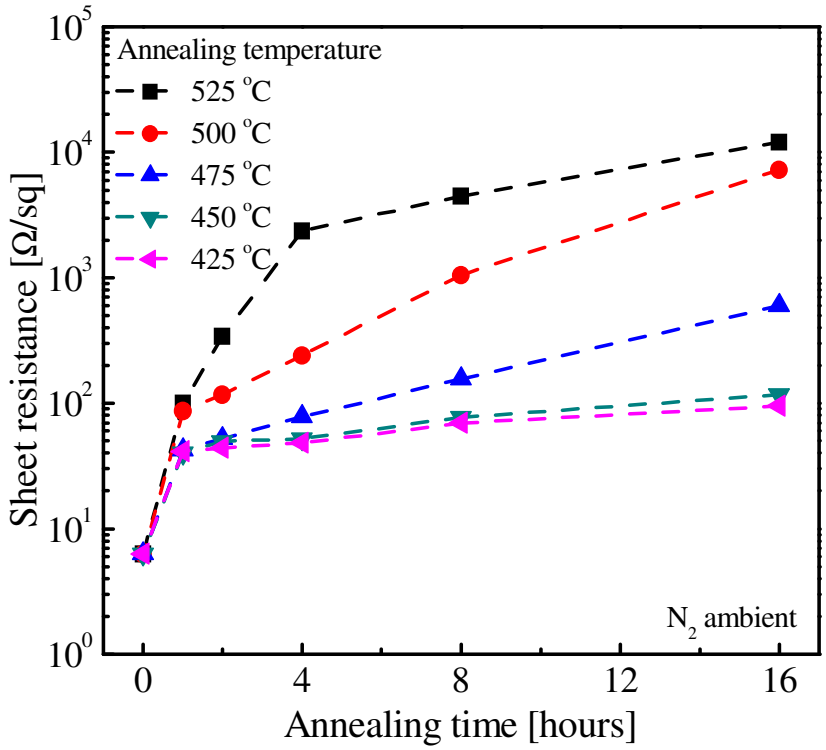

Figure 4. 1: Sheet resistances of ZnO:Al films on borofloat33 glass as a function of annealing time and annealing temperature.

4.3 PROPERTIES OF ZnO:Al/POLY-Si STACKS

In this section, the properties of ZnO:Al films capped with Si are investigated. For the ALILE-based experiments the sample is annealed in a tube furnace with nitrogen ambient at 425 and 450 °C for 16 hours and at 475…525 °C for 16 hours. For the SPC-based experiments intrinsic a-Si layers were deposited on ZnO:Al coated glass by electron beam (e-beam) evaporation at room temperature. The thickness of the a-Si layer was about 290 nm. The initial glass/ZnO:Al/a-Si stacks were annealed in a tube furnace at 600 °C for 24 hours in nitrogen ambient. During annealing the initially amorphous silicon was crystallized and therefore finally glass/ZnO:Al/poly-Si stacks were formed. For comparison, the different annealing steps were also applied to (i) glass/ZnO:Al samples, (ii) glass/Al/a-Si samples (ALILE process without ZnO:Al), and (iii) glass/a-Si samples (SPC process without ZnO:Al). The sheet resistances were measured by a 4-point probe.

Fig 4.2 shows the sheet resistance of the different samples as a function of the annealing temperature: glass/ZnO:Al (open circles), glass/poly-Si (open triangles), and glass/ZnO:Al/poly-Si (solid squares). For comparison the sheet resistance of an as-deposited ZnO:Al layer (6.3 Ω/sq) is indicated with a dashed line. The sheet resistance of the annealed glass/ZnO:Al samples (open circles) is significantly increased compared to the as deposited value despite the nitrogen ambient as shown in Fig 4.1, in which ZnO:Al is known to more stable as compared to air or oxygen ambient [Ham05]. In contrast, the sheet resistances of the glass/ZnO:Al/poly-Si samples (solid squares) are even lower than the sheet resistance of as deposited ZnO:Al layer. This is due to an increased conductivity of the ZnO:Al as the poly-Si on top does not contribute to the total resistance of the stack considerably. The resulting sheet resistance of the glass/ZnO:Al/poly-Si samples formed at 425 °C by the ALILE process and at 600 °C by the SPC process is around 4 Ω/sq. Hence, the Si layer on top of the ZnO:Al effectively prevents the degradation of the ZnO:Al films. For the SPC sample annealed at 600 °C for 24 hours the difference between the sheet resistance of the glass/ZnO:Al sample (open circle) and the glass/ZnO:Al/poly-Si sample (solid square) is more than three orders of magnitude as shown in Fig 4.2. This very promising result strongly motivated

further effects to study the application of sputtered ZnO:Al layers in poly-Si thin-film solar cells because the capped ZnO:Al layers do not degrade and provide a high quality transparent front contact.

In addition to the electrical properties the influence of the annealing on the optical properties was studied. Fig 4.3 shows the absorption spectra of three different samples (SPC experiments): (i) glass/ZnO:Al before annealing (dashed line), (ii) glass/ZnO:Al after annealing (solid line) at 600 °C for 24 hours, (iii) glass/ZnO:Al/poly-Si after annealing (solid circle) at 600 °C for 24 hours. It can be clearly seen that the heat treatment of the glass/ZnO:Al samples leads to a disappearance of free carrier absorption in the near infra-red (NIR) region indicated by an arrow. The reduction of free carriers can explain the strong increase of resistivity as can be seen in Fig 4.2. For the glass/ZnO:Al/poly-Si stack, however, the free carrier absorption in the NIR is preserved although the stack has been annealed for the same time. Bare poly-Si films have no absorption in this spectral region. In case of the glass/ZnO:Al/poly-Si sample the presence of the absorption in the ultra-violet (UV) region is caused by the absorption of the poly-Si film.

For a better understanding of the change of the electrical properties during crystallization Hall measurements were carried out on three samples, namely the as-deposited ZnO:Al film, the glass/ZnO:Al/poly-Si stack formed by ALILE at 425 °C for 16 hours (sample was treated by CMP after the ALILE process) and the glass/ZnO:Al/poly-Si stack formed by SPC at 600 °C for 24 hours. The resistivity of the glass/ZnO:Al/poly-Si (ALILE) and the glass/ZnO:Al/poly-Si (SPC) sample was $(2.2\pm0.1)\times10^{-4}$ Ωcm and $(3.4\pm0.1)\times10^{-4}$ Ωcm, respectively. This is lower than the resistivity of the as-grown glass/ZnO:Al sample ($(4.3\pm0.1)\times10^{-4}$ Ωcm). It should be noted that in all cases the Si layer does not contribute to the electrical transport noticeably, so the measured values could be solely attributed to the ZnO:Al layer. Table 4.1 shows resistivity ρ, carrier concentration N_e and hall mobility μ_H. As can be seen from Table 4.1, while the decreased resistivity of the ALILE sample is due to higher carrier concentration N_e in the ZnO:Al film, no change in carrier concentration can be observed for the SPC sample. Instead the mobility μ increases strongly. The measured

value of 52.6 cm^2/Vs is close to the theoretical limit proposed by Ellmer [Ell01], and thus higher than the experimental limit investigated by C. Agashe [Aga04]. This indicates that two different processes are responsible for the decrease of the resistivity. The higher mobility for the SPC sample is most likely caused by an improved crystallinity of the ZnO:Al film after the annealing. The increased electron concentration of the ALILE sample probably results from a diffusion of Al into the ZnO:Al film during the annealing and thus is a peculiarity of the ALILE process. The effect of the improved crystallinity of the ZnO:Al film expected after the annealing on the mobility is probably compensated by increased ionized impurity scattering.

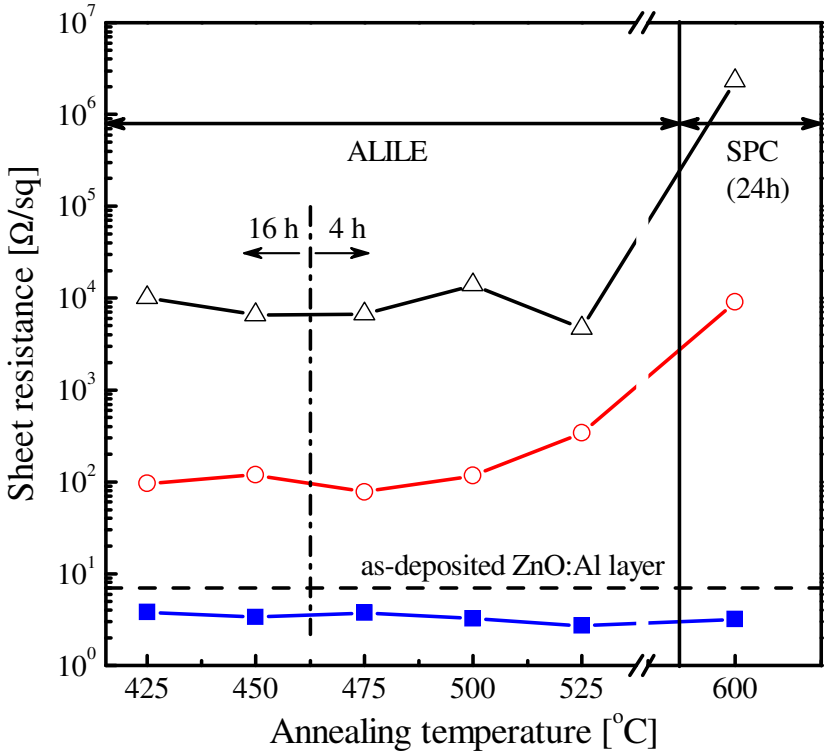

Figure 4. 2: The sheet resistance of glass/ZnO:Al/poly-Si (squares), glass/ZnO:Al (circles) and glass/poly-Si (triangles) stacks as a function of the annealing temperature. For reference, the sheet resistance of the glass/ZnO:Al layers before annealing is indicated with a dashed line. The poly-Si films were formed by either ALILE (450 - 525 °C) or SPC (600 °C).

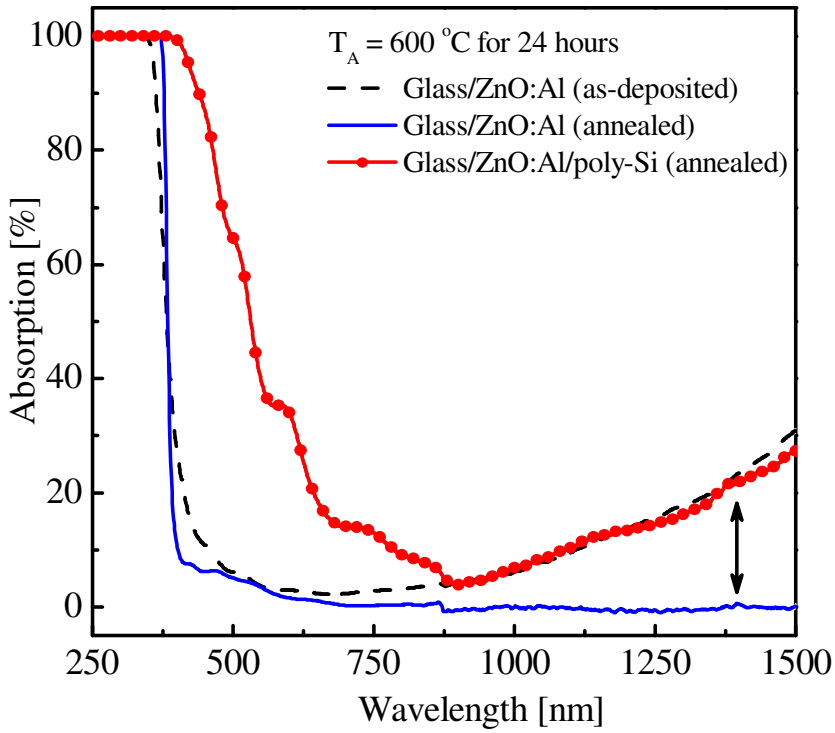

Figure 4. 3: Absorption spectra of ZnO:Al films on glass before (dashed line) and after (solid line) annealing, as well as of a glass/ZnO:Al/poly-Si stack after annealing (solid circles). Annealing was performed at 600 °C for 24 hours in nitrogen ambient (SPC experiments). The arrow highlights that the remaining free carrier absorption of the glass/ZnO:Al/poly-Si stack is maintained after annealing. In case of the glass/ZnO:Al/poly-Si sample the presence of the absorption in the ultra-violet (UV) region is caused by the absorption of the poly-Si film.

TABLE 4.1: Resistivity ρ, carrier concentration N_e and hall mobility μ_H of the as deposited ZnO:Al film and ZnO:Al films coated with poly-Si produced by the ALILE and the SPC process.

Sample	Crystallization conditions	ρ [$\times 10^{-4}$ Ωcm]	N_e [$\times 10^{20}$ cm^{-3}]	μ_H [cm^2/Vs]
ZnO:Al as dep.	-	4.3 ± 0.1	3.5 ± 0.1	42.0 ± 0.1
SPC	24 h @ 600 °C	3.4 ± 0.1	3.5 ± 0.1	52.6 ± 0.1
ALILE	16 h @ 425 °C	2.2 ± 0.1	6.8 ± 0.2	41.8 ± 0.2

4.4 ELECTRICAL PROPERTIES OF ZnO:Al/POLY-Si STACKS FORMED BY THE ALILE PROCESS

Fig 4.4 shows the resistivity, the hall mobility and the carrier concentration of ZnO:Al/poly-Si stacks which were formed by the ALILE process as a function of the annealing temperature. The black straight line is a linear fit to the open triangles data points to emphasize the increasing carrier concentration with increasing annealing temperature. Thus, it does not mean that the increasing carrier concentration is only due to the increasing Al concentration in the ZnO:Al films. In the case of ZnO:Al, the carrier concentration is not the same as the Al concentration. Usually, the Al concentration is a factor of 2-10 higher than the carrier concentration. This increasing carrier concentration is accompanied by a decreasing Hall mobility. The highest mobility value of 42 cm^2/Vs was obtained for a ZnO:Al/poly-Si stack formed at 425 °C and equals the as-deposited value. However, annealing at 525 °C leads to a mobility of 33 cm^2/Vs. Again, the red dashed line is a linear fit to the open squares to show the general trend of decreasing Hall mobility. Nevertheless, measured Hall mobilities were typically between 39 and 42 cm^2/Vs for all the samples up to 500 °C. These values are in the range of the mobility of single ZnO crystals which have similar doping levels [Ell08]. It is unclear why the sample annealed at 525 °C shows a different behavior.

In order to investigate whether Al atoms diffuse into the ZnO film during the ALILE process the sheet resistance of poly-Si on intrinsic ZnO (i-ZnO) coated glass is compared with that of poly-Si on ZnO:Al coated glass. The sheet resistance of (i) glass/i-ZnO, (ii) glass/i-ZnO/poly-Si, (iii) glass/ZnO:Al, (iv) glass/ZnO:Al/poly-Si stacks and (v) glass/poly-Si were measured by 4-point probe. The results are summarized in Table 4.2. The sheet resistance of the i-ZnO film could not be measured due to a high sheet resistance (> 1 MΩ). After ALILE process the sheet resistance of the ZnO/poly-Si stack is more than one order lower than the sheet resistance of the poly-Si film on glass. The sheet resistance of i-ZnO/poly-Si stack and poly-Si film on glass is around 400 Ω/sq and around 10 kΩ/sq, respectively. The change of the sheet resistance

of glass/i-ZnO/poly-Si could be explained by Al diffusion into the i-ZnO film during the ALILE process.

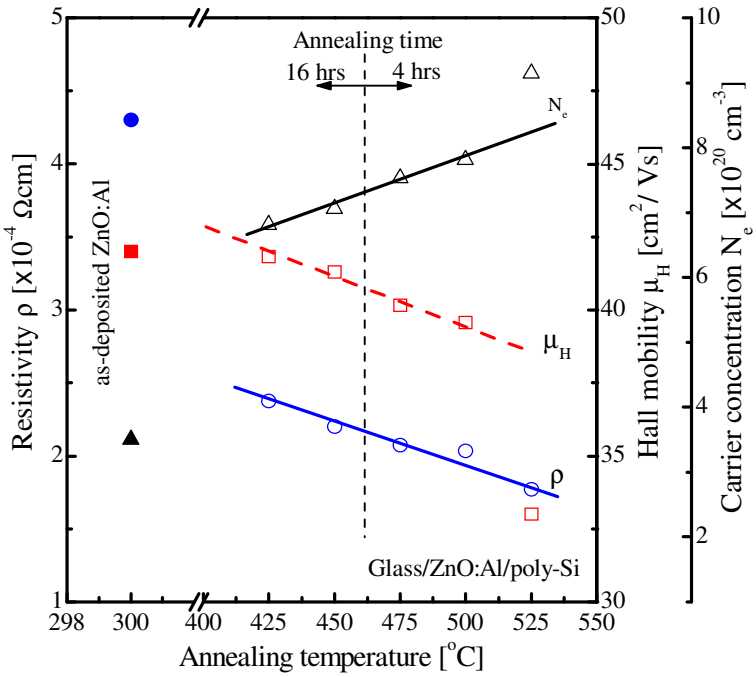

Figure 4. 4: Resistivity ρ (open circle), Hall mobility μ_H (open square), and carrier concentration N_e (open triangle) of ZnO:Al/poly-Si stacks formed by the ALILE process as a function of annealing temperature. For comparison the resistivity (solid circle), Hall mobility (solid square), and carrier concentration (solid triangle) of the ZnO:Al film deposited on glass at 300 °C are shown.

TABLE 4.2: Sheet resistance of (i) glass/i-ZnO (as-deposited), (ii) glass/i-ZnO/poly-Si, (iii) glass/ZnO:Al (as-deposited), (iv) glass/ZnO:Al/poly-Si, and (v) glass/poly-Si stacks. The poly-Si films were formed at 425 °C for 16 hours in nitrogen ambient.

Structure	Sheet resistance [Ω/sq]
Glass/i-ZnO (as-deposited)	> 1M
Glass/i-ZnO/poly-Si	413.4
Glass/ZnO:Al (as-deposited)	3.8
Glass/ZnO:Al/poly-Si	3.5
Glass/poly-Si	~ 10k

4.5 COMPARISON

The hall mobility of ZnO:Al/poly-Si stacks formed at 425 °C for 16 hours by the ALILE (star) and at 600 °C for 24 hours by SPC (solid circle) and the hall mobility of the as-deposited ZnO:Al on glass (open circle) are shown in Fig 4.5. The mobility is plotted as a function of carrier concentration. Indicated are mobility data from various publications [Ell06, Bre03, Kon03, Min92]. The data for single crystals were fitted by Ellmer using Masetti's formular [Ell05], resulting in the green line. Additionally the influence of grain boundary scattering for polycrystalline layers was calculated for different trap densities (blue and red straight lines). The trap density is 1.3×10^{13} cm^{-2} for the blue line and 3×10^{13} cm^{-2} for the red line.

The Masetti mobility model μ_H^{ma} [Mas83] was used to simulate the doping dependent mobility in Si and takes into account the scattering of the carriers by charged impurity ions which lead to a degradation of the carrier mobility (ionized impurity scattering). It is a model that combines lattice and impurity scattering.

$$\mu_H^{Ma} = \mu_{min} + \frac{\mu_{max} - \mu_{min}}{1 + (n / n_{ref1})^{\alpha_1}} - \frac{\mu_1}{1 + (n_{ref2} / n)^{\alpha_2}} \tag{4.1}$$

where μ_{max} is the lattice mobility at low carrier concentrations, μ_{min} is the ionized impurity mobility at higher carrier concentrations, and μ_{min}-μ_1 is the clustering mobility at very higher carrier concentrations. n is the carrier concentration.

The dotted line in Fig 4.5 by M. Kon et al. was fitted by Brooks–Herring–Dingle (BHD) theory [Kon03]. The BHD theory is based on charged impurity scattering.

$$\mu_1 = \frac{24\pi^3(\varepsilon_0\varepsilon_r)^2\hbar^3 n}{e^3 m^{*2} g_{(x)} Z^2 n_I} \tag{4.2}$$

where ε_0 and ε_r are the dielectric constant of free space and the relative permittivity, and Z and n_I are the charge and the density of the ionized scattering centers, respectively.

m* and $g_{(x)}$ is the effective mass and the screening function, respectively. n is the integer and h is Planck's constant.

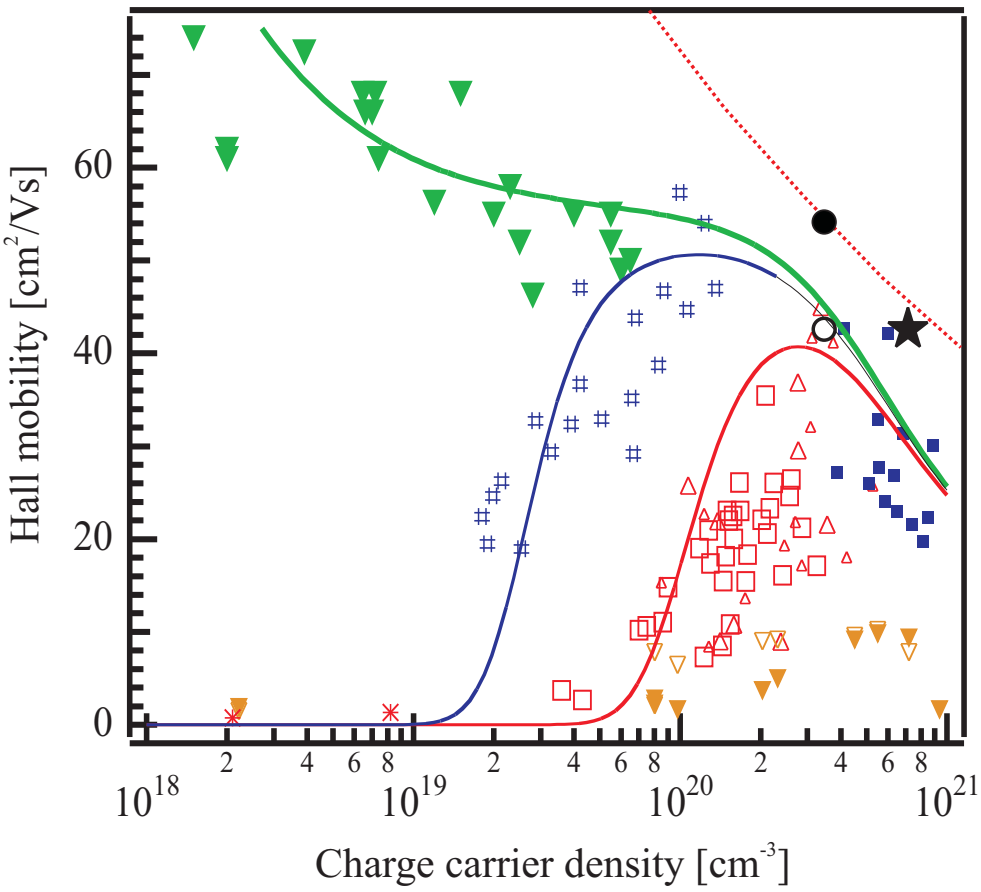

Figure 4. 5: Hall mobilities achieved in this thesis are shown for ZnO:Al/poly-Si stack formed at 425 °C for 16 hours by the ALILE (★) and at 600 °C for 24 hours by the SPC (●) process and for the as-deposited ZnO:Al film on glass (○).The straight green line is the hall mobility of single crystal ZnO:Al which is fitted by Masetti's formula [Mas83]. The dotted line was fitted by M. Kon [Kon03]. For comparison mobility data of other groups were added, which have been measured for ZnO films deposited by magnetron sputtering: Ellmer (□) [Ell06], Minami (■, #) [Min92], Brehme et al. (▼, ▽) [Bre03] and Kon et al. (△) [Kon03]. The mobility values of ZnO single crystals are indicated by green triangles. Additionally the influence of grain boundary scattering for polycrystalline layers was calculated for different trap densities (blue and red straight lines). The trap density is 1.3×10^{13} cm^{-2} for the blue line and 3×10^{13} cm^{-2} for the red line.

The hall mobility of ZnO:Al/poly-Si stacks formed at 425 °C for 16 hours by the ALILE (star) and at 600 °C for 24 hours by SPC (solid circle) process are comparable to the hall mobility of single ZnO crystals showing the high quality of the films. Ellmer et al. showed the improvement of the hall mobility of annealed ZnO:Al samples at 500 °C in vacuum and concluded that no recrystallization occurred and instead, it is plausible that point defects or dislocations have been annealed, reducing the scattering at such centers [Ell05]. Thus, the improvement of the hall mobility of ZnO:Al/poly-Si stack annealed at 600 °C in a furnace with nitrogen ambient seems to be a reduction of points defect or dislocations within ZnO:Al layer during an annealing process.

4.6 INFLUENCE OF SiN_X AS A BARRIER LAYER

SiN_X layers were applied to prevent a contamination with impurities from the glass substrate during the ALILE process [Abe06]. Resistivity ρ, carrier concentration N_e and hall mobility μ_H of ZnO:Al/poly-Si stacks with and without SiN_X as a barrier layer are summarized in Table 4.3. For comparison, resistivity ρ, Hall mobility μ_H, and carrier concentration N_e of as-deposited ZnO films on glass are shown. The resistivity, hall mobility, and carrier concentration did not change significantly in both cases (with and without SiN_X layer). SiN_X does not influence the properties of the ZnO:Al.

TABLE 4.3: Resistivity ρ, Hall mobility μ_H, and carrier concentration N_e of ZnO:Al/poly-Si stack formed on glass and on SiN_X coated glass at 425 °C. For comparison resistivity, Hall mobility, and carrier concentration of as-deposited ZnO film on glass is shown.

Sample	ρ [$\times 10^{-4}$ Ωcm]	N_e [$\times 10^{20}$ cm^{-3}]	μ_H [cm^2/Vs]
ZnO:Al as dep.	4.3 ± 0.1	3.5 ± 0.1	42.0 ± 0.1
Glass/ZnO:Al/poly-Si	2.4 ± 0.1	6.8 ± 0.2	41.8 ± 0.2
Glass/SiN_X/ZnO:Al/poly-Si	2.3 ± 0.1	7.3 ± 0.2	38.8 ± 0.2

4.7 INFLUENCE OF POST TREATMENTS

The investigations shown so far demonstrated that the capped ZnO:Al films can withstand process temperatures up to 650 °C. However, high quality poly-Si further process steps - i.e. Hydrogen (H)-passivation and rapid thermal annealing (RTA). The influence of these process steps on the electrical properties of the ZnO:Al layer are described in the following. For this investigation a 1"×1" sample after the CMP process was divided into 4 pieces (0.5"×0.5"). Each piece was treated with different post treatments. The electrical resistivity (triangles), Hall mobility (circles), and carrier concentration (squares) of the ZnO:Al/poly-Si stack formed on SiN_X coated glass at 425 °C for 16 hours with different kinds of post treatments (H-passivation, RTA, and RTA & H-passivation) are shown in Fig 4.6. For the H-passivation the hydrogen plasma was applied for 10 minutes at a substrate temperature of 600 °C. The RTA process was applied at 850 °C for 200 seconds. Even though the electrical properties of ZnO:Al/poly-Si stack did not change significantly after H-passivation, the electrical properties of ZnO:Al/poly-Si stack were improved dramatically after RTA treatment.

The H-passivation is practically interesting, as hydrogen has been identified as a donor in ZnO [Wal03]. The theoretical findings are backed by many experimental results. Thomas et al. [Tho56] investigated the influence of hydrogen on the conductivity of ZnO single crystal. They annealed the ZnO single crystal at 650 °C for a short time in hydrogen ambient. They found that the conductivity in ZnO is increased by the hydrogen. Also Oh et al. [Oh05] investigated the influence of H-passivation on the electrical properties of ZnO:Al layer. They applied an H-passivation process at 300 °C for 10 ~ 120 min. They found that the resistivity of the ZnO:Al layer is reduced after the H-passivation. The influence of hydrogen gas during the deposition of Al doped and undoped ZnO:Al layers on the hall mobility and carrier concentration was investigated by many researchers [Due08, Myo03]. They found a decrease of the Hall mobility of the Al doped and undoped ZnO layer with increasing hydrogen content during the deposition. The decrease of the Hall mobility could be explained by excessive hydrogen atoms acting as centers of interstitial sites in the lattice or let to an increase ionized or neutral impurity scattering. Both Al and H could constitute scattering centers or

combine to form the neutral defect complexes [Li05]. It has been stated by several groups that the carrier scattering at ionized impurities limits the mobility in the ZnO:Al films for carrier concentrations above 10^{19} cm^{-3} [Bel92, Min00, Ell01, Ell08]. From the literature the increase of carrier concentration and the decrease of the Hall mobility could be expected after H-passivation treatment. The results obtained here, show that the resistivity of ZnO:Al/poly-Si stack was slightly improved after H-passivation. But the improvement of the resistivity is within the error range. The Hall mobility and the carrier concentration of the as-grown ZnO:Al/poly-Si stacks and the RTA treated ZnO:Al/poly-Si did not exhibit significant changes after H-passivation. The reason could be that the highly Al doped poly-Si thin film acts as a barrier layer and prevents a diffusion of H atoms into the ZnO:Al layer.

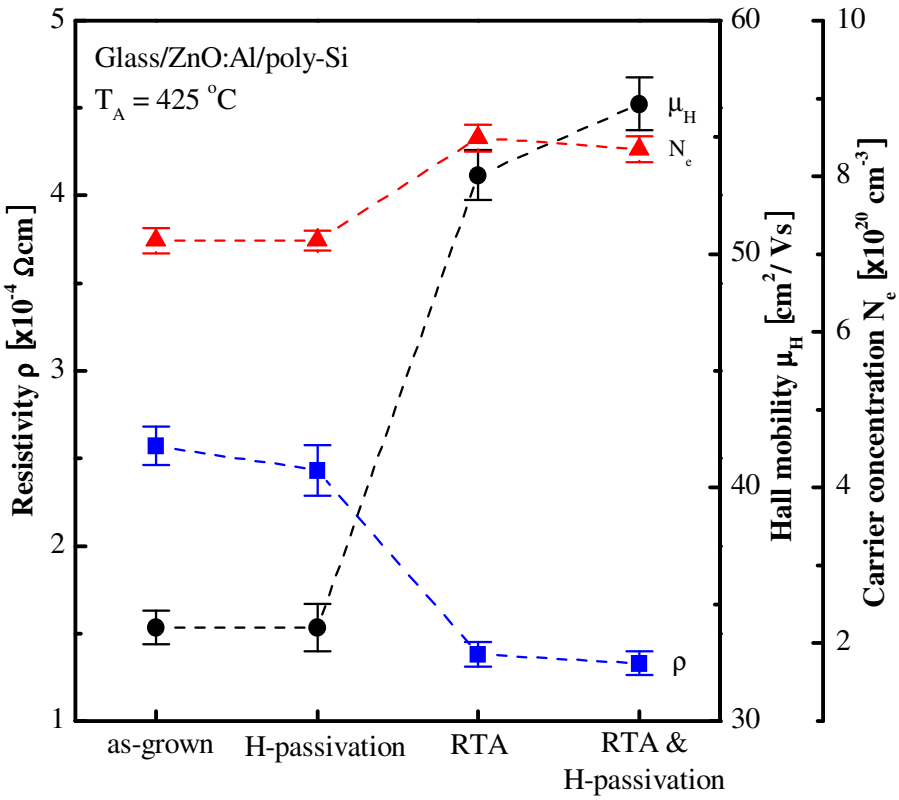

Figure 4. 6: Electrical resistivity ρ (squares), Hall mobility μ_H (circles), and carrier concentration N_e (triangles) of ZnO:Al/poly-Si stacks formed on SiN_X coated glass at 425 °C for 16 hours with different kinds of post treatment (H-passivation and RTA).

The hall mobility of ZnO:Al/poly-Si stack after RTA treatment was increased compared to the hall mobility of the as-grown ZnO:Al/poly-Si stack. The hall mobility of ZnO:Al/poly-Si stack before and after RTA treatment is 36 and 53 cm^2/Vs, respectively. This result is well matched with the results by Kim et al. [Kim05b]. They investigated the influence of RTA at 900 °C for 3 min in nitrogen ambient on the electrical properties of Al doped and undoped ZnO layer. They concluded that the enhancement of the mobility could be attributed to the combined effects of the improved crystallinity and the activation of Al dopants through de-oxidation of Al-oxide. As can be seen in Fig 4.7 the Hall mobility of ZnO:Al/poly-Si stack after H-passivation and after RTA treatment is 34 and 56.4 cm^2/Vs, respectively. It is concluded that in the ZnO:Al/poly-Si stack the RTA is more effective than the H-passivation in order to improve the Hall mobility and the resistivity of the ZnO:Al layer. From this results it is extracted that ZnO:Al/poly-Si stack withstand post-treatments (RTA and H-passivation), ZnO:Al can be improved by RTA and can be applied for poly-Si thin film solar cells.

4.8 APPLICATION OF SnO_2:F FILMS

SnO_2:F thin films could be an alternative to ZnO:Al layers as mentioned in the beginning of this chapter. Kawashima et al. [Kaw03] investigated the dependence of the resistivity of the SnO_2:F layer grown on Corning7059 glass substrate on annealing temperature (up to 600 °C) for 1 hour in the air. The resistivity of SnO_2:F layer was maintained after annealing. Bae et al. [Bae07] investigated the sheet resistance of the SnO_2:F layer in different ambient at 450 °C for 30 min. The sheet resistance of the SnO_2:F layer does not depend on the ambient. Thus SnO_2:F thin films should be suitable for the high temperature process in poly-Si formation.

The sheet resistance of SnO_2:F/poly-Si stacks formed using the ALILE process and the SPC process were investigated and compared. Fig 4.7 shows the sheet resistance of glass/SnO_2:F/poly-Si stacks (solid squares), glass/SnO_2:F (open circles) as a function of annealing temperature. The poly-Si films were formed by either ALILE at 425 and

450 °C for 8 hours or SPC at 600 °C for 24 hours. The SnO_2:F layers were deposited on borofloat33 glass (from Schott) using atmosphere pressure chemical vapor deposition (APCVD) method by Saint-Gobain-Recherche (SGR) in France. The thickness of SnO_2:F films used in this experiment is about 450 nm. For SPC experiments the thickness and the B doping concentration of amorphous silicon (a-Si) films deposited using electron beam (e-beam) evaporation is 290 nm and 4×10^{16} cm^{-3}, respectively. The sheet resistance of the SnO_2:F film in the as-deposited state is 27.3 Ω/sq. The sheet resistance of the SnO_2:F/poly-Si stack formed at 425 °C and 450 °C for 8 hours by the ALILE process is about 33 and 50 Ω/sq, respectively. The sheet resistance of the SnO_2:F/poly-Si stack formed by the SPC process is around 70 Ω/sq. The sheet resistance of the glass/SnO_2:F/poly-Si stacks treated in parallel increases with increasing temperature. However, the sheet resistance of the glass/SnO_2:F/poly-Si stacks is still suitable for the application in solar cells. The sheet resistance of the poly-Si films formed on bare glass using ALILE process is about 10 kΩ/sq. The reason for the degradation of the SnO_2:F layer capped with poly-Si formed by either the ALILE process or the SPC process is unclear.

For the properties of SnO_2:F/poly-Si stack the following study will be investigated in a future.

1. The interface of SnO_2:F layer and poly-Si layer is investigated in order to understand the degradation of SnO_2:F layers capped with Si.
2. Electrical properties (i.e. Hall mobility, carrier concentration and resistivity) of SnO_2:F/poly-Si stack are investigated.
3. Optical properties (i.e. absorption and HAZE) of SnO_2:F/poly-Si stack are investigated.
4. Characterization of solar cells on SnO_2:F coated substrate

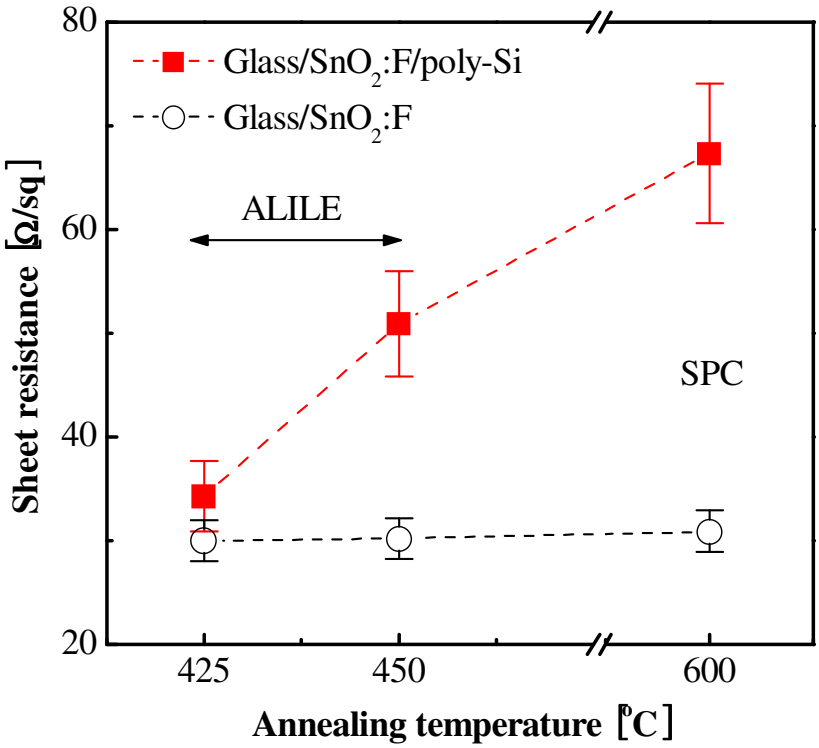

Figure 4. 7: The sheet resistance of glass/SnO_2:F/poly-Si stacks (solid squares), glass/ SnO_2:F (open circles) as a function of annealing temperature. The poly-Si films were formed by either ALILE (at 425 and 450 °C for 8 hours) or SPC (at 600 °C for 24 hours).

4.9 CONCLUSION

It was shown that crystallization of a-Si layers can also be carried out on ZnO:Al coated glass substrates using both ALILE and SPC. While uncoated ZnO:Al films show a strong increase of the sheet resistance upon heat treatment, ZnO:Al layers with Si on top used in this study resulted in electrical properties that were not only stable but considerably improved. While for SPC this is a consequence of a higher mobility, a strong increase of carrier density was observed during the ALILE process. The temperature-stable conductivity of ZnO:Al/Si stacks opens up appealing options for poly-Si thin-film solar cells including transparent conductive oxides (TCOs).

In the investigation of the influence of post-treatments (H-passivation and/or RTA) the electrical properties of ZnO:Al/poly-Si stack were not changed by H-passivation while the electrical properties (mobility and resistivity) of ZnO:Al/poly-Si stacks were improved by RTA treatment. The highst mobility of ZnO:Al/poly-Si stack was achieved 56.4 cm^2/Vs after the RTA treatment.

Although the sheet resistance of the glass/SnO_2:F/poly-Si stacks treated in parallel increases with increasing temperature, the sheet resistance of the glass/SnO_2:F/poly-Si stacks is still suitable for the application in solar cells.

CHAPTER 5
POLY-Si FILMS ON ZnO:Al COATED GLASS

In this chapter the properties of poly-Si films formed on ZnO:Al coated glass and on glass are characterized and compared in order to understand and optimize the aluminium induced layer exchange (ALILE) process for poly-Si thin film solar cells.

5.1 KINETICS OF CRYSTALLIZATION

In this section the kinetics of the crystallization on glass and on ZnO:Al coated glass in the aluminium-induced layer exchange (ALILE) process is studied in order to understand the influence of the ZnO:Al layer. Studies of the nucleation and grain growth using appropriate tools can elucidate the mechanisms of the crystallization of a-Si and will allow the control of the quality of the resulting polysilicon silicon (poly-Si) film formed by ALILE process.

The kinetics of crystallization by aluminium-induced crystallization (AIC) process was already addressed by several researchers [Manj78, Nas00, Gal02, Wid02, Kis03, Hsu03, Sch05, Pih07]. The driving force of the AIC process is described in literatures by [Nas00, Wid02, Rob04, Yu97, Sch06]. From some literature [Nas00b, Kon95, Sch06] the fact is agreed that the concentration of Si dissolved in the Al in the Al/a-Si system is different from that in the Al/c-Si system. Nast et al. [Nas00] and Konno et al. [Kon95] suggested that this concentration gradient is generated by the difference in Gibbs free energy between the initial and the final state. Pihan et al. [Pih07] argued that this difference in Gibbs free energy of the initial and the final state in the case of a crystalline Si layer as the precursor is associated to the grain boundary density and energy changes during crystallization.

A wide range of activation energies is found for the layer exchange process varying from 1.2 to 2 eV in the literature [Man78, Kim02, Pih07, Gal02]. The difference in activation energies from one author to another may originate from the complexity in the kinetics of the process since dissolution of Si, diffusion through the oxide at the interface Al/a-Si, and competition between grains influence the Si oversaturation in the Al layer and therefore modify the activation energy. The activation energy deduced from the diffusion coefficient of Si in Al layers and for Si diffusion in a thin Al layer is in the range of 0.8~1.36 eV [Hul98, McC71]. The activation energy of self-diffusion of Si and of the epitaxial regrowth of implanted Si is 4.1~4.6 eV) [Hir79, Kal79] and 2.4 eV [Cse75, Cse78], respectively. The activation energy of grain-boundary diffusion of Al in polycrystalline Si is 2.64 eV [Hwa80]. The activation energy for a-Si is 3~4 eV in the solid phase crystallization (SPC) process [Spi98, Lee97].

In the presented study, the crystallization (nucleation and grain growth) was observed in a heating stage of an optical microscope described in section 3.2.1.1. Therefore the samples were placed upside down on the heating stage such that the initial ZnO:Al/Al interface could be observed through the glass/ZnO:Al during annealing. The formation of poly-Si grains at the initial ZnO:Al/Al interface leads to a local change of the reflectivity as Si reflects less light than Al. The corresponding optical micrographs were analyzed to determine the crystallized fraction. The crystallized fraction as a function of the annealing time for different annealing temperatures (T_A) is shown in Fig 5.1. The annealing temperature was varied from 375 to 550 °C with an increment of 25 °C. At higher temperatures, the crystallized fraction increases very rapidly and then saturates while at low temperature a long incubation time is necessary before the crystallization starts and then the crystallized fraction increases moderately and saturates after a long time. The time necessary to get complete poly-Si films is found to depend strongly on the annealing temperature. The crystallized fraction reached nearly 100% at all annealing temperatures, which means that at all annealing temperatures continuous poly-Si film were formed on top of the ZnO:Al coated glass. The crystallization process on ZnO:Al coated glass at 425 °C takes around 4 hours. The crystallization process at annealing temperatures above 500 °C is very fast (below 20 min). Pihan et al. [Pih07] mentioned that the dentritic growth behaviour of Si grains is typical for metal-induced

crystallization of a-Si below the eutectic point, especially during the Al-induced layer exchange process and the shape of the Si grains is strongly depending on the crystallization temperature. In spite of the dentritic growth behaviour of Si grains formed on thermal oxidized Si wafer at 450 °C in his studies, the growth behaviour of Si grains in our experiment have circular shape at higher temperatures (> 425 °C). Dentritic growth behaviour was obtained on some Si grains formed at 400 °C and obviously on most of Si grains formed at 375 °C.

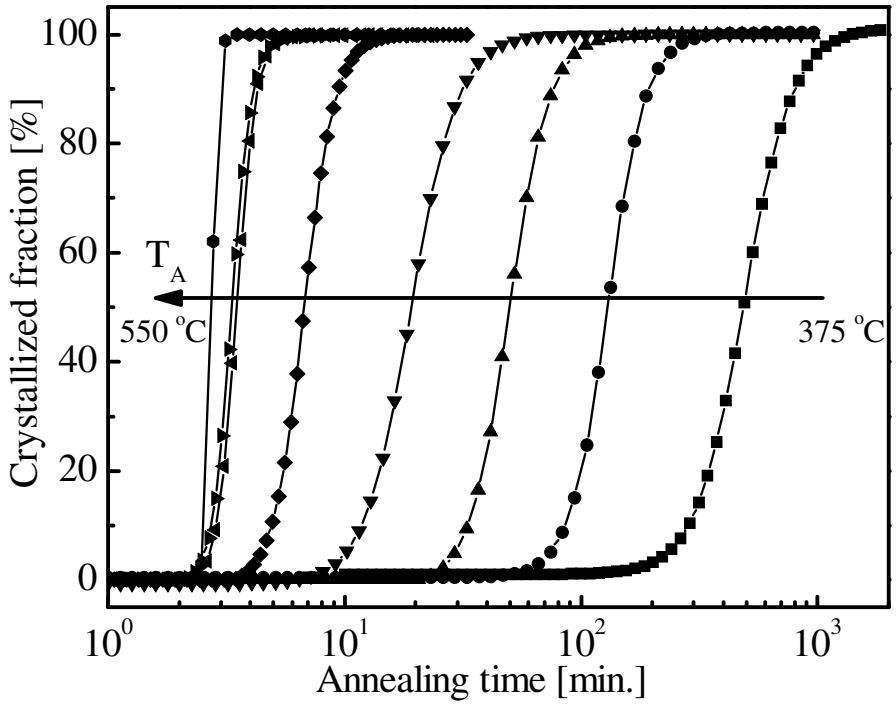

Figure 5. 1: Crystallized fraction versus annealing time for poly-Si films formed on ZnO:Al coated glass at eight different annealing temperature T_A (375…550 °C). The arrow indicates increasing annealing temperature.

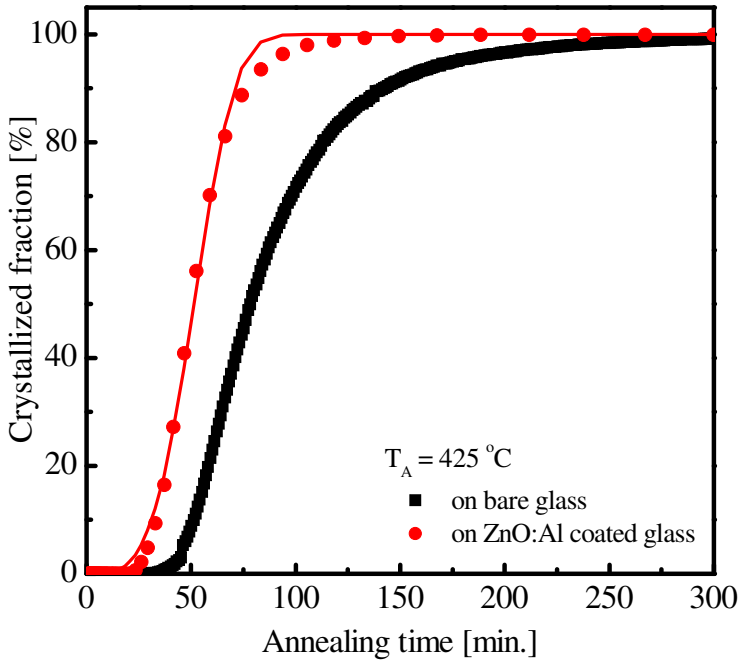

Figure 5. 2: Comparison of the crystallized fraction of poly-Si films on bare glass and on ZnO:Al coated glass at 425 °C.

The crystallized fraction of poly-Si films on bare glass and on ZnO:Al coated glass is compared in Fig 5.2. It was observed that the process time for the ALILE process on ZnO:Al coated glass is slightly shorter compared to the process time of the ALILE process on bare glass by the investigation of in-situ annealing. The reason could be that the surface of the ZnO:Al coated glass is rougher than the surface of the bare glass itself. The root-mean-squared (RMS) roughness of the ZnO:Al film and the Borofloat33 glass measured by atomic force microscopy (AFM) were 1.37 and 0.75 nm, respectively.

Fig 5.3 shows the increase of the crystallized fraction and the variation of the grain density on ZnO:Al coated glass as a function of an annealing time at the annealing temperature of 425 °C. Nucleation and grain growth does not occur in region (I). Both nucleation and grain growth occur in region (II). In region (III) only grain growth occurs (no nucleation). Here the grains grow until the film is fully crystallized. During the isothermal transformation, the cystallized fraction (α) of Si is represented by Avrami's equation [Joh39, Avr39, Avr40].

$$\alpha(t) = 1 - \exp(-Kt^n) \tag{5.1}$$

Here t is the process time, *K* is rate constant and *n* is the order parameter which depends upon the mechanism of crystal growth. *n* is held to have an value between 1-4 which reflected the nature of the transformation in question [Jen92]. The lines in Fig 5.2 and Fig 5.3 are based on Avrami's equation shown in Eq (5.1). For the fitting of the crystallized fration on ZnO:Al coated glass in Fig 5.2 the fitting parameter K and *n* was 5.21×10^{-14} and 3.76, respectively. For the fitting of the crystallized fration on bare glass in Fig 5.2 the fitting parameter K and *n* was 8.45×10^{-11} and 2.68, respectively.

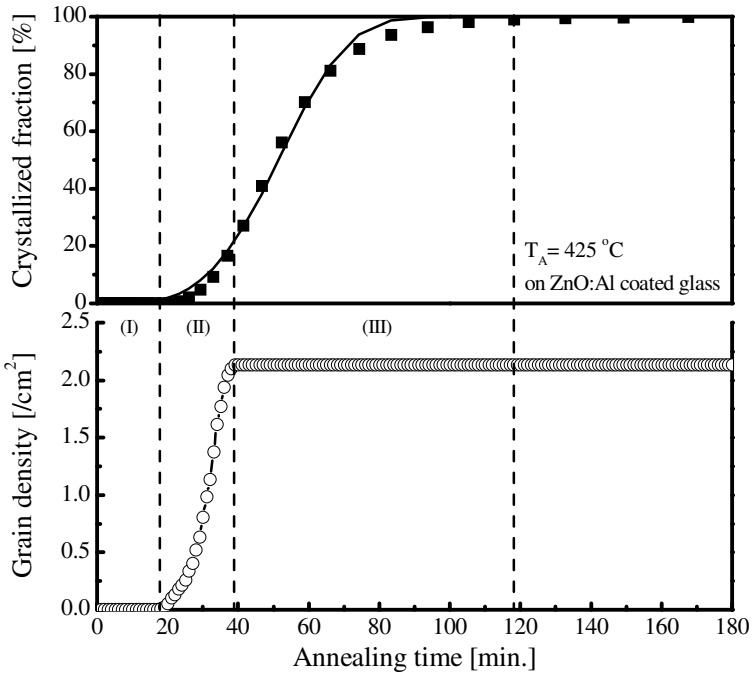

Figure 5. 3: Crystallized fraction and the grain density as a function of the annealing time at 425 °C as the annealing temperature; region (I): no nucleation and no grain growth, region (II): nucleation and grain growth, region (III): no further nucleation and grain growth but no nucleation until full crystallization.

5.1.1 NUCLEATION

Fig 5.4 shows the nucleation time of silicon on glass (solid squares) and on ZnO:Al coated glass (open circles) as a function of the annealing temperature. The nucleation time corresponds to the time when the first grain exceeding the optical microscope resolution (~ 0.5 μm) appears in the optical microscope. Open circles and open squares are the experimental data and straight lines are the Arrhenius fitting curves. The equation used for calculation of the activation energy E_A is shown below.

$$t = A \exp\left(-\frac{E_A}{kT_A} \right) \tag{5.2}$$

where A is the pre-exponential factor or simply the prefactor, t is the nucleation time, E_A is the activation energy for the nucleation, k is the Boltzmann constant and T_A is the annealing temperature (K). In Eq. (5.2), E_c and A are calculated to be practically independent of the temperature (at least in the temperature interval accessible in the calorimetric measurements).

The slope of the curve is hence related to the magnitude of the activation energy E_A that reflects the rate-limiting mechanism during the entire nucleation process. The activation energy for nucleation on glass and on ZnO:Al coated glass below 500 °C is 1.4 and 1.2 eV, respectively. The activation energy for the nucleation on ZnO:Al coated glass is lower than that for the nucleation on glass. This means that ZnO:Al films have an influence on the Si nucleation. Generally, the surface roughness of a substrate influences the nucleation time. The surface roughness of ZnO:Al films is higher than that of glass. It might be the reason why the crystallization time on ZnO:Al coated glass is shorter than that on glass substrates. The activation energy on ZnO:Al coated glass was calculated to be 1.2 eV for T < 500 °C and 0.2 eV for T > 500 °C. And also the activation energy of poly-Si films on bare glass shows the same behaviour. This behaviour is different to the behaviour reported in the literature [Sch04]. According to Schneider et al., the activation energy is 1.9 eV at the annealing temperature range of 400 ~ 540 °C. The activation energy for the nucleation on bare glass is lower than 1.9

eV reported by Gall et al. [Gal02b] and Schneider et al. [Sch04]. It can be explained with the different glass substrate used. Schneider et al. used Corning1737 glasses as a substrate. The reason could be the change of glass substrate from Corning 1737 glass (from Corning) to Borofloat33 glass (from Schott). Corning1737 glass and Borofloate33 glass have different thermal expansion coefficients and different strain points as seen in section 3.1.1. Hsu et al. [Hsu03] argued that the thermal energy at higher temperatures can release the film stress in a short time.

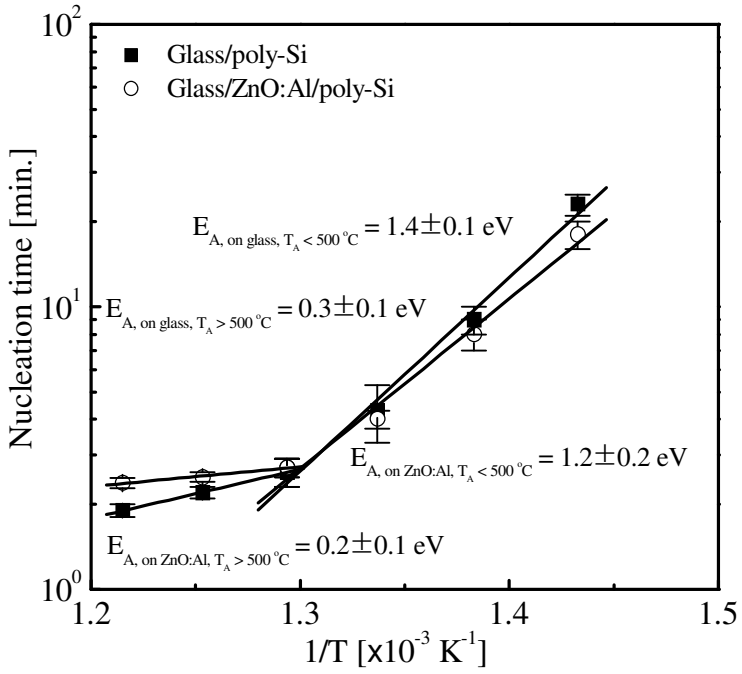

Figure 5. 4: Arrhenius-plot of the temperature dependence of the nucleation time of poly-Si on glass (solid squares) and on ZnO:Al coated glass (open circles). The nucleation time corresponds to the time when the first grain appears in the optical microscope (~ 0.5 µm).

5.1.2 GRAIN GROWTH

As can be seen in Fig 5.5, the activation energy for the grain growth determined in region III (see Fig 5.3) for the crystallization of 99 % on ZnO:Al coated glass and on

bare glass is 1.9 and 1.8 eV, respectively. The activation energy for the grain growth on ZnO:Al coated glass and on bare glass is quite similar. The value of 1.8 ~ 1.9 eV compares well with the activation energy of 1.8 eV calculated from the grain growth velocity reported by Schneider [Sch04]. This means that the ZnO:Al film and the kind of glass substrate should not influence the activation energy for the grain growth. But the ZnO:Al film can reduce the total crystallization time because the pre-factor A is lower. The pre-factor for the grain growth on ZnO:Al coated glass and on bare glass is 4×10^{-12} and 2×10^{-11} min, respectively. The pre-factor for the grain growth on ZnO:Al coated glass is one order magnitute lower than that on bare glass. In the perspective of an industrial application in the future the enhanced crystallization speed on ZnO:Al is desired to reduce a process time.

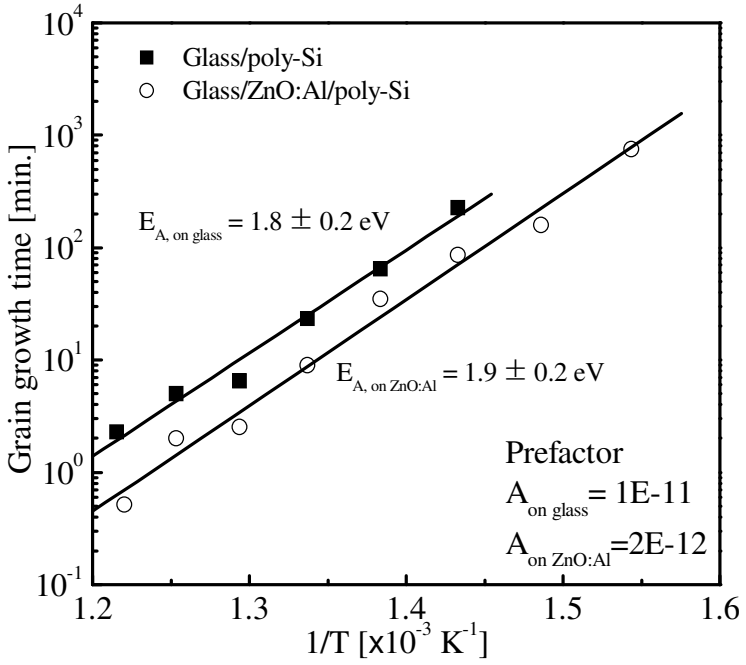

Figure 5. 5: Arrhenius-plot of the temperature dependence of the grain growth time on ZnO:Al coated glass (open circles) and on bare glass (solid squares). The error range is smaller than indicators.

5.2 STRUCTURAL PROPERTIES

The structural properties of poly-Si films formed on ZnO:Al coated glass and on glass were intensively studied and are compared in this section. In the ALILE process the process temperature is a crucial parameter which can change grain size and preferential (100) orientation. O. Nast [Nas00b] concluded that the process temperature is one of the most important parameters which influence the grain size.

5.2.1 CRYSTALLINE QUALITY

SEM tilted image and surface image of a glass/ZnO:Al/poly-Si stack after chemical mechanical polishing (CMP) are shown in Fig 5.6(a) and (b), respectively. The annealing is applied at 450 °C for 16 hours. As shown in Fig 5.6 a continuous poly-Si film is formed on ZnO:Al coated glass but few holes are visible at the grain boundaries. These holes are a typical feature of poly-Si films formed by ALILE process. O. Nast et al. [Nas00S] concluded that these holes in the poly-Si film are caused by intergrain Al clusters. The straight lines from top left the bottom right shown in Fig 5.6(a) were caused by the CMP process.

The crystalline nature of poly-Si thin films on ZnO:Al coated glass and on glass after ALILE process was verified using Raman spectroscopy. Raman measurements can also give a first impression of the crystallographic quality of the poly-Si material. Fig 5.7 shows the normalized Raman spectra of poly-Si thin films (a) on glass and (b) on ZnO:Al coated glass for different annealing temperatures. The Raman peaks corresponding to the transverse optical (TO) phonon of poly-Si thin films on glass and on ZnO:Al coated glass annealed within the whole process temperature range from 425 °C to 525 °C are at 520 cm^{-1} and exhibit a similar line shape for all the samples. In all cases, there is no Raman signal at 480 cm^{-1} that would indicate an amorphous phase in the poly-Si thin films [Sch98].

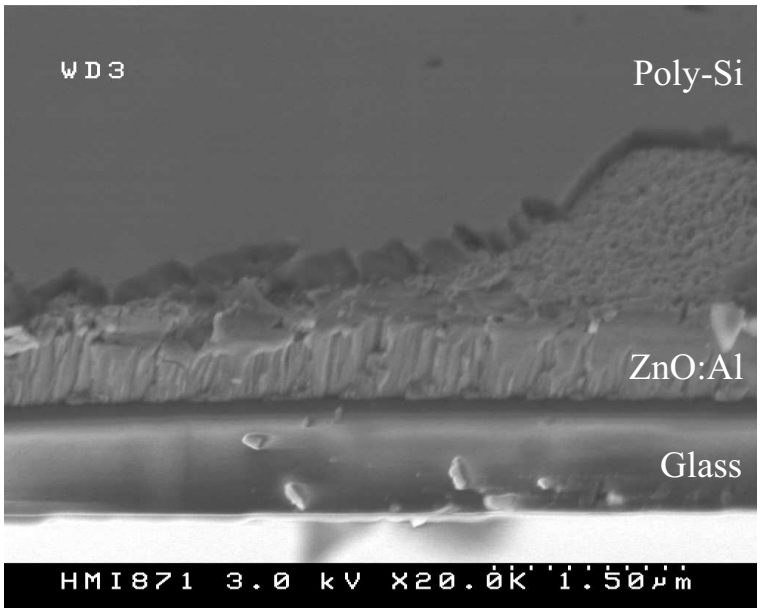

(a)

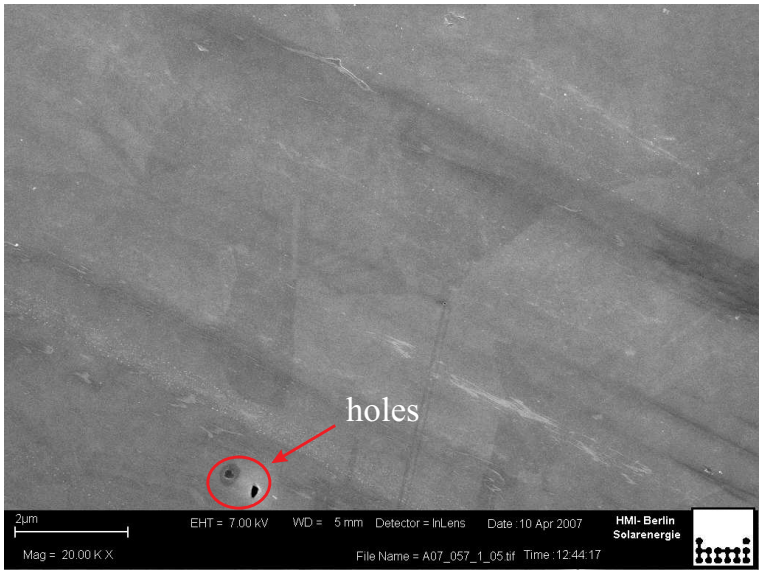

(b)

Figure 5. 6: (a) SEM tilted image and (b) surface image of glass/ZnO:Al/poly-Si stack after CMP.

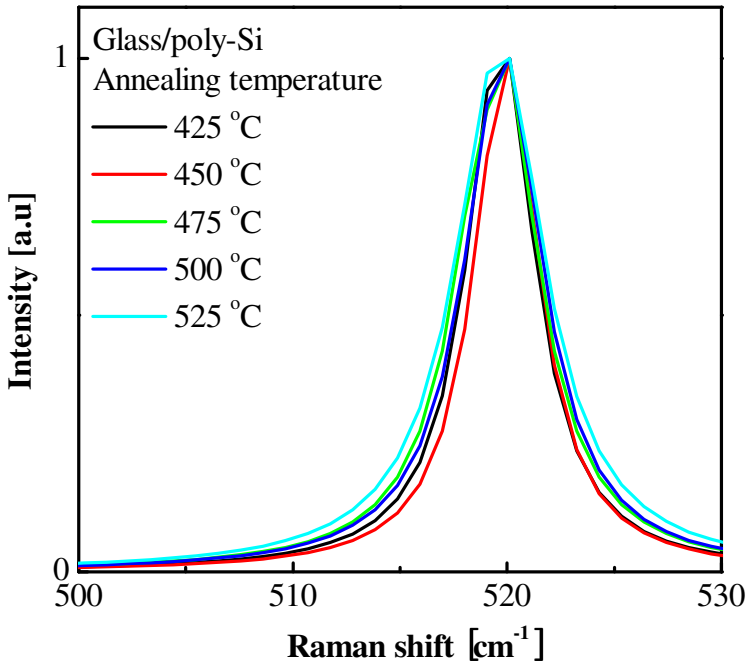

(a)

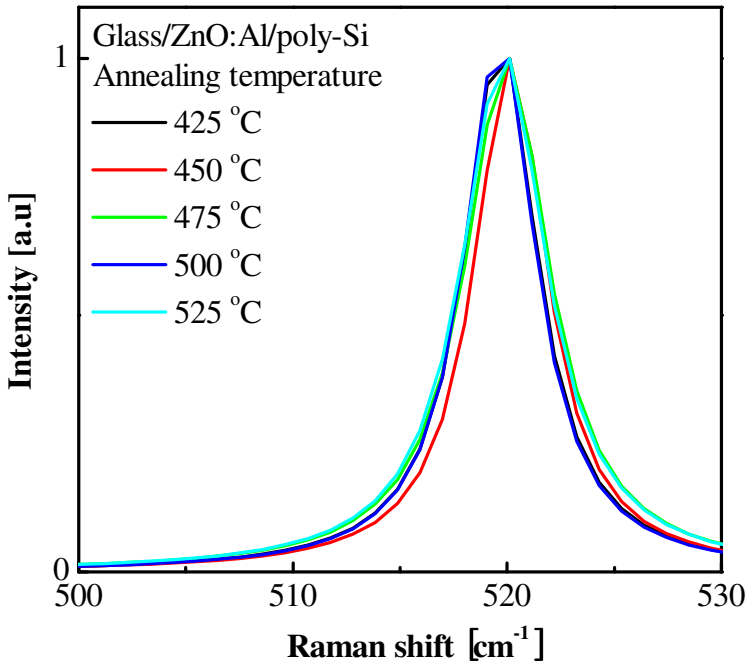

(b)

Figure 5. 7: Normalized Raman spectra of poly-Si thin films (a) on glass and (b) on ZnO:Al coated glass for different annealing temperatures.

To determine the Full-Width at Half Maximum (FWHM) of the TO phonon line a Lorentzian peak has been used as fit function [Kam98, Vou95]. The spectral width is interpreted in terms of phonon confinement, i.e. it is a measure for the density of defects in the films. The FWHM of poly-Si thin films on ZnO:Al coated glass and on glass as a function of the annealing temperature are shown in Fig 5.8. For comparison the FWHM of FZ-Si wafer is indicated with a dashed line. The FWHM value of both poly-Si films on glass and on ZnO:Al coated glass shows no significant change with increasing annealing temperature. The FWHM values of 4.1 cm^{-1} and 3.8 cm^{-1} have been calculated for the poly-Si films formed on ZnO:Al coated glass and on glass at 425 °C as a ALILE process temperature, respectively. The value of the FWHM of poly-Si thin films formed on glass and on ZnO:Al coated glass at 525 °C is 5 and 4.8 cm^{-1}, respectively. The FWHM of FZ Si wafer is 3 cm^{-1}, which is still much lower than the obtained values for poly-Si films. Hence, no significant difference has been observed for both types of poly-Si films. From the Raman results it could be concluded that poly-Si films formed on glass and on ZnO:Al coated glass have the same crystalline quality.

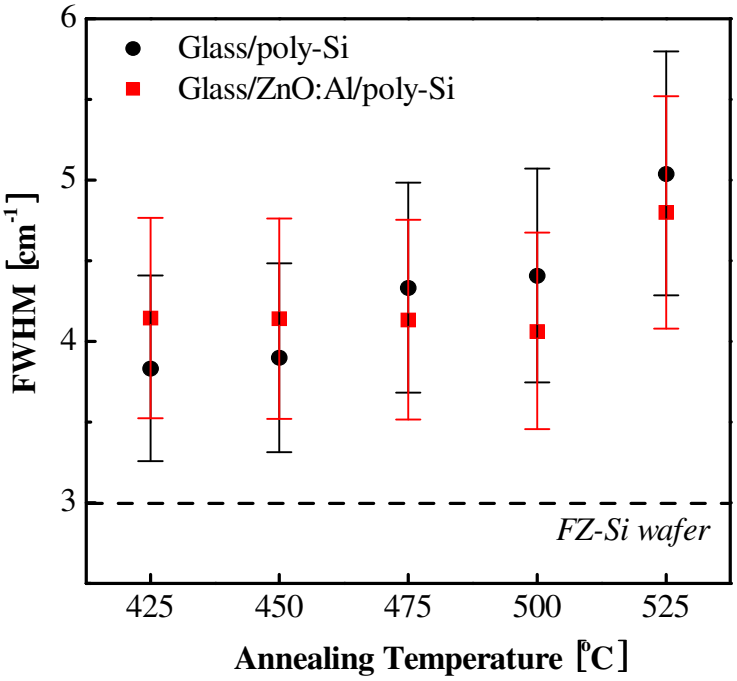

Figure 5. 8: FWHM of poly-Si films on glass and on ZnO:Al coated glass as a function of the annealing temperature. For comparison the FWHM of FZ-Si wafer is indicated with a dashed line.

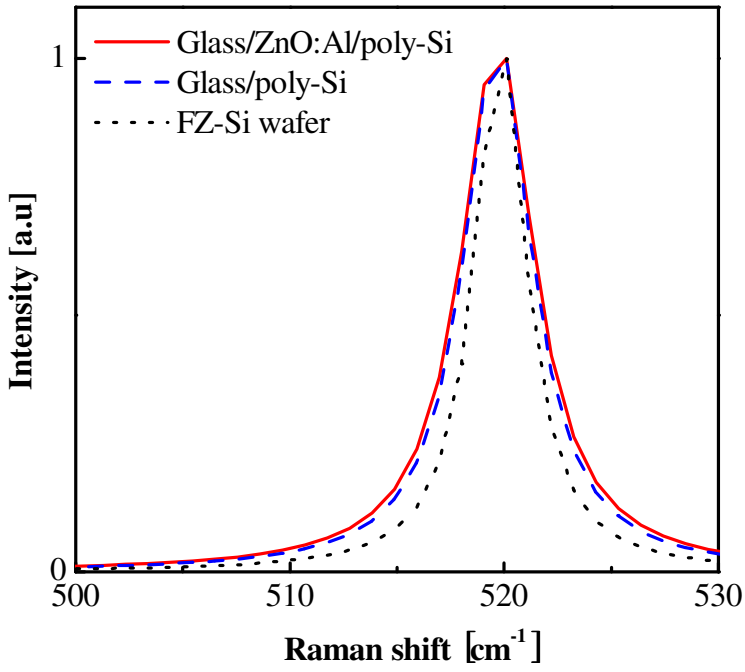

Figure 5. 9: Normalized Raman spectra of poly-Si films grown on ZnO:Al coated glass (red solid line) and on glass (blue dashed line). The samples were annealed at 425 °C for 16 hours. The normalized Raman spectrum of a FZ silicon wafer (black dotted line) is shown as a reference. Each spectrum is normalized to its maximum.

The normalized Raman spectra of poly-Si thin films grown on glass (blue dashed line) and on ZnO:Al coated glass (red solid line) annealed at 425 °C for 16 hours are compared in Fig 5.9. The normalized Raman spectrum of a FZ silicon wafer is shown as a reference. Each spectrum is normalized to its maximum. The Raman spectra of poly-Si films on glass and on ZnO:Al coated glass have no significant difference.

UV reflectance is an excellent characterization tool for the evaluation of the near-surface crystalline quality of poly-Si thin-film materials [Wid05, Str04, Wid07]. Fig 5.10 shows the measured UV reflectance of poly-Si films on glass and ZnO:Al coated glass, together with that of a polished c-Si wafer for comparison. The UV reflectance of poly-Si films on glass and on ZnO:Al coated glass are quite similar to the UV reflectance of the Si wafer. Using the ‘‘crystalline quality figure of merit’’ (Q) proposed in Ref. [Str04, Wid05], the poly-Si films formed on glass and on ZnO:Al coated glass at 425 °C have a crystalline quality in the surface region of about 99 %, compared to a

figure of merit of 100% of a polished high-quality Si wafer. The crystalline quality factor Q is obtained by dividing the measured reflectances of the sample at two specific wavelengths, ~ 367 nm (e1 peak) and ~ 275 nm (e2 peak), by the reflectances of a polished high-quality Si wafer at these wavelengths and then calculating the mean of the two values. The equation is the following:

$$Q = 100 \times \frac{1}{2}\left(\frac{R_{e1}}{R_{e1,c-Si}} + \frac{R_{e2}}{R_{e2,c-Si}}\right) \ [\%] \qquad (5.3)$$

where R_{e1} and R_{e2} is the measured reflectance of the sample at 367 nm and 275 nm, respectively. $R_{e1,\,c\text{-}Si}$ and $R_{e2,\,c\text{-}Si}$ is the measured reflectance of the polished high-quality Si wafer as a reference at 367 nm and 275 nm.

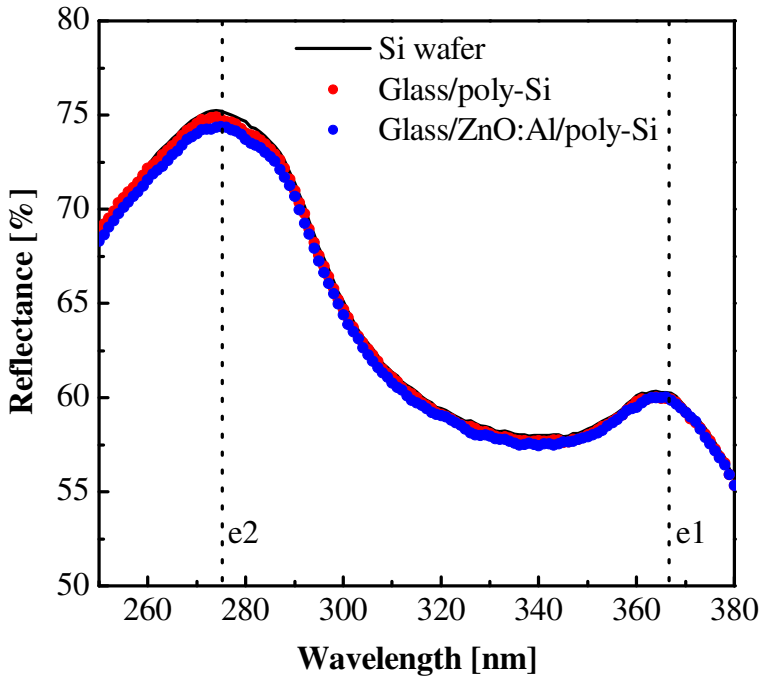

Figure 5. 10: Measured UV reflectance of a polished Si wafer (black line) and poly-Si films formed on glass (red circles) and on ZnO:Al coated glass (blue circles) at 425 °C for 16 hours.

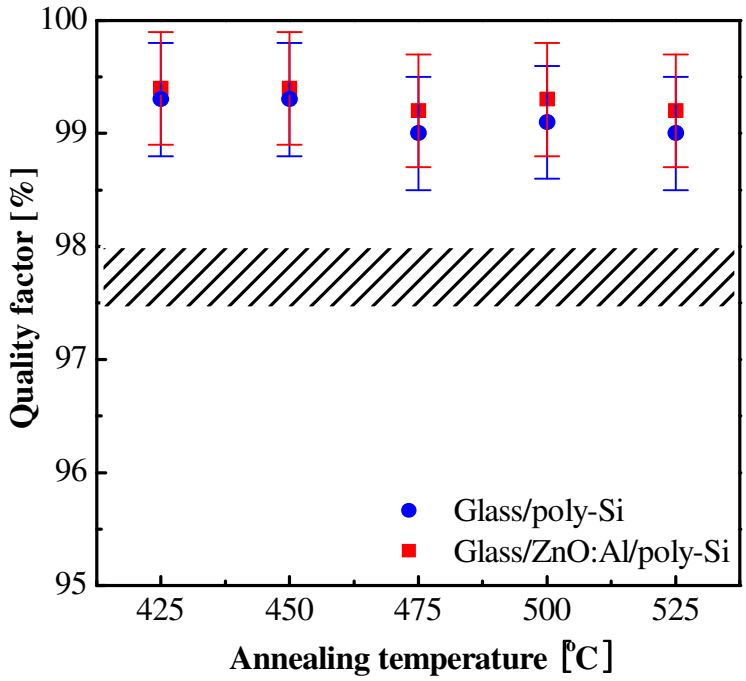

Figure 5. 11: The quality factor Q of poly-Si films on ZnO:Al coated glass (red squares) and on glass (blue circles) as a function of annealing temperature. The quality factors were calculated by the equation (5.2). The marked area indicates data from Widenborg et al. [Wid05].

The crystalline quality of poly-Si films on glass and on ZnO:Al coated glass calculated as a function of annealing temperature by Eq (5.3) is shown in Fig 5.11. All poly-Si films formed on glass and on ZnO:Al coated glass have a similar crystalline quality (98.5 ~ 99.4%). Hence Raman results and UV reflectance are in agreement with respect to the poly-Si film quality. The quality factor Q of poly-Si films formed using the ALILE process from Widenborg et al. [Wid05] is 97.4 ~ 98% as shown in Fig 5.11. The crystalline quality of poly-Si films on ZnO:Al coated glass is slightly better than the data of Widenborg et al. for both on glass and on ZnO:Al coated glass.

Some researcher investigated the influence of post treatments (H-passivation, rapid thermal annealing (RTA)) in terms of open-circuit voltage and short-current density of solar cells [Ter07, Gor07, Rau06]. But the characterization of the ALILE poly-Si films itself after post treatments were not studied so far. Raman was used to investigate the influence of post-treatments on the crystalline quality of ZnO:Al/poly-Si stacks.

Fig 5.12 shows the Raman spectra of glass/ZnO:Al/poly-Si stacks after H-passivation (red), RTA (green), and RTA+H-passivation (blue). The black line is the Raman spectrum of glass/ZnO:Al/poly-Si stack after the ALILE process and before the application of post-treatments. H-passivation treatment does not have any influence on the position of the Si-Si TO (transverse optical)-LO (longitudinal optical) phonon band. But the Si-Si TO-LO phonon band position was shifted from 520.3 to 521.3 cm^{-1} by the RTA treatment. It is known that stress causes the shift of the optical-phonon line at 520 cm^{-1} [Cer72]. The stress can be estimated from the frequency shift in the case of FWHM < 8 cm^{-1} [Kit02]. The dominant origin of stress in poly-Si thin films was attributed to thermal stress. The frequency is also modified by the presence of micro-crystals. It can be concluded that the RTA treatment introduces compressive stress in ZnO:Al/poly-Si stacks. The FWHM of poly-Si films treated by H-passivation does not change.

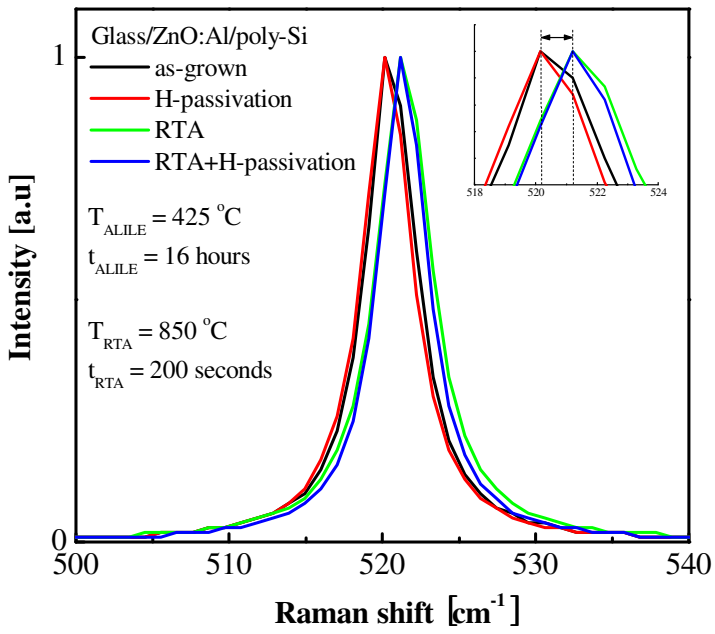

Figure 5. 12: Raman spectra of glass/ZnO:Al/poly-Si stacks treated by H-passivation (red), RTA (green), and RTA+H-passivation (blue). The black line is the Raman spectrum of glass/ ZnO:Al/poly-Si stack after ALILE process and before post-treatments.

5.2.2 PREFERENTIAL ORIENTATION

To investigate the crystallographic orientation of poly-Si thin films formed on glass and on ZnO:Al coated glass, electron backscatter diffraction (EBSD) and X-ray diffraction measurements were performed.

Fig 5.13 shows the EBSD orientation maps of poly-Si films formed on glass and on ZnO:Al coated glass by the ALILE process at different annealing temperatures. The color scale for the orientation maps is: Red color is (100) orientation, blue color is (111) orientation, and green color is (101) orientation. From the orientation maps shown in Fig 5.13, two important parameters concerning the poly-Si thin films can be extracted: The grain size and the orientation of the grains. The orientation maps are mainly red what is assigned to (100) orientation. Fig 5.14 shows the preferential (100) orientation $R_{(100)}$ of poly-Si films on ZnO:Al coated glass (solid squares) and on glass (open circles). The fraction of the poly-Si surface showing an orientation within 20° of the perfect (100) direction is defined as the preferential (100) orientation $R_{(100)}$. The preferential (100) orientation of poly-Si films is about 60% on both substrates. No significant change of a preferential (100) orientation with increasing annealing temperature was observed. A (100) orientation of the seed layer is very advantageous for subsequent epitaxial thickening. In previous publications [Kim02, Gal06] it was shown that the preferential (100) orientation decreases with increasing annealing temperature. In this study Borofloat 33 glass (from Schott) was used instead of Corning 1737 glass that was used in other studies. The thermal expansion coefficient of Borofloat 33 glass, crystalline silicon, and Corning 1737 glass is about 3.25×10^{-6} K^{-1}, 2.6×10^{-6} K^{-1}, and 3.76×10^{-6} K^{-1}, respectively. The thermal expansion coefficient of Borofloat33 glass is close to the thermal expansion coefficient of crystalline silicon. The thermal stress applied on the glass substrate during the ALILE process with different temperatures is changed due to the change of thermal expansion coefficient of the glass substrate. The change of the thermal stress at different temperatures could lead to the change of an orientation of the crystallized silicon thin film. The preferential (100) orientation of the poly-Si films on ZnO:Al coated glass can make these layers act as favorable seed layers for epitaxial growth of silicon absorber layers.

	Glass/poly-Si	Glass/ZnO:Al /poly-Si
425 °C	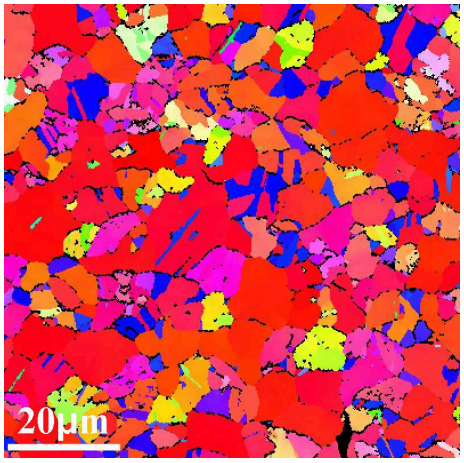	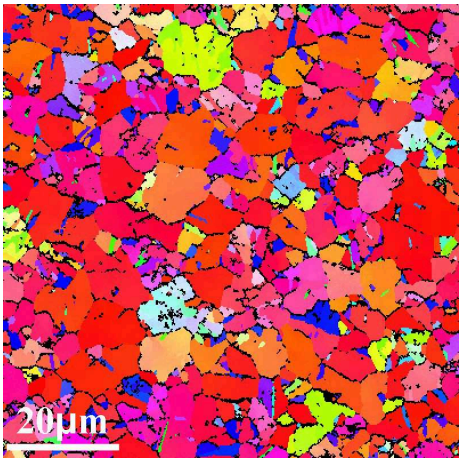
450 °C	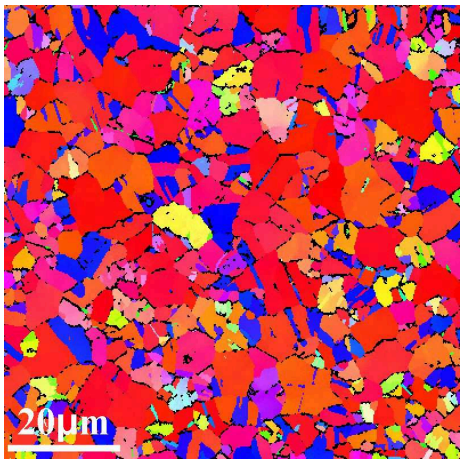	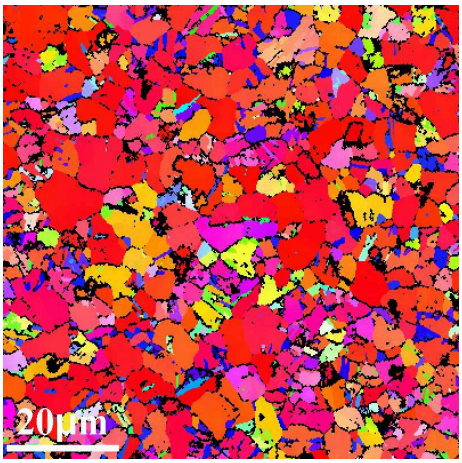
475 °C	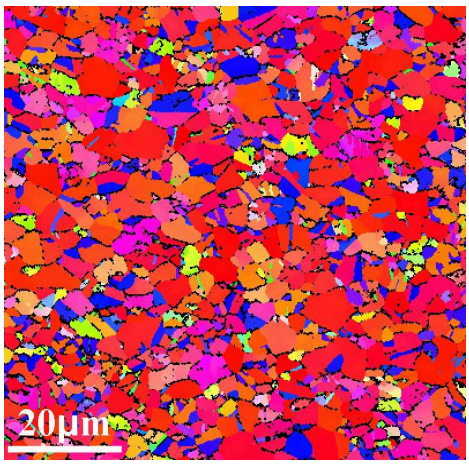	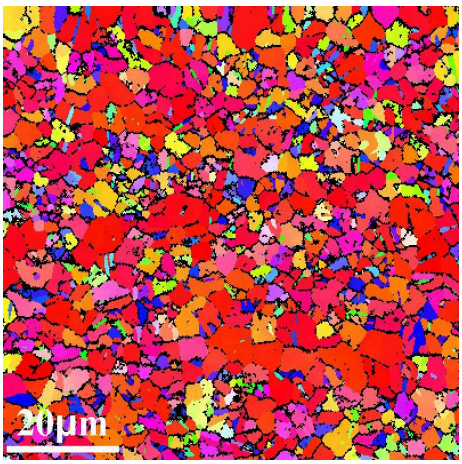

See the next page for the caption

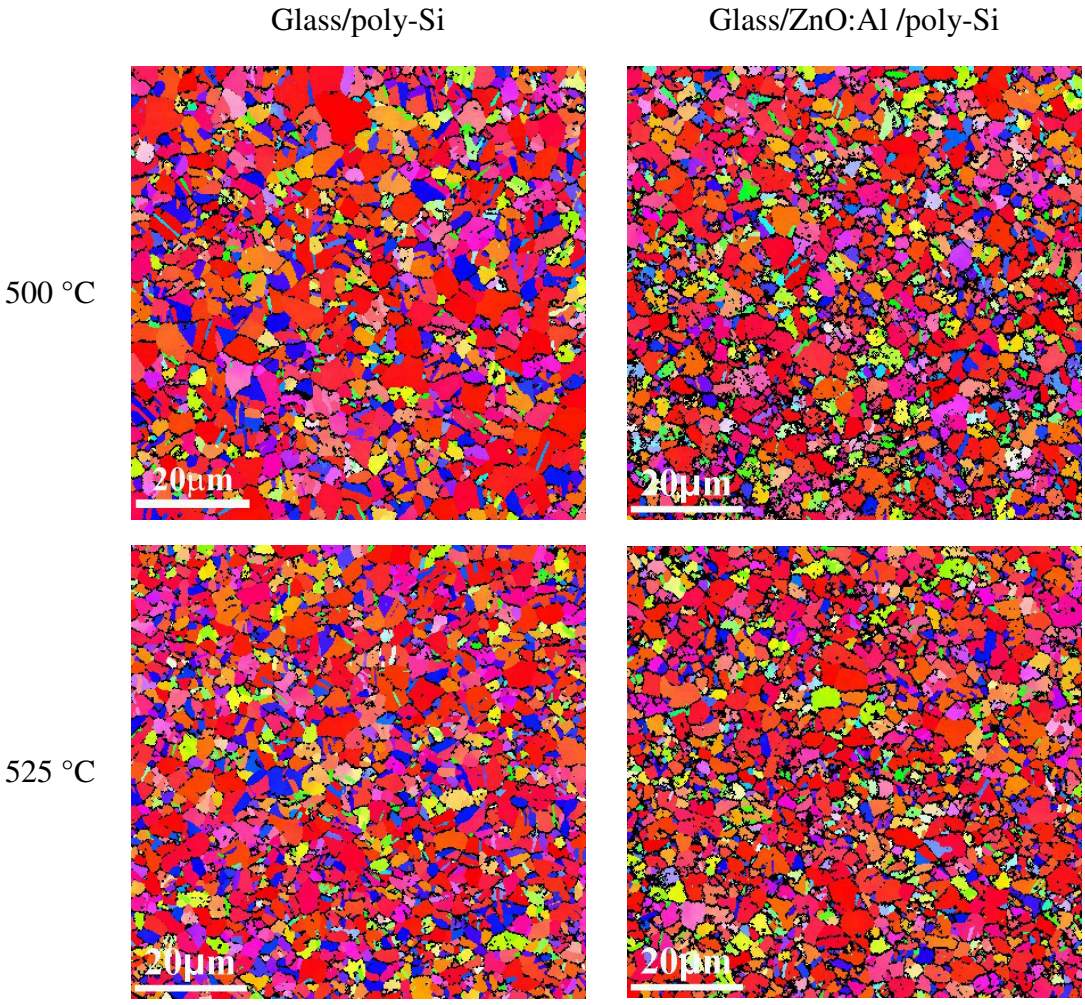

Figure 5. 13: EBSD orientation maps for poly-Si thin films on glass and on ZnO:Al coated glass annealed at 425 °C, 450 °C, 475 °C, 500 °C and 525 °C. Color scale for the orientation maps: Red color is (100) orientation, blue color is (111) orientation, and green color is (101) orientation.

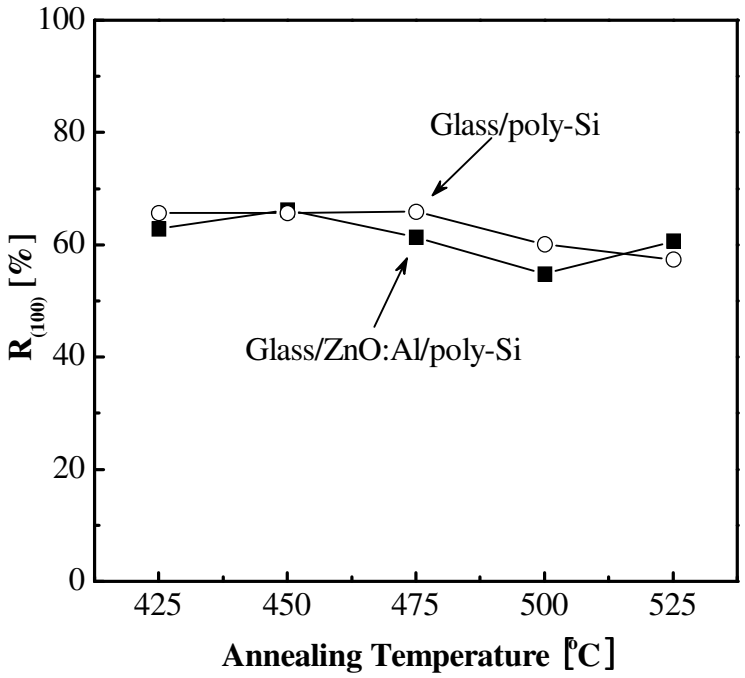

Figure 5. 14: Preferential (100) orientation $R_{(100)}$ of poly-Si films prepared on ZnO:Al coated glass (solid squares) and on glass (open circles) as a function of annealing temperature.

Even though the preferential (100) orientation of poly-Si films on glass and ZnO:Al coated glass is similar as shown in Fig 5.14, the different behavior of grain orientations of poly-Si film formed on glass and on ZnO:Al coated glass is shown in Fig 5.15. As can be seen in Fig 5.15(a) many grains of poly-Si film on glass are oriented to (111) orientation even though few grains of poly-Si film on ZnO:Al coated glass have a (111) orientation. Also the tilted angles of grains from a perfect (100) orientation show a different behavior between the glass/poly-Si stack and the glass/ZnO:Al/poly-Si stack. In case of glass/poly-Si stack most of grains are located in a range of 10 ~ 20° tilted from a perfect (100) orientation, but in case of glass/ZnO:Al/poly-Si stack most of grains are located in a range of 0 ~ 10° tilted from a perfect (100) orientation.

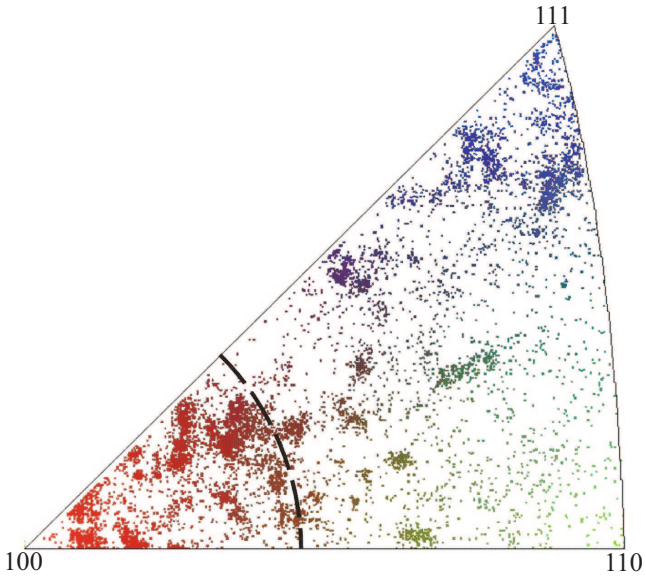

(a)

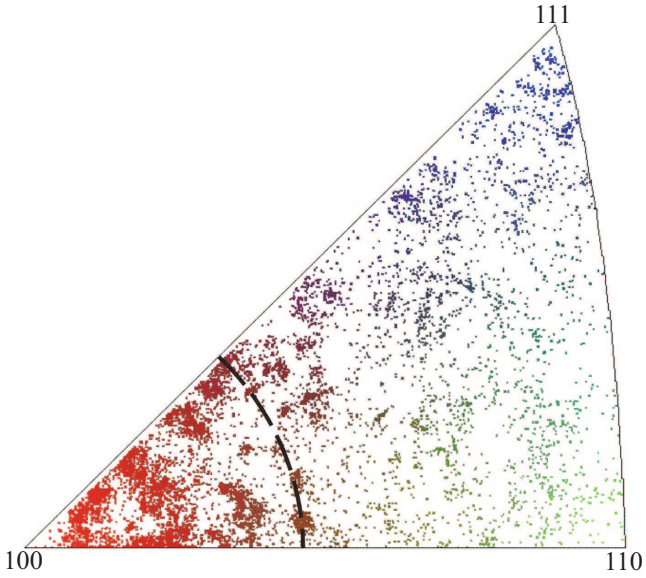

(b)

Figure 5. 15: Inverse pole figure of an electron back scatter diffraction (EBSD) orientation map of a poly-Si film (a) on glass and (b) on ZnO:Al coated glass prepared at 425 °C for 16 hours as annealing temperature of the ALILE process. In both cases about 60% of the area under investigation is tilted by less than 20° with respect to the (100) orientation (the corresponding region is indicated by a dashed line).

Both EBSD and X-ray diffraction (XRD) method are powerful techniques for determining orientation of poly-Si films, but a very flat sample surface is required in case of EBSD measurements. Due to this fact, XRD was measured to compare with the orientation of poly-Si films extracted from EBSD measurements. The XRD spectra of poly-Si films on ZnO:Al coated glass and on glass are shown in Fig. 5.16. Due to the high texture of the underlying ZnO:Al film only the (002) and the (004) reflections of zinc oxide are seen in the spectrum. Apart from these peaks, the positions of all silicon reflexes expected in the examined diffraction angle range are indicated. For a real investigation of film texture, i.e. preferential crystal growth in certain crystallographic directions, the measured peak areas first have to be corrected for the X-ray absorption for different incident angles and the structure factors of the individual peaks. The latter can be done by comparing the relative peak intensities to the ones of powder diffraction standards [ICDD]. In our case it was found that only orientations along (111), (100) and mixtures thereof play a significant role, while (110) orientation could not be found.

Based on this finding a tentative calculation of the fraction of grains oriented along the four crystal directions indicated in Fig 5.16 were carried out. The result is shown in Fig 5.17. The open circles indicate the fraction of each orientation of the glass/ZnO:Al/poly-Si stack and the open squares indicate the fraction of each orientation of the glass/poly-Si stack. The fraction of (400) orientation of poly-Si films on glass and on ZnO:Al coated glass was determined to 31% and 48%, respectively. And the fraction of (511) orientation of poly-Si films on glass and on ZnO:Al coated glass was determined to 27% and 23%, respectively. These results suggest that the preferential (400) orientation of poly-Si film on ZnO:Al coated glass is stronger than the preferential (400) orientation of poly-Si film on glass. For the calculation of a preferential (400) orientation both the fraction of (400) and (511) orientation were considered. As can be seen in Table 5.1, (411) and (511) orientations are tilted within 20° of the perfect (400) direction. Nevertheless, (411) orientation was not detected in the poly-Si films. The preferential (400) orientation $R_{(400)}$ (i.e. the sum of (400) and (511) peak) of poly-Si films on glass and on ZnO:Al coated glass is 58% and 71%, respectively. The numbers are similar to those determined using EBSD on samples prepared in the same way, but the difference between glass and ZnO:Al was not

observed previously. Grigorov et al. [Gri07] showed XRD results of poly-Si film on ZnO:Al coated glass. According to their investigation poly-Si films on ZnO:Al coated glass have a preferential (111) orientation. This result is different from our results where a preferential (100) orientation is observed. There are two differences: (a) the different orientation of ZnO:Al films and (b) a different preferential orientation of poly-Si films on glass. ZnO:Al films have a (101) orientation for their experiment and a (100) orientation in our experiments. Poly-Si films on glass have a preferential (111) orientation in their experiment [Dim06] and a preferential (100) orientation in this experiment as shown in Fig 5. 13.

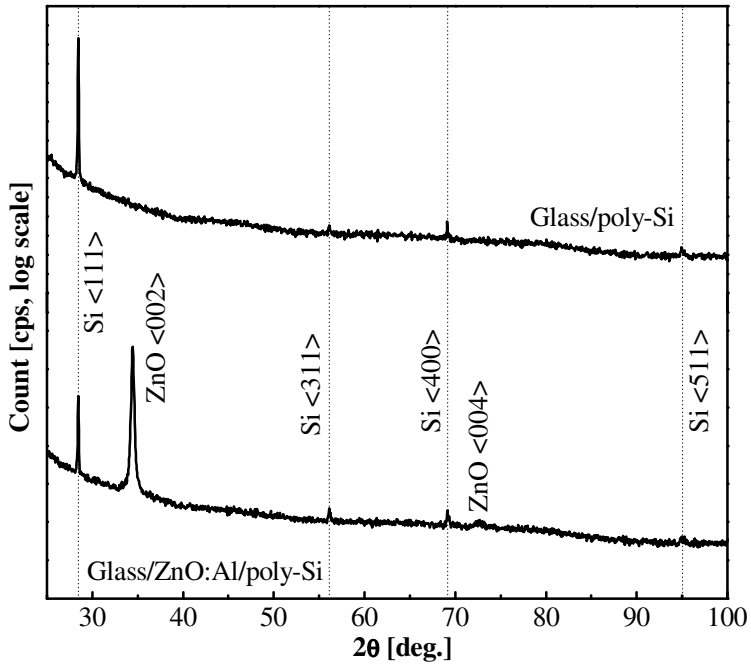

Figure 5. 16: XRD spectra of poly-Si films on glass (upper) and on ZnO:Al coated glass (below).

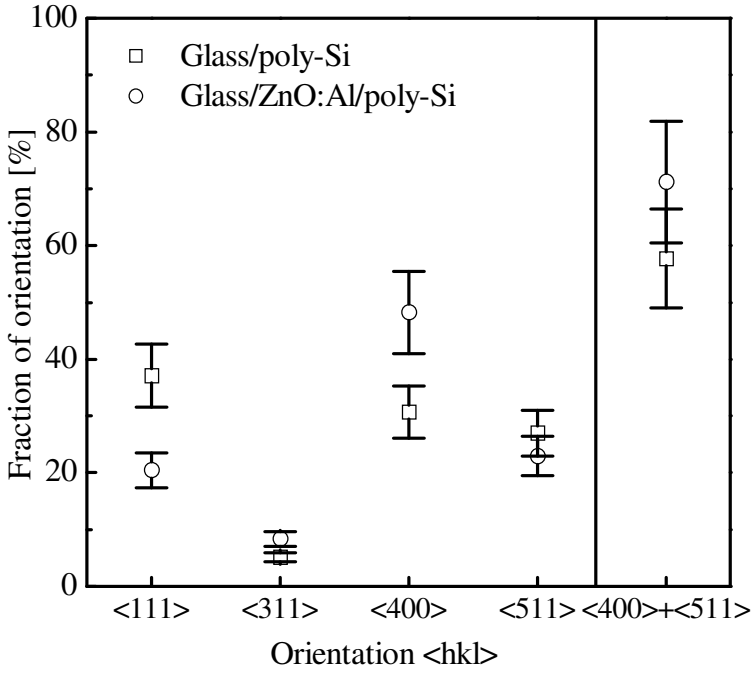

Figure 5. 17: The percentages of grain orientation of poly-Si films formed on glass and on ZnO:Al coated glass at 425 °C for 16 hours calculated from XRD measurement.

TABLE 5. 1: Tilted Angles between (400) orientation and different orientations.

Angle	(111)	(211)	(311)	(411)	(511)
(400)	54.7	35.2	25.2	19.47	15.8

5.2.3 GRAIN SIZE

To investigate the grain size of poly-Si films on glass and on ZnO:Al coated glass prepared at different annealing temperatures EBSD measurements and in-situ optical microscope measurements were used.

Fig 5.18 shows (a) the maximum grain size and (b) the average grain size of the poly-Si thin films on glass (open circles) and on ZnO:Al coated glass (solid squares) as a function of the annealing temperature. The maximum and average grain size of the poly-Si thin films was extracted from orientation maps measured by EBSD data (see Fig 5.13). The maximum grain size and the average grain size of poly-Si films on ZnO:Al coated glass are about 16 µm and 5 µm at 425 °C, respectively. The maximum grain size (solid squares) and the average grain size (solid circles) of the poly-Si thin films on glass are 18 µm and 7 µm at the same annealing temperature, respectively. The grain size decreases with increasing annealing temperature on ZnO:Al coated glass as well as on glass. For all temperatures, the grain size of the poly-Si films on ZnO:Al coated glass is slightly smaller than that of the poly-Si films on glass. This might be due to the surface roughness of ZnO:Al film. The surface of ZnO:Al layer is rougher than the surface of glass substrates. Due to this reason, the ALILE process time on ZnO:Al coated glass is shorter than that on glass and more nucleation sites of silicon and hence smaller grains lead to the faster crystallization process. As mentioned before, the time between the time needed for first nucleation and the time needed for the last grain nucleation has an impact to determine average grain size. The small time gap leads to similar grain sizes of the sample. Even though the maximum grain size of poly-Si films on glass is bigger than the maximum grain size of poly-Si films on ZnO:Al coated glass, the average grain size of poly-Si films on glass is slightly bigger than the average grain size of poly-Si films on ZnO:Al coated glass.

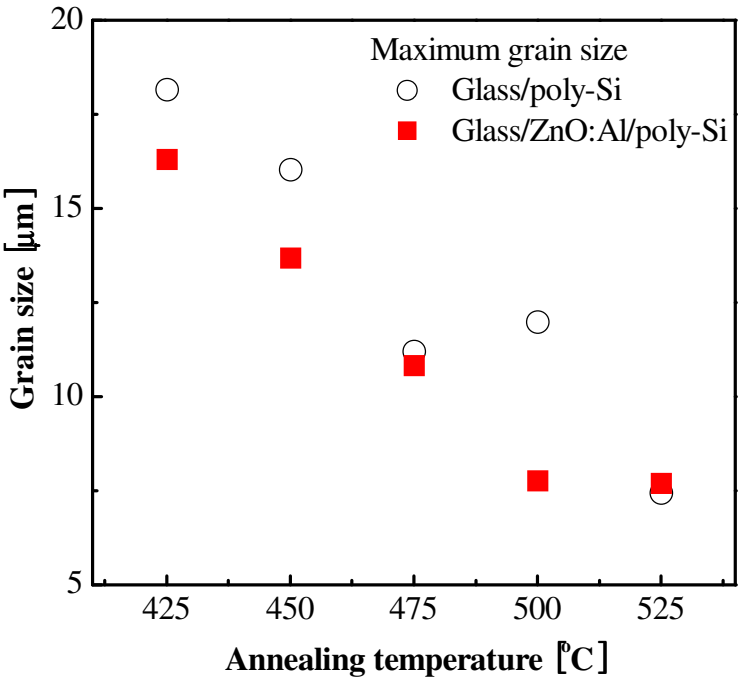

(a)

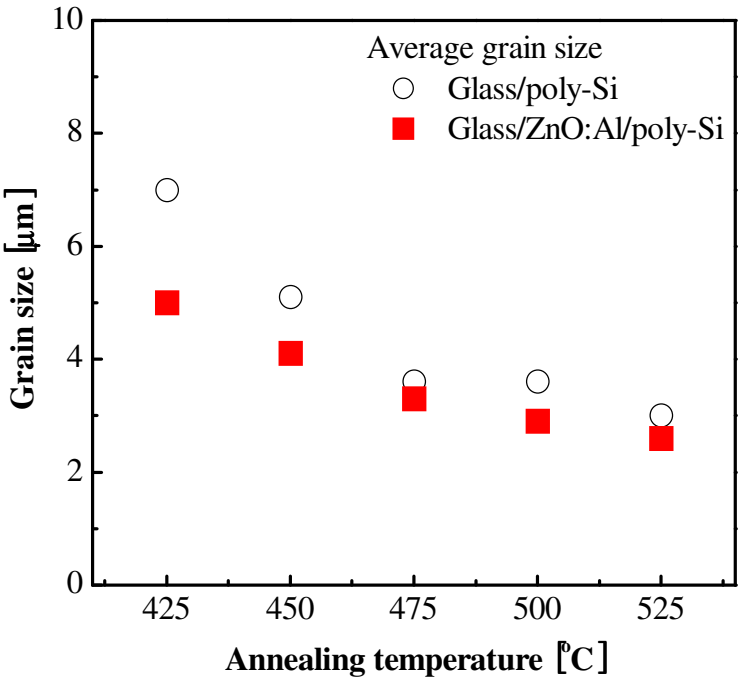

(b)

Figure 5. 18: (a) maximum grain size and (b) average grain size extracted from EBSD data of poly-Si films formed on glass (open circles) and on ZnO:Al coated glass (solid squares) as a function of the annealing temperature.

The grain size distribution as a function of the annealing temperature for the poly-Si films formed on glass and on ZnO:Al coated glass are shown in Fig 5.19. The data were obtained from electron backscatter diffraction (EBSD) measurements. The lines are Gaussian fitting curves. When the poly-Si films are formed at high temperatures (475 ~ 525 °C) by the ALILE process, the distribution of grain size is quite compact with a maximum at a grain size of about 3 µm. On the other hand, a very large distribution of the poly-Si grain diameter is obtained for low annealing temperatures (425 ~ 450 °C) and no real maximum of the grain size can be found. Although in this regime most of the surface is determined by the large grains it is expected that the quality of the resulting poly-Si layer will be determined by the low-quality (small grains) regions.

Fig 5.20 shows the grain density on ZnO:Al coated glass versus annealing time for different annealing temperatures. Si grains larger than 0.5 µm were considered due to the resolution of the optical microscope. At 425 and 450 °C, a different behavior is observed: the grain density is found to increase slightly and both nucleation and grain growth are taking place at the same time. Above 475 °C, the nucleation stops at an early stage as shown in Fig 5. 20. The formed Si grains continue to grow until they coalesce without significant additional nucleation and it ends with the formation of a continuous poly-Si layer. An interpretation of this behavior is that suppression of nucleation can take place over a large distance at high temperatures. Information on the grain size distribution will be greatly helpful to validate such assumption.

In Fig 5.21 the average grain size of poly-Si films extracted by EBSD (squares) is compared with the estimated average grain size of poly-Si films calculated by in-situ optical microscopy (circles) measurements. The estimated average grain size of poly-Si films observed by in-situ optical microscopy (OM) is calculated from the maximum nucleation density N_G shown in Fig 5.20. The maximum of the nucleation density N_G was used to determine the final estimated grain size d_G of grains ($d_G = \sqrt{A / N_G}$). A is the image size of the optical micrographs. The average grain size of poly-Si films calculated by in-situ optical microscopy is slightly larger than the average grain size of poly-Si films calculated by EBSD. A simple technique like optical microscopy can give good information locally.

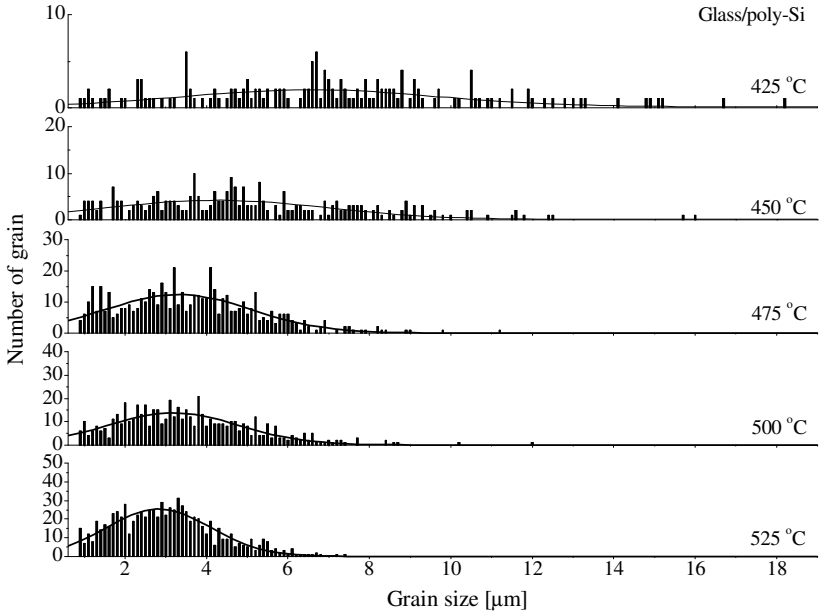

(a)

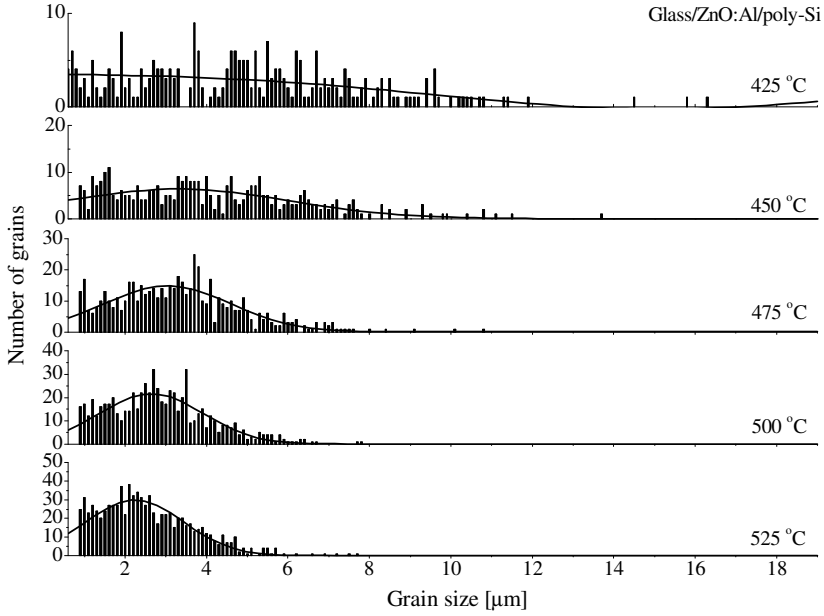

(b)

Figure 5. 19: Grain size distribution as a function of the annealing temperature for the poly-Si films formed (a) on glass and (b) on ZnO:Al coated glass. The data were extracted from electron backscatter diffraction (EBSD) data.

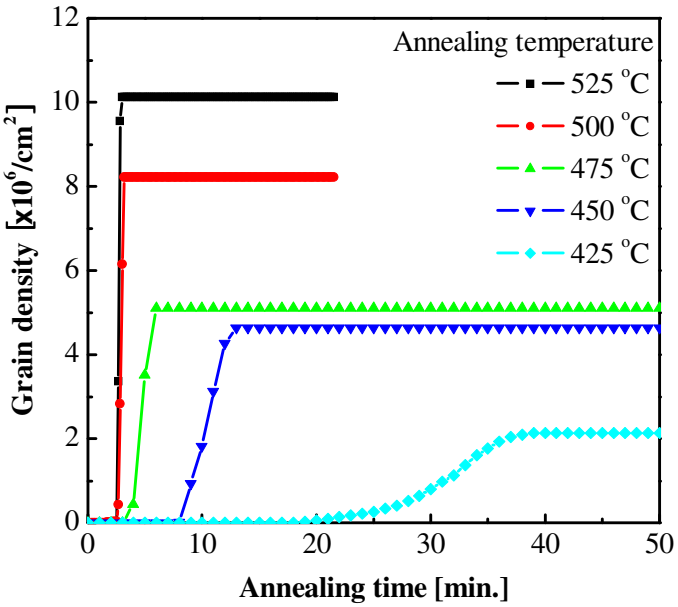

Figure 5. 20: Grain density vs. annealing time for different annealing temperatures. The substrate is ZnO:Al coated glass. Si crystals larger than 0.5 μm were considered due to the resolution of optical microscope. The size of images from in-situ optical microscope is 350×260 μm^2.

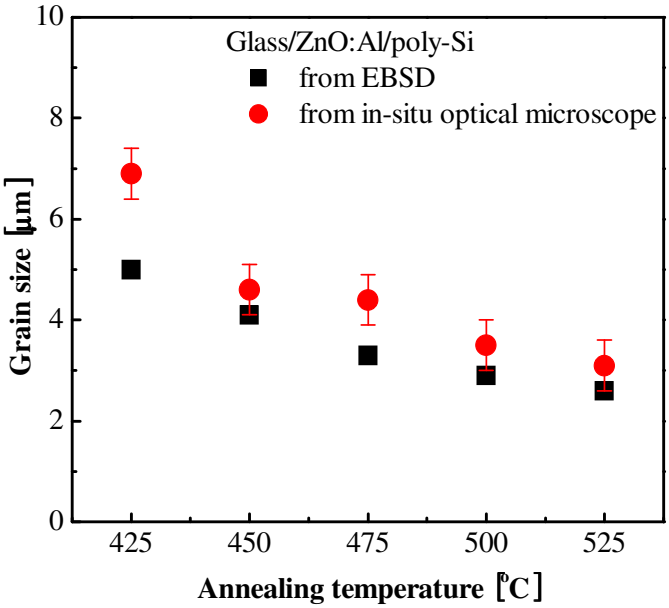

Figure 5. 21: The average grain size of poly-Si films on ZnO:Al coated glass extracted by EBSD (squares) and calculated by in-situ optical microscopy (circles) measurements.

5.2.4 DEFECT ANALYSIS

As can be seen in Fig 5.22 (a), there are numerous twin grain boundaries within the poly-Si film formed on ZnO:Al coated glass at 425 °C. These twin grain boundaries can be identified using EBSD analysis. Coincident site lattice (CSL) boundaries are shown by color. CSL boundaries are mainly twin boundaries of the first order (Σ3), second order (Σ9) and third order (Σ27). It is a highly symmetrical interface; also, atoms are shared by the two crystals at regular intervals. This is also a much lower-energy interface than the grain boundaries that form when crystals of arbitrary orientation grow together. Higher order twins are formed by the subsequent influence of twinning or by the reaction of lower order twins [Pih07]. For example, the Σ27 boundary is formed by Σ3 and Σ9 boundaries. CSL boundaries generally present low-energy configurations compared to random grain boundaries [Pih07, Bro81].

Knowledge of the density of these twins is very important in order to understand the formation of these twins and to improve the crystalline quality of the poly-Si layer. As shown in Fig. 5.22 (b), twin boundaries of Σ3 and Σ9 are present for poly-Si film formed on ZnO:Al coated glass at 425 °C. A very high distribution of Σ3 boundaries is observed while a very low proportion of third order (Σ27) twin boundaries are present. CSL Boundaries for poly-Si film formed on glass at 425 ^{o}C are shown in Fig 5.23. Twin boundaries of Σ3, Σ9 and Σ27 are present. The boundaries of the twins are mainly Σ3 for both cases.

In order to study the extended defects Secco etching [Sec72] was used. Secco etching can not be applied directly to the poly-Si film prepared by the ALILE process because they are highly doped with Al. Therefore, epitaxially thickened poly-Si films were used to study extended defects. For the epitaxial thickening of the poly-Si seed layer the surface of poly-Si layers was polished by the chemical mechanical polishing (CMP) process followed by a RCA cleaning and an oxide layer removal by a 1% HF dip. Then the thin poly-Si seed layers have been epitaxially thickened. The thickness of layers grown at 600 °C by e-beam evaporation was around 2 µm and the doping concentration of Boron was about 4×10^{16} cm^{-3}. To make extended defects visible, on the sample

surface Secco etching solution was applied. The Secco solution is HF/$K_2Cr_2O_7$/H_2O obtained by mixing 2 parts of HF (49%) with 1 part of 0.15 Mol $K_2Cr_2O_7$/H_2O. The samples were etched at room temperature for 7 seconds and the resulting etch pits were analyzed by scanning electron microscopy (SEM).

Fig 5.24 (a) and (b) show the SEM images of Secco-etched poly-Si seed layer/absorber layer stacks (epitaxial poly-Si films) on bare glass and on ZnO:Al coated glass, respectively. From the images it is seen that while some of the grains exhibit better quality epitaxial growth, some other grains exhibit more defective regions. The area of the more defectively grown grains corresponds to about 35% of the total area of the sample surface analyzed by SEM images. We know from EBSD and XRD analysis that about 60% of the grains feature a (100) orientation and about 48% of the grains feature a (400) orientation and 23% of the grains feature a (511) orientation for the poly-Si film on ZnO:Al coated glass, which is favorable for epitaxial thickening at low temperatures. This means that the more defective regions (35% of the total area) could be related to underlying grains with orientations towards (110) and (111) orientation.

Fig 5.25 shows intragrain defects of poly-Si films (a) on glass and (b) on ZnO:Al coated glass. It can be also seen that even less defectively grown grains exhibit dislocations (circular pits in the figure). Comparison of Fig 5.25 (a) and (b) shows that underlying ZnO:Al layer has no significant influence on the intra grain defect density. These circular etch pits are characteristic for dislocations in Si (100) grains [Dog08]. A cross sectional TEM image of a glass/poly-Si/epi-Si sample is shown in Fig 5.26. The glass substrate is located at the bottom. The sample was shortly defect etched before sample preparation for TEM to facilitate the selection of interesting regions for TEM analysis. The traces of this short defect etching are visible at the top of the sample. The left and the right part of the image show a clear difference of the surface. The absorber layer on the right hand side contains a high density of twins within the cone that is visible and twin and dislocations on the right side of this cone. The extended defects on the left hand side are mainly dislocations. Because dislocations can not stop suddenly but end by forming a loop, merging together or reaching a surface, the dislocations in the left

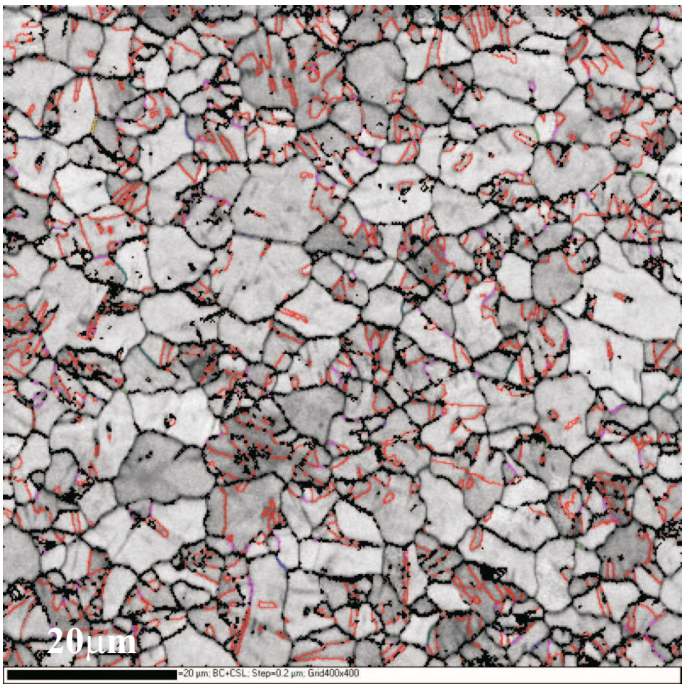

(a)

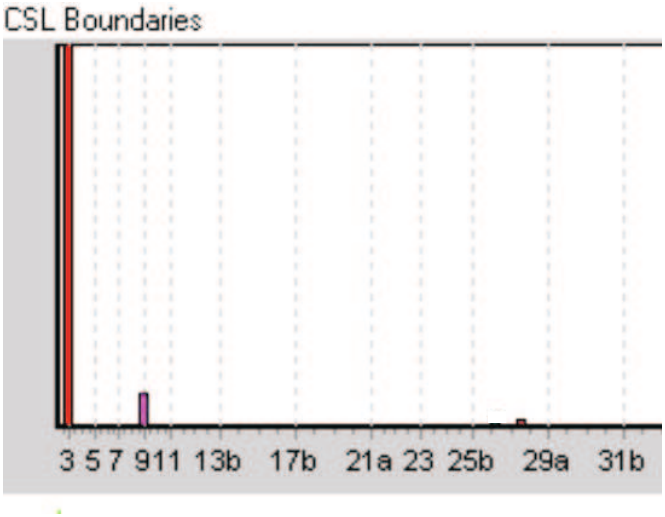

(b)

Figure 5. 22: EBSD analysis of a poly-Si film formed on ZnO:Al coated glass at 425 °C: (a) map of the twins (red = Σ3, violet = Σ9, green = Σ27), and (b) distribution of coincident site lattice boundaries.

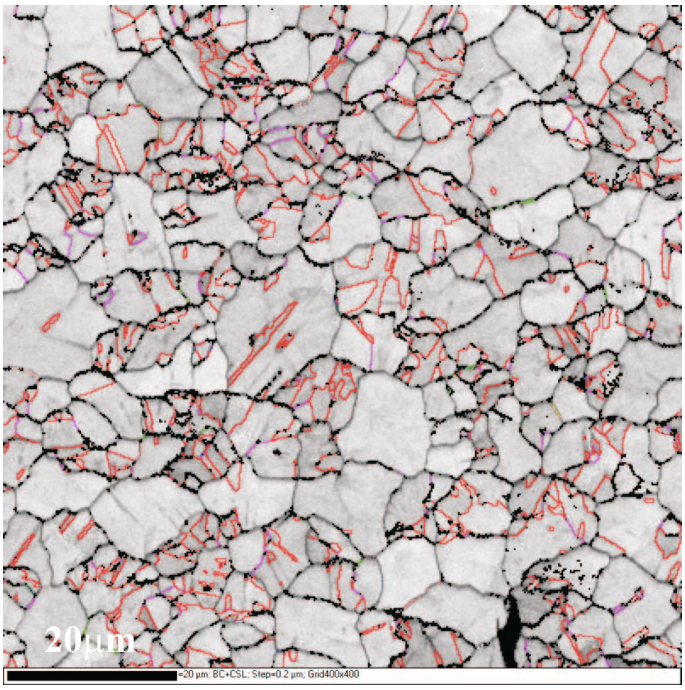

(a)

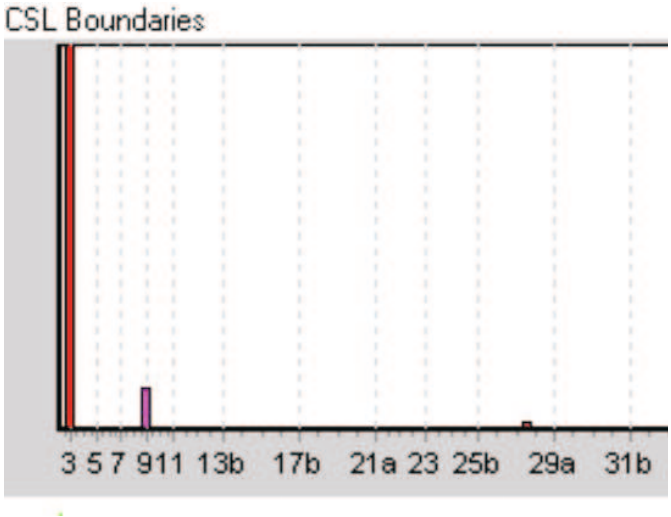

(b)

Figure 5. 23: EBSD analysis for poly-Si film formed on bare glass at 425 °C: (a) map of the twins (red = Σ3, violet = Σ9, green = Σ27), and (b) distribution of coincident site lattice boundaries.

part of the image are in a direction not parallel to the image plane. Many of stacking faults are present in the seed layer as can be seen in Fig 5.26.

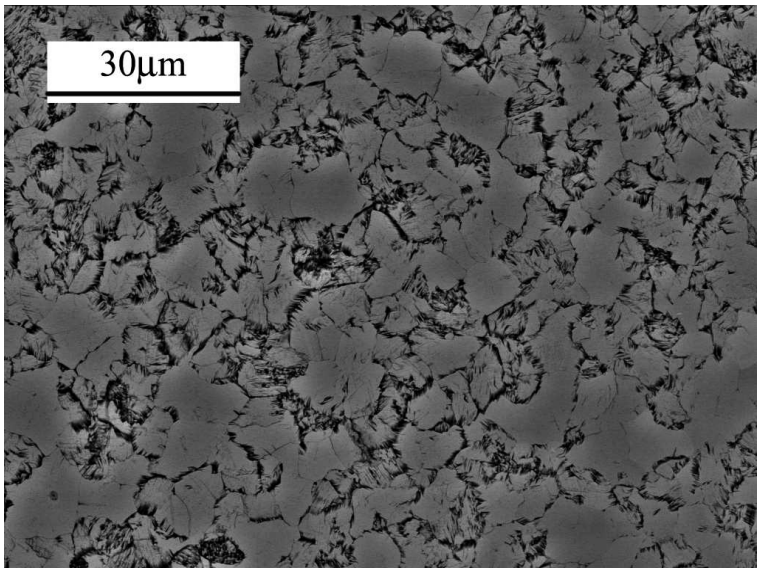

(a)

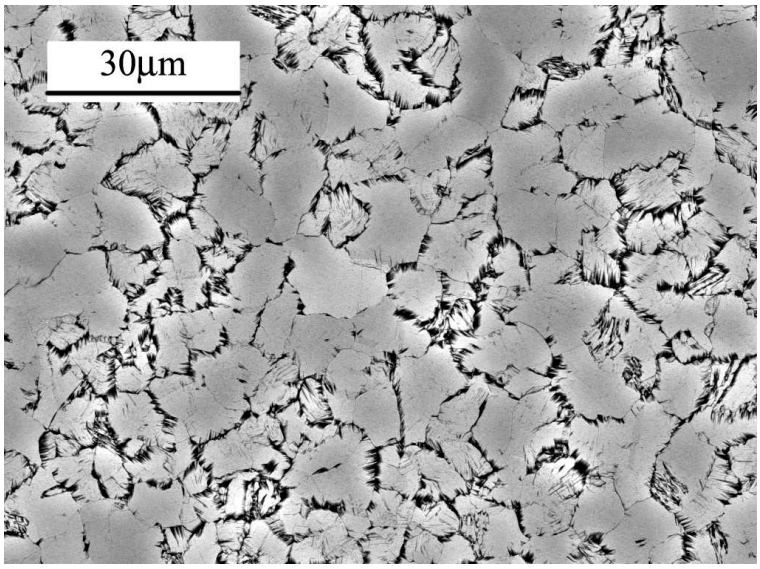

(b)

Figure 5. 24: SEM images of Secco-etched thickened poly-Si films (~ 2µm) (a) on glass and (b) on ZnO:Al coated glass.

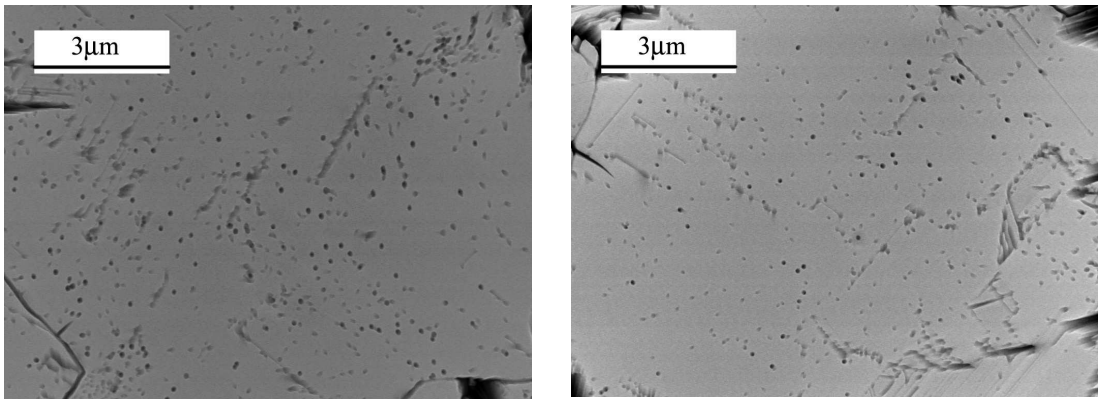

(a) (b)

Figure 5. 25: SEM images of Secco-etched epitaxial poly-Si films (a) on glass and (b) on ZnO:Al coated glass.

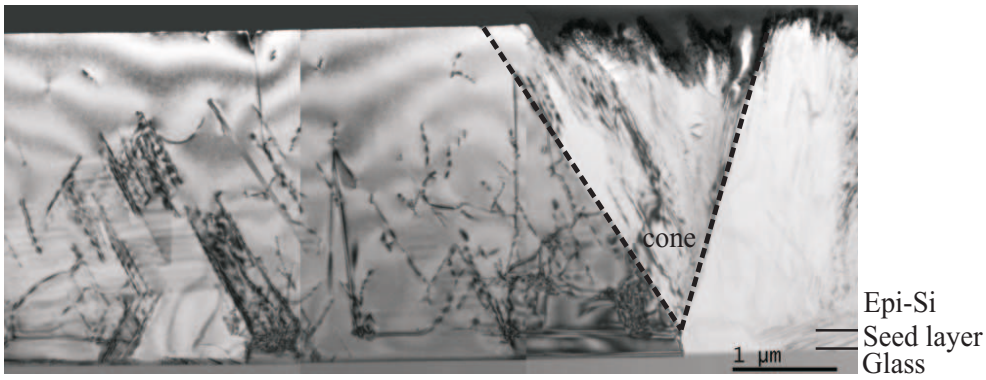

Figure 5. 26: Cross section TEM image of a glass/poly-Si/epi-Si sample. The glass substrate is located at the bottom [Ges08b].

5.2.5 CONCENTRATION OF IMPURITIES

Fig 5.27 shows the secondary ion mass spectroscopy (SIMS) depth profile for Aluminum and Boron in the poly-Si seed layer grown on ZnO:Al coated glass and on glass at 425 °C annealing temperature, respectively. The calibration is only valid for the poly-Si film. The concentration of Boron in the glass/ZnO:Al/poly-Si stack is one order of magnitude lower than that in poly-Si on glass. This means that ZnO:Al films act as a

diffusion barrier for Boron coming from the glass substrate. The concentration of Al in the poly-Si film grown on ZnO:Al is similar to the Al concentration of poly-Si film grown on glass.

Nast et al. [Nas01] showed by Hall Effect measurement that roughly 10% of the Al content in poly-Si film on glass is electrically active at room temperature. As can be seen in Fig. 5.27, the SIMS results revealed that the average Al concentration in the poly-Si film formed on glass at 425 °C is about 9×10^{19} cm^{-3}. This means that the Al concentration in poly-Si on glass is 3 times higher than 3×10^{19} cm^{-3} published by Nast et al. [Nas01]. However, the carrier concentration of 3×10^{17} cm^{-3} in poly-Si film on bare glass was measured at room temperature by the Hall measurements in our case. This carrier concentration is one order lower than the carrier concentration measured by Nast et al.. In case of glass/ZnO:Al/poly-Si stacks, the concentration of electrically active Al in poly-Si films could not be deduced by Hall measurements. The resistivity of as-deposited ZnO:Al layers and poly-Si films is 2.3×10^{-4} and 2×10^{-1} Ωcm, respectively. Therefore the carrier concentration and the Hall mobility of the ZnO:Al layer itself can be measured. But the concentration of electrically active Al in poly-Si film on ZnO:Al coated glass can be inferred from the result of poly-Si on glass. From SIMS data in Fig. 5.27 the average Al concentration in poly-Si film formed on ZnO:Al coated glass at 425 °C is about 3×10^{20} cm^{-3}. The 1% of the Al content in poly-Si film on ZnO:Al coated glass would be assumed, the concentration of electrically active Al would be 3×10^{18} cm^{-3}.

During heat treatment steps (epitaxial growth, RTA, and H-passivation) boron atoms can diffuse from the glass substrate to the thickened poly-Si films. The SIMS profile of the boron concentration in the glass/SiN_X/ZnO:Al/p+poly-Si seed layer/p-epi-Si stack and the glass/p+poly-Si seed layer/p-epi-Si stack after RTA and H-passivation is shown in Fig 5.28. The main boron source in thickened poly-Si seed layers is the glass substrates. The boron concentration in the ALILE poly-Si film on glass is higher than the boron concentration in the ALILE poly-Si film on SiN_X/ZnO:Al coated glass. The SiN_X/ZnO:Al stack seems to act as a barrier layer for a diffusion of boron from the glass substrates. Although the poly-Si seed layer has a high boron concentration, the B

concentration in the epi-Si film is not influenced. It seems that the poly-Si seed layer act as a barrier for a diffusion of boron. As can be seen in SIMS profile of Fig 5.28 the boron concentrations in the epi-Si layer have similar values. This shows that boron impurities could not diffuse from the glass substrate to the epi-Si layer during RTA and H-passivation treatments.

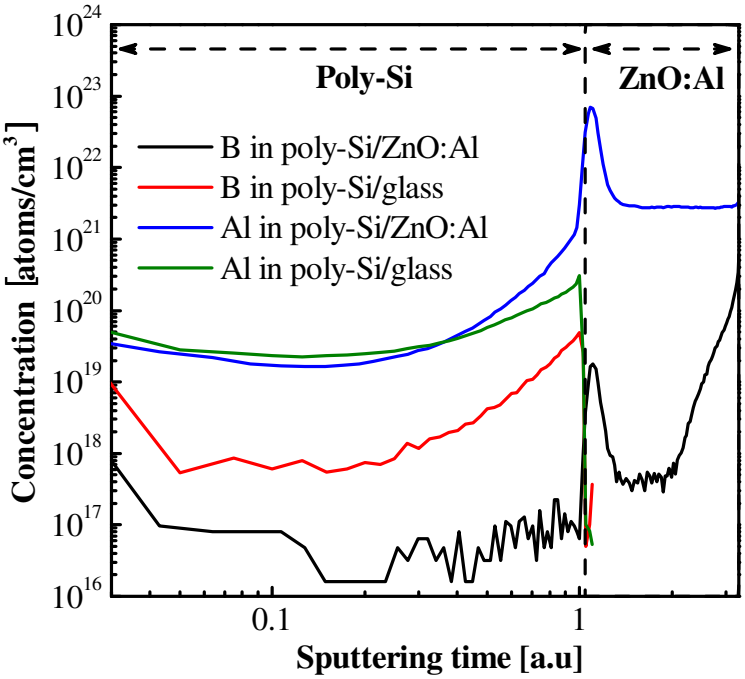

Figure 5. 27: SIMS depth profile of the Al and the B concentration in the poly-Si seed layer grown on ZnO:Al coated glass and bare glass (annealed at 425 °C for 16 hours).

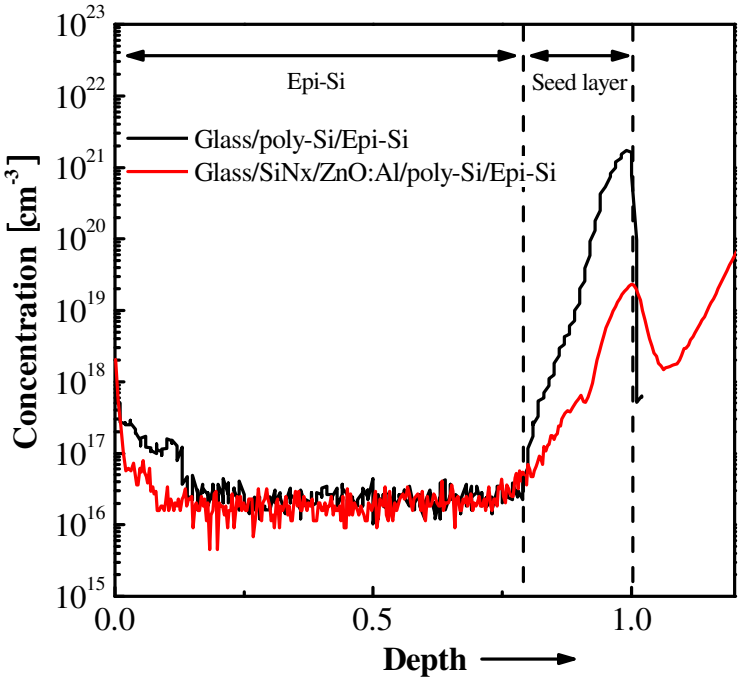

Figure 5. 28: SIMS profile of boron concentration in the thickened poly-Si seed layer on glass and on SiN_x/ZnO:Al coated glass after RTA and H-passivation treatment.

5.3 CONCLUSION

Studying the kinetics of the crystallization revealed that the activation energy for the nucleation on ZnO:Al coated glass and on bare glass has similar values. Also the activation energies for the grain growth on ZnO:Al coated glass and on bare glass have similar values (1.8~1.9 eV). But the crystallization time on ZnO:Al coated glass is shorter than the crystallization time on bare glass due to differnet value of the pre-factor (see Fig 5.5) for the grain growth.

Continuous poly-Si films were formed on ZnO:Al coated glass by the ALILE process and it was measured by Raman spectroscopy and UV-VIS spectroscopy method that the crystalline quality of poly-Si films on ZnO:Al coated glass is similar to the crystalline quality of poly-Si films on bare glass. The FWHM values of 4.1 cm^{-1} and 3.8 cm^{-1} have been calculated for the poly-Si films formed on ZnO:Al coated glass and on bare glass

at 425 °C as a ALILE process temperature, respectively. The crystalline quality calculated from UV-VIS results (reflectance) is in the range of 98.5 ~ 99.4% (on both ZnO:Al coated glass and bare glass).

The average grain size and maximum grain size of poly-Si films on ZnO:Al coated glass is smaller than the average grain size and maximum grain size of poly-Si films on bare glass. Although the preferential (100) orientation of poly-Si films on both ZnO:Al coated glass and bare glass is about 60%, in case of poly-Si film on ZnO:Al coated glass most of grains are located in a range of 0 ~ 10° (in a range of 10 ~ 20° in case of poly-Si films on bare glass). No significant change of a preferential (100) orientation with increasing annealing temperature was observed.

The surface of the thickened poly-Si films on ZnO:Al coated glass and on bare glass observed with Secco etching shows only circular etch pits which are characteristic for Si (100) dislocations in grains and it was observed that the ZnO:Al layer has no significant influence.

CHAPTER 6
POLY-Si THIN-FILM SOLAR CELLS

Polycrystalline silicon (poly-Si) thin-film solar cells on low-cost substrates can significantly reduce manufacturing cost due to their potential for high efficiencies. In practical efficiencies almost as high as far wafer based silicon solar cells should be provided, however, the realisation of these efficiencies exceeding 15% remains challenging. The application of ZnO:Al coated glass substrates would enable an integrated series connection of solar cells simultaneously processed on large substrates, and could provide an effective incoupling light and an efficient light trapping when surface textured ZnO:Al films are applied [Rec06, Ber08].

The previous chapters described the electrical, optical, and structural properties of poly-Si films on ZnO:Al coated glass. It has been shown that ZnO:Al films prepared by sputtering and over coated by a thin Si film exhibit excellent electrical and optical properties. Moreover, high structural quality of poly-Si films could be demonstrated. The ZnO:Al coated glass is a promising alternative route for the preparation of low cost thin film solar cells on nonconductive substrates. This chapter describes on the realization of poly-Si thin film solar cells on ZnO:Al coated glass by using the aluminum-induced layer exchange (ALILE) process described in the previous chapter.

6.1 PREPARATION AND STRUCTURE

The solar cell concept investigated here is based on the preparation of a thin, active silicon base layer on a low-cost substrate covered with a conductive layer. Typical features of a thin-film solar cell on a substrate covered with a conductive layer are the following:

(i) The implementation of diffusion barriers for impurities from the glass and/or highly conductive layers between substrate and silicon film for simplifying the structure of solar cells, and

(ii) The application of ALILE process to enlarge the grain size of polycrystalline silicon layers.

The preparation of ALILE poly-Si seed layers has been described in detail in section 3.1. For the solar cells on ZnO:Al coated glass, the thin poly-Si seed layers produced by the ALILE process at 450 ^{o}C on ZnO:Al coated glass have been epitaxially thickened to form the absorber layer of the solar cell. The epitaxial absorbers are ~ 2 µm thick grown at 600 °C by e-beam evaporation and the doping concentration of boron is about 4×10^{16} cm^{-3}. To prevent crystallization of the a-Si:H emitter, defect passivation is realized at 600 °C by exposing the samples to a hydrogen plasma prior to the deposition of n^{+}-type a-Si:H hetero-emitter with TCO (Al doped ZnO) on top. For the defect passivation of the poly-Si seed layer/absorber layer stacks the hydrogen plasma was applied for 10 minutes at a substrate temperature of 600 °C. It features a hollow-cathode RF high density plasma source (13.56 MHz) that was used in a simple diode configuration [Gor07c]. A defect annealing process typically performed at 900-1000 °C [Rau08] was not applied. A hetero-junction emitter layer of about 10 nm n^{+}-type a-Si:H has been deposited by using plasma enhanced chemical vapor deposition (PECVD) using conditions optimized for wafer based Si solar cells [Kor07]. Interdigitated contacting using Al is done by photolithography. The sample area is 4×4 mm^2 with an emitter area of 8.6 mm^2. The schematics of the solar cell on ZnO:Al coated glass is shown in Fig 6.1.

The solar cells on ZnO:Al coated glass were designed in the so-called “substrate-type” (the light enters the cell through the air side) configuration. The structure of solar cells is glass/ZnO:Al/p^{+} seed layer/p^{-} epi-Si/n^{+} a-Si/ZnO/Al. The total thickness of the solar cells is ~ 2.3 µm. During the current-voltage measurements, a white reflector (several sheets of white papers) was used on the backside while the light was irradiated on the layer side. The efficiency and short-current density was calculated using the emitter area.

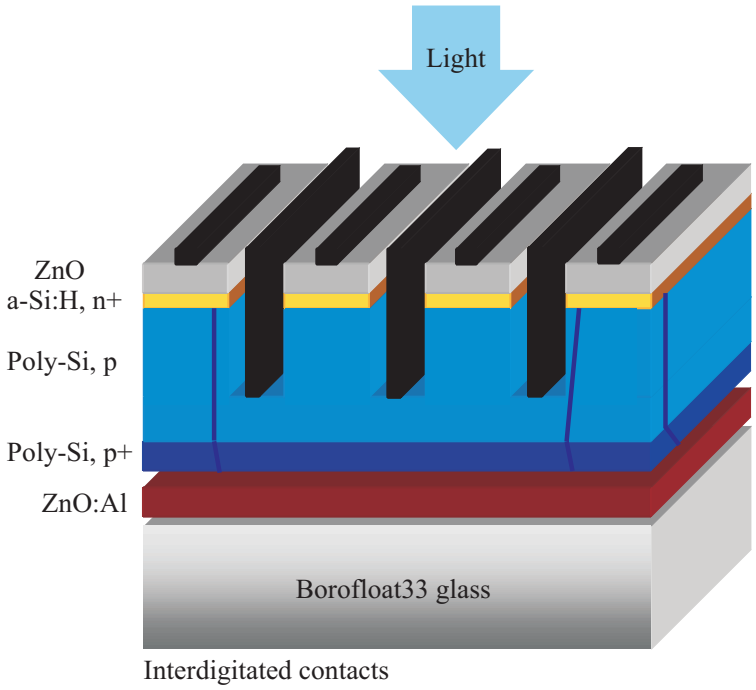

Figure 6. 1: Schematics of the solar cell on ZnO:Al coated glass: "substrate-type" (the light enters the cell through the air side) configuration and interdigitated contacts.

6.2 SOLAR CELL RESULTS

In this section solar cell the results achieved on ZnO:Al coated glass obtained in this study are described (section 6.2.1) and compared to previous solar cell results on bare glass which are reviewed and discussed (section 6.2.2).

6.2.1 SOLAR CELL ON ZnO:Al COATED GLASS

The current-voltage (I-V) curve of the first solar cell on ZnO:Al coated glass is plotted in Fig 6.2 (for standard test conditions: AM1.5, 100 mW/cm^2, 25 °C). The thin poly-Si seed layer was produced on ZnO:Al coated glass at 450 ^{o}C for 16 hours by ALILE process. The solar cell on ZnO:Al coated glass showed an open-circuit voltage (V_{OC}) of

389 mV, a short-current density (J_{SC}) of 9.1 mA/cm^2 and an efficiency of 2%. The emitter area (8.6 mm^2) of the solar cell was considered for calculating the efficiency of the solar cell. The series resistance of the solar cell on ZnO:Al coated glass is 7 Ωcm^2.

As a first test of the feasibility of poly-Si rear junction cells based on ALILE process, the illuminated I-V parameters of an existing poly-Si cell on ZnO:Al coated glass were measured in both substrate and superstrate configuration (see Table 6.1). We note that the structure of this cell was designed for the substrate configuration (see Fig. 6.1). The absorber layer was grown by e-beam evaporation method and its thickness was around 2 µm. Due to the fact that the as-processed devices are essentially bifacial, white paper was used as reflector in both configurations. In superstrate configuration, the short-current density of the cell is slightly lower than in substrate configuration. Gordon et al. [Gor07a] asserted that J_{SC} is decreased due to the absence of an anti-reflective coating (ARC) in superstrate configuration. In the case of solar cells illiuminated throughthe glass, the thickness of the ZnO:Al layer is about 700 nm and does not act as an ARC layer. The difference in V_{OC} between both configurations corresponds to what is expected from the decrease in short-circuit current density [= n × (kT/q) × ln(9.1/7.7)] taken from the simple diode equation for solar cell as a rough estimate. Here, n is the ideality factor, k is the Boltzmann's constant, T is the temperature, and q is the Planck's constant.

The distribution of the efficiency and the open-circuit voltage of solar cells on a single ZnO:Al coated glass substrate is shown in Fig 6.3. The entire size of the ZnO:Al coated glass substrate is 2.54 by 1.25 cm^2. Most of the measured open-circuit voltages are quite similar. This means that most of the areas feature a similar material quality. The open-circuit voltage of solar cells on ZnO:Al coated glass with poly-Si seed layers formed at 425 and 450 °C is compared in Table 6.2. The V_{OC} of solar cells with poly-Si seed layer formed at 425 °C is lower than that of solar cells with poly-Si seed layer formed at 450 °C. This reason could be that a poly-Si film formed on ZnO:Al coated glass at 425 °C has a lot of very small grains (less than 1 µm) which were not observed at higher temperature (as shown in Fig 5.16 (b)). Although large grains cover on most of the

surface it is expected that the performance of the resulting poly-Si layers will be mainly limited by the low-quality (small grains) regions.

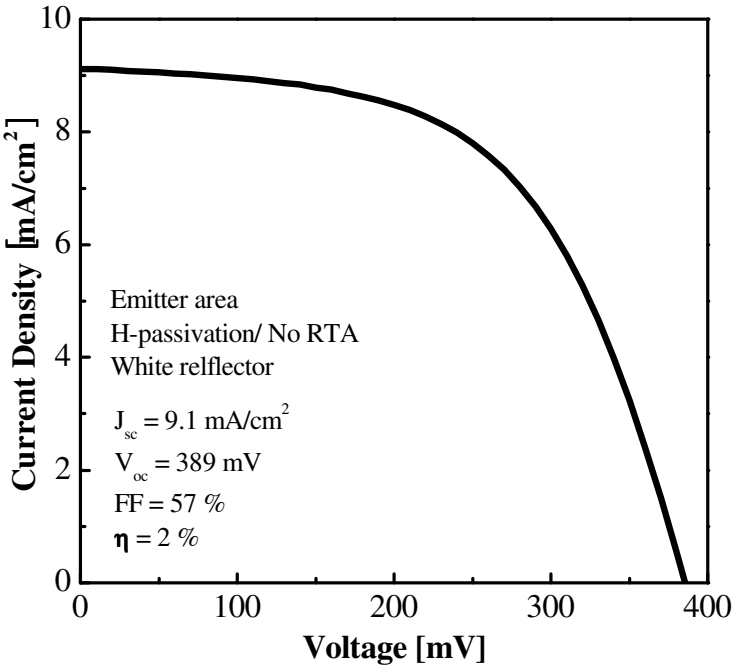

Figure 6. 2: Current density versus voltage (I-V) of the solar cell structure of glass/ ZnO:Al/p+ seed layer/p- epi-Si/n+ a-Si/ZnO/Al stacks.

TABLE 6. 1: Comparison of substrate and superstrate structure of solar cell on ZnO:Al coated glass.

Structure	J_{SC} (mA/cm^2)	V_{OC} (mV)	FF (%)	η (%)
Substrate	9.1	389	57	2.0
Superstrate	7.7	376	57.4	1.5

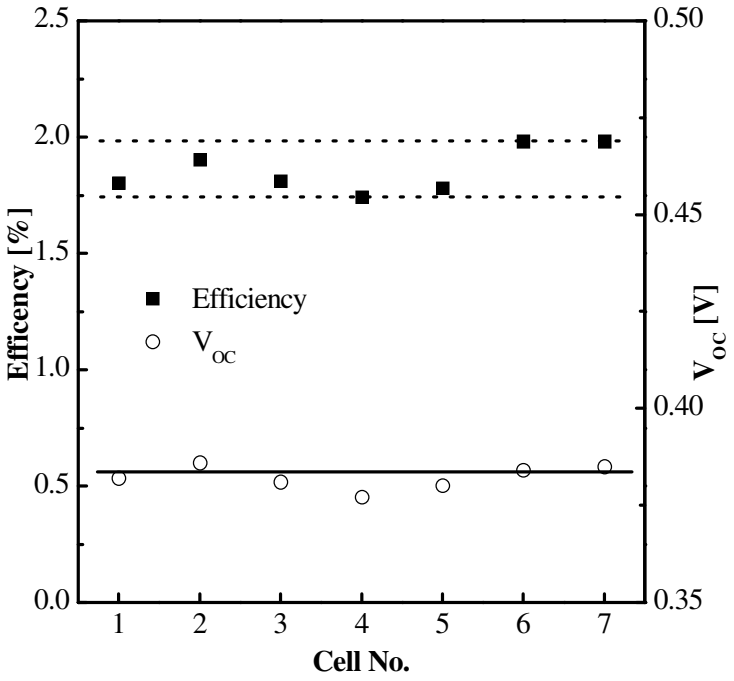

Figure 6. 3: Distribution of efficiency and open-circuit voltage of solar cells on ZnO:Al coated glass on a single substrate.

TABLE 6. 2: Comparison of open-circuit voltage (V_{OC}) of solar cells on ZnO:Al coated glass for poly-Si seed layers formed at 425 and 450 °C.

T_A (°C)	V_{OC} (mV)
425	316
450	372

6.2.2 SOLAR CELL ON GLASS

In the section 6.2.2 the solar cell results on Borofloat33 glass reported recently are reviewed and compared with the solar cell result on ZnO:Al coated glass. These solar cells on bare glass were also based on the seed layer formed at 450 °C for 16 hours by the ALILE process.

The current-voltage characteristic of the poly-Si thin-film solar cell on bare glass obtained by Dogan et al. [Dog08] is shown in Fig 6.4 (for standard test conditions: AM1.5, 100 mW/cm^2, 25 °C). The solar cell on bare glass was measured with white reflector. For the measurements a white paper was placed below the glass substrate. The solar cell has interdigitated contacts and an area of 16 mm^2. The short-current density was calculated using the emitter area of the solar cell: 8.6 mm^2. Together with an open-circuit voltage V_{OC} of 406 mV, a short circuit current density J_{SC} of 10.3 mA/cm^2 and a fill factor FF of 67.4% this had led to an emitter area efficiency of 2.8%. For comparison the current-voltage characteristics of the thin-film solar cell prepared so far on an 'ideal seed layer' (a p^+-type mono-crystalline Si(100) wafer) was measured (see ref. [Dog08]). The wafer-based thin-film solar cell showed an emitter area short circuit current density J_{SC} of 15.9 mA/cm^2. The emitter area efficiency of this wafer-based thin-film solar cell was 7.3% (V_{OC} = 583 mV, FF = 78.7%).

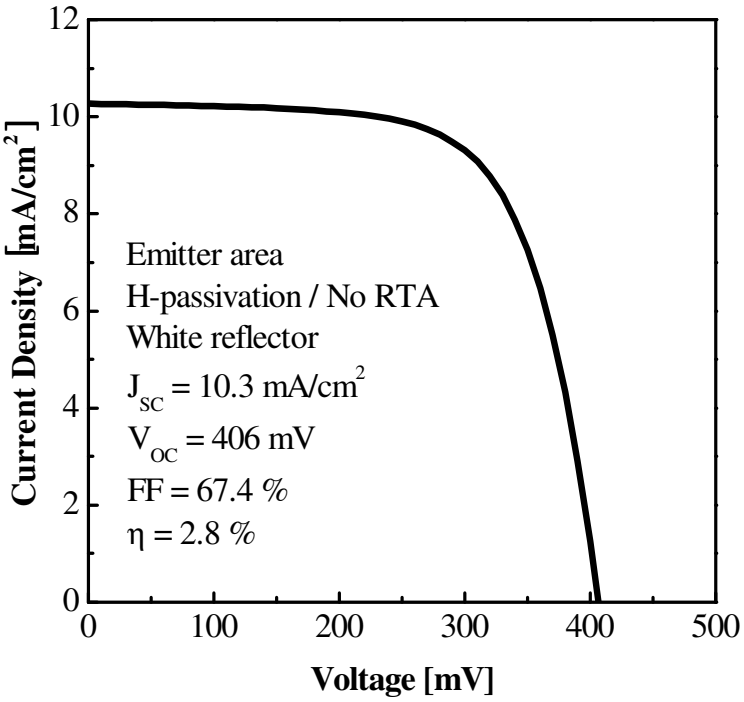

Figure 6. 4: Emitter area current density versus voltage for the thin-film solar cell on bare glass. The 2 µm thickness of absorber layer was grown at 600 °C. The solar cell was measured with a white reflector.

Current-voltage curves of the solar cell on bare glass before (black line) and after H-passivation (red line) are shown in Fig 6.5. The influence of H-passivation on solar cells was investigated by Gorka et al. [Gor08]. Current-voltage measurements of the solar cell test structures were carried out under standard test conditions (AM1.5 illumination, 100 mW/cm^2, 25 °C). The emitter area was taken for the calculations and an underlying black reflector was used during the measurements to discard any reflections. After H-passivation the V_{OC} increased strongly for the solar cell on glass from 223 mV (as-grown) to 351 mV. It seems that mostly the V_{OC} is affected by the passivation. The short circuit current J_{SC} and the fill factor (FF) were improved by a factor of 1.2 so that the overall efficiency is more than doubled after H-passivation. In this study the solar cell was passivated by Hydrogen plasma at 520°C for 10 min. Fig 6.6 shows the dependence of the average open-circuit voltage (red circles) and the short circuit current density (black squares) on the substrate temperature during H-passivation. The V_{OC} increased notably with the temperature. The highest average value of 385 mV was achieved for hydrogenation at 620 °C. The short circuit current densities were not influenced significantly by different temperatures.

The influence of the rapid thermal annealing process (RTA) on solar cells was investigated by B. Rau [Rau08]. In this study a condition of the RTA process was 900 °C for 200 seconds. Improved solar cell performances were achieved by applying the RTA process. And the external quantum efficiency (EQE) of solar cells applied only H-passivation and both RTA and H-passivation was discussed. In the shorter wavelength region, i.e. close to the pn-junction, both spectra are almost identical. The additional RTA treatment increased the EQE for wavelengths above 450 nm indicating the improved material quality. The EQE maximum shifts slightly to longer wavelengths. The improved material quality can also be seen on the solar cell parameters: V_{OC} = 405 mV, J_{SC} = 8.3 mA/cm², Fill factor (FF) = 63% and efficiency (η) = 2.1% for the sample with both treatments and V_{OC} = 360 mV, J_{SC} = 7.4 mA/cm², FF = 56% and η= 1.5% for the sample with hydrogenation only.

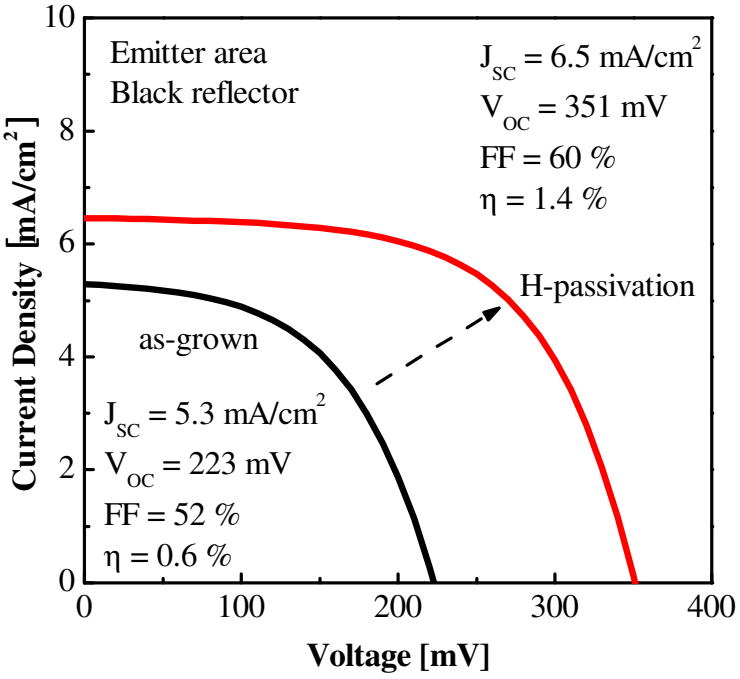

Figure 6. 5: Current density versus voltage characteristics of solar cells on glass before (black line) and after H-passivation (red line).

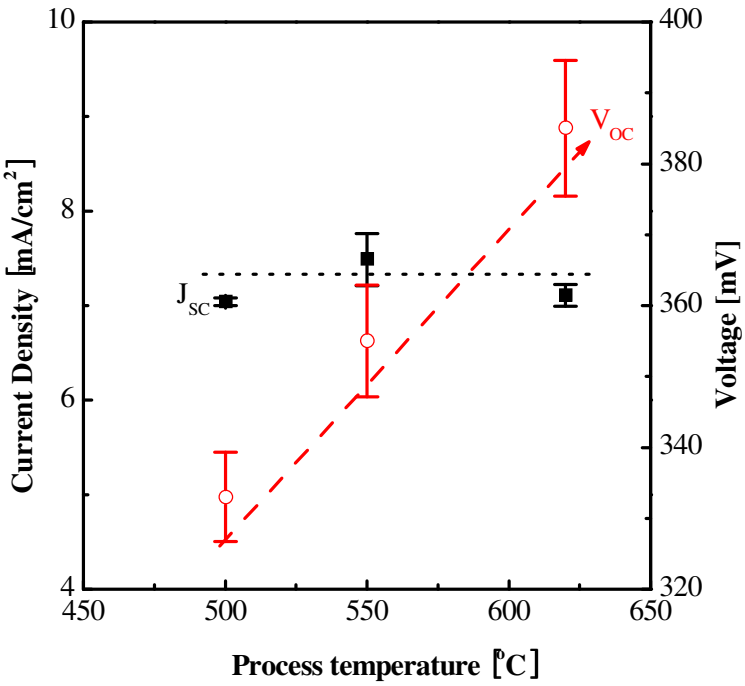

Figure 6. 6: Dependence of the average open-circuit voltage (red circles) and the short circuit current density (black squares) on the substrate temperature during H-passivation.

The solar cell performances on bare glass reviewed above are summerized in Table 6.3. The best efficieny of the solar cell on bare glass is 2.8% realized by by P. Dogan [Dog08]. Although this efficency is a higher than an efficiency of 2% of the solar cell on ZnO:Al coated glass achieved in this study, it can not be compared directly. The deposition parameters of the absorber layer were changed during the fabrication of the best solar cell on bare glass. Nevertheless, the solar cell on ZnO:Al coated glass shows a possibility to be improved.

The solar cell on ZnO:Al coated glass shows a better performance compared to the solar cell results on bare glass measured by B. Gorka [Gor08] and B. Rau [Rau08]. These results measured by B. Gorka and B. Rau show the lower values compared to the results achieved in this study. A short circuit current density (J_{SC}) of the solar cell on ZnO:Al coated glass measured with black reflector and with white reflector in this study is 7.8 and 9.1 mA/cm², respectively. A J_{SC} of the solar cell on bare glass with black reflector and with white reflector was 6.5 from [Gor08] and 7.4 mA/cm² from [Rau08], respectively. An open-circuit voltage (V_{OC}) of the solar cell on ZnO:Al coated glass is a slightly higher than a V_{OC} of the solar cells on bare glass. But a Fill Factor (FF) of the solar cells on bare glass and on ZnO:Al coated glass are similar. An improved J_{SC} and V_{OC} on the solar cell on ZnO:Al coated glass were achieved.

TABLE 6. 3: Recent results in our laboratory.

Ref.	η [%]	J_{SC} [mA/cm^2]	V_{OC} [mV]	FF [%]
[Dog08]	2.8	10.3	406	67.4
[Gor08]	1.4	6.5	351	60
[Rau08]	1.5	7.4	360	56
This study	2	9.1	389	57

6.3 CONCLUSION AND OUTLOOK

The best poly-Si solar cell on ZnO:Al coated glass has achieved an open-circuit voltage (V_{OC}) of 389 mV, a current density (J_{SC}) of 9.1 mA/cm^2 and an efficiency of 2%. V_{OC} and J_{SC} results on ZnO:Al coated glass are only slightly lower than results recently published for the solar cell on bare glass [Dog08]. One of the reasons for the difference in the efficiency should be the series resistance of the solar cell.

These world-wide first large-grained poly-Si solar cells realized on ZnO:Al coated glass may serve as a first proof of concept. However, there are still many open questions which have to be addressed and solved on the path to a potentially highly efficient solar cell.

1) High temperature treatments for defect annealing have to be developed which are applicable to the glass/ZnO:Al/Si device structure
2) Adapted barrier coatings have to be developed to avoid cross contamnations
3) Chemical processes which are compatible with the ZnO:Al coated glass substrate have to be developed.

CHAPTER 7
CONCLUSIONS

In this study the formation of large-grained poly-Si films on transparent conductive oxide (TCO) coated glass is addressed in order to open up new possibilities for the fabrication of photovoltaic devices. Being ahead of the objective the realization of temperature stable Al doped ZnO and the successful formation of poly-Si layers on the ZnO:Al layer should be preceded for the above purpose. The investigated key aspects have been (i) the temperature stability of the ZnO:Al films which are capped with a poly-Si layer, (ii) the study of poly-Si thin films formed on ZnO:Al coated glass and ,for comparison, on bare glass by the aluminium-induced layer exchange (ALILE) process, and (iii) the fabrication of first poly-Si thin film solar cells on ZnO:Al coated glass.

The resistivity of ZnO:Al layers covered with poly-Si films formed by ALILE or SPC is improved even though the resistivity of uncapped ZnO:Al layer is decreased by heat treatment in nitrogen ambient. The resulting sheet resistance of the glass/ZnO:Al/poly-Si samples formed by ALILE and by SPC is almost independent of the annealing temperature.

On both ZnO:Al coated glass substrates and bare glass substrates the activation energy for the nucleation and the grain growth during the ALILE process is 1.1~1.4 eV and 1.7~1.9 eV, respectively. Nevertheless, the ALILE process time on ZnO:Al coated glass is shorter than the ALILE process time on bare glass.

Poly-Si films formed on ZnO:Al coated glass and on bare glass have the same crystalline quality as determined from the FWHM values deduced from the Raman results, thereof it could be concluded that ZnO:Al films did not determine the change of the crystal quality of poly-Si films. The quality factors calculated from the optical reflectance spectra of poly-Si films on ZnO:Al coated glass and on bare glass show the same values (~ 99%) and are not affected by the annealing temperature. Hence we

conclude that ZnO:Al layer and the ALILE process temperature cut down the crystallization time without a falling-off in the crystalline quality of poly-Si films .

The preferential (100) orientation of poly-Si films on both ZnO:Al coated glass and bare glass is about 60% and no significant change of the preferential (100) orientation with increasing annealing temperature was observed using EBSD. Also the total fractions of the (400) and (511) orientations, tilted within 20° of the perfect (400) orientation, calculated from XRD resuls and measured on larger areas have similar values as the values extracted by EBSD results which give information on a small area.

Even though few holes which are a typical feature of the ALILE process are revealed at grain boundaries by SEM investigations, it can be stated that the poly-Si film formed on ZnO:Al coated glass by ALILE process is continuous in general.

The electrical properties of ZnO:Al/poly-Si stacks and the Si-Si TO-LO phonon band position of poly-Si film on ZnO:Al coated glass are not significantly influenced by H-passivation while the electrical properties (mobility and resistivity) of ZnO:Al/poly-Si stacks are improved and the Si-Si TO-LO phonon band position of poly-Si film on ZnO:Al coated glass is shifted by RTA treatment.

The solar cell on ZnO:Al coated glass has achieved a open-circuit voltage (V_{OC}) of 389 mV, a short-current density (J_{SC}) of 9.1 mA/cm^2 and an efficiency of 2%.

In this thesis large-grained poly-Si films and solar cells on ZnO:Al coated glass were realized for the first time and it was shown that the utilization of the ZnO:Al is a promising option for the preparation of high efficiency poly-Si thin-film soalr cells.

ABBREVIATIONS, SYMBOLS AND UNITS

ABBREVIATION	MEANING
AIC	Aluminium-induced crystallization
ALILE	Aluminum-induced layer exchange process
APCVD	Atmospheric pressure chemical vapor deposition
a-Si:H	Hydrogenated amorphous silicon
CIS	Copper-indium-selenide (sulfite)
CIGS	Copper indium gallium selenide
CdTe	Cadmium telluride
CMP	Chemical mechanical polishing
CSG	Crystalline silicon on glass
EBSD	Electron back scatter diffraction
ECRCVD	Electron cyclotron resonance chemical vapor deposition
EPIA	European photovoltaic industry association
FOx	Flowable oxide
HR-TEM	High resolution transmission electron microscope
IAD	Ion assisted deposition
LC	Laser crystallization
MW	Megawatts
nc-Si	Nano-crystalline silicon
PECVD	Plasma enhanced chemical vapor deposition
Poly-Si	Large-grained polycrystalline silicon
PV	Photovoltaic
PVD	Physical vapor deposition
RTA	Rapid thermal annealing
SAC	Selected area channeling
SPE	Solid phase epitaxy
SPC	Solid phase crystallization
TEM	Transmission electron microscope
TCO	Transparent conductive oxide
μc-Si:H	Hydrogenated microcrystalline silicon
W_p	Watt peak
ZnO:Al	Al doped ZnO

SYMBOL	UNIT	MEANING
A	μm^2	Area of optical microscope image
d_G	µm	Grain size
E_A	eV	Activation energy
FF	%	Fill Factor
I_{SC}	mA/cm^2	Short circuit current
k	eV/K	Boltzmann constant (8.6215×10^{-5} eV/K)
n		ideality factor ($1 < n < 2$)
N_G	mm^{-2}	Nucleation density
Q	%	Quality factor
q	C	Absolute value of electron charge
R_{e1}	%	Reflectance at e1 peak
R_{e2}	%	Reflectance at e2 peak
T_A	°C	Annealing temperature
T_{ALILE}	°C	Process temperature of ALILE
T_{RTA}	°C	Process temperature of RTA
t	min	Time
t_N	min	Nucleation time
V_{OC}	mV	Open-circuit voltage
η	%	Efficiency of solar cell

REFERENCES

[CHAPTER 1]

[And06] G. Andra, J. Bergmann, A. Bochmann, F. Falk, A. Gawlik, E. Ose, J. Plentz, S. Dauwe, and T. Kieliba, Conference Record of the 2006 IEEE 4th World Conference on Photovoltaic Energy Conversion. Waikoloa, HI, USA, (2006) 4

[Deb00] Satyen K. Deb, NREL/CP-590-28060 (2000)

[Dim07] D. Dimova-Malinovska, O. Angelov, M. Kamenova, A. Vaseashta, and J. C. Pivin, J. Optoelectron Adv Mater. 9 (2007) 355

[Ear07] http://www.earthpolicy.org/Indicators/Solar/2007.htm (Dec. 27, 2007)

[EPIA] www.epia.org/

[EPI08] EPIA, Solar Generation V 2008

[Fuh04] W. Fuhs, S. Gall, B. Rau, M. Schmidt, and J. Schneider, Solar Energy 77 (2004) 961

[Ges06] D. Van Gestel, I. Gordon, L. Carnel, K. Van Nieuwenhuysen, J. D´Haen, J. Irigoyen, G. Beaucarne, and J. Poortmans, Thin Solid Films 511/512 (2006) 35

[Gre04] M.A. Green, P.A. Basore, N. Chang, D. Clugston, R. Egan, R. Evans, D. Hogg, S. Jarnason, M. Keevers, P. Lasswell, J. O'Sullivan, U. Schubert, A. Turner, S.R. Wenham, and T. Young, Solar Energy 77 (2004) 857

[Im93] J. S. Im, H. J. Kim, and M. O. Thompson, Appl. Phys. Lett. 63 (1993) 1969

[Kee07] M.J. Keevers, T.L. Young, U. Schubert, and M.A. Green, Proc. of the 22nd European Photovoltaic Solar Energy Conference, Milan, Italy (2007) 1783

[Kim02] H. Kim, D. Kim, G. Lee, D. Kim, and S.H. Lee, Sol. Energy Mater. Sol. Cells 74 (2002) 323

[Klu03] O. Kluth, G. Schöpe, J. Hüpkes, C. Agashe, J. Mueller, and B. Rech, Thin Solid Films 442 (2003) 80

[Mat01] Y.Matsumoto and Z. Yu, Jpn. J. Appl. Phys. 40 (2001) 2110

[Mat90] T. Matsuyama, K. Wakisaka, M. Kameda, M. Tanaka, T. Matsuoka, S. Tsuda, S. Nakano, Y. Kishi, and Y. Kuwano, Jpn. J. Appl. Phys. 29 (1990) 2327

[Mul04] J. Muller, B. Rech, J. Springer, and M. Vanecek, Solar Energy 77 (2004) 917

[Nas00] O. Nast and A. J. Hartmann, J. Appl. Phys. 88 (2000) 124

[Nas98] O. Nast, T. Puzzer, L.M. Koschier, A.B. Sproul, and S.R. Wenham, Appl. Phys. Lett. 73 (1998) 3214

[Rau04] B. Rau, I. Sieber, J. Schneider, M. Muske, M. Stöger-Pollach, P. Schattschneider, S. Gall, and W. Fuhs, J. Cryst. Growth 270 (2004) 396

[Rec06] B. Rech, T. Repmann, M.N. van den Donker, M. Berginski, T. Kilper, J. Hüpkes, S. Calnan, H. Stiebig, and S. Wieder, Thin Solid Films 511/512 (2006) 548

[Sch05] J. Schneider, J. Klein, M. Muske, S. Gall, and W. Fuhs, Appl. Phys. Lett. 87 (2005) 031905

[She08] S. Sheng, Y.K. Chae, L. Li, J. Su, and X. Yang, Semiconductor International (Nov. 1, 2008)

[Sol08] http://www.solarbuzz.com/Marketbuzz2008-intro.htm (March 17, 2008)

[Sta77] D. L. Staebler and C. R. Wronski, Appl. Phys. Lett. 31 (1977) 292

[Tan03] M. Tanaka, S. Okamoto, S. Tsuge, and S. Kiyama, Proc. 3rd world conference (2003)

[Vou03] A.T. Voutsas, Appl. Surf. Sc. 208/209 (2003) 250

[CHAPTER 2]

[Abe05] A.G. Aberle, P.I. Widenborg, D. Song, A. Straub, M.L. Terry, T. Walhs, A. Sproul, P. Campbell, D. Inns, and B. Beilby, In Proc. of the 31st IEEE PV Conference (2005)

[Ada05] S. Adachi, Properties of Group-IV, III-V and II-VI Semiconductors, John Wiley and Sons, Ltd,West Sussex, England, 2005.

[Add99] M.L. Addonizio, A. Antonaia, G. Cantele, C. Privato, Thin Solid Films 349 (1999) 93

[Aga04] C. Agashe, O. Kluth, J. Hüpkes, U. Zastrow, B. Rech and M. Wuttig, J. Appl. Phys. 95 (2004) 1911

[Al05] M. Al-Barghouti, H. Abu-Safe, H. Naseem, W.D. Brown, and M. Al-Jassim, J. Electrochem. Soc. 152 (2005) G354

[Boa76] R.L. Boatright and J.O. McCaldin, J. Appl. Phys. 47 (1976) 2260

[Boh96] E. Böhmer, F. Siebke, B. Rech, C. Beneking and H. Wagner, Mater. Res. Soc. Symp. Proc. 426 (1996) 519

[Bos96] S. Bose, S. Ray, A.K. Barua, J. Appl. Phys. 29 (1996) 1659

[Bre83] M.J. Brett, R.W. McMahon, J.D. Affinito and R. Parsons, J. Vac. Sci. Technol. A 1 (1983) 352

[Bre99] S. Brehme, F. Fenske, W. Fuhs, E.Nebauer, M. Poschenrieder, B. Selle, I. Sieber, Thin Solid Films 342 (1999) 167

[Cai92] W. Cai, and D. Wan, Thin Solid Films 219 (1992) 1

[Ceb98] R. Cebulla, R. Wendt, K. Ellmer, J. Appl. Phys. 83 (1998) 1087

[Cha80] B. Chapman, Glow Discharge Processes. John Wiley & Sons, 1980

[Cho83] K. L. Chopra, S. Major and D. K. Pandya, Thin Solid Films 102 (1983) 1

[Con50] E. Conwell and V.F. Weisskopf, Phys. Rev. 77 (1950) 388

[Dim06] D. Dimova-Malinovska, V. Grigorov, M. Nikolaeva-Dimitrova, O. Angelov, and N. Peev, Thin Solid Films 501 (2006) 358

[Dim07] D. Dimova-Malinovska, O. Angelov, M. Kamenova, A. Vaseashta and J. C. Pivin, J. Optoelectron Adv Mater. 9 (2007) 355

[Dog08] P. Dogan, E. Rudigier, F. Fenske, K.Y. Lee, B. Gorka, B. Rau, E. Conrad, and S. Gall, Thin Solid Films 516 (2008) 6989

[Eka03] G. Ekanayake, S. Summers, and H. S. Reehal, Proc. of the 3rd WCPEC, volume B (2003) 1867

[Eka04] G. Ekanayake, Z. Lu, and H. S. Reehal, Proc. of the EPVSEC 19th (2004)

[Ell01] K. Ellmer, J. Phys. D: Applied Physics 34 (2001) 3097

[Ell94] K. Ellmer, F. Kudella, R. Mientus, R. Schieck and S. Fiechter, Thin Solid Films 247 (1994) 15

[Fay00] S. Fay, S. Dubail, U. Kroll, J. Meier, Y. Ziegler and A. Shah, Proceedings of the 16th European Photovoltaic Solar Energy Conference. Glasgow, UK, 2000

[Gal06] S. Gall, J. Schneider, J. Klein, K. Hübener, M. Muske, B. Rau, E. Conrad, I. Sieber, K. Petter, K. Lips, M. Stöger-Pollach, P. Schattschneider, and W. Fuhs, Thin Solid Films 511/512 (2006) 7

[Ges08a] D.V. Gestel, I. Gordon, A. Verbist, L. Carnel, G. Beaucarne, and J. Poortmans, Thin Solid Films 516 (2008) 6907

[Gju04] M. Gjukic, M. Buschbeck, R. Lechner, and M. Stutzmann, Appl. Phys. Lett. 85 (2004) 2134

[Gju05] M. Gjukic, R. Lechner, M. Buschbeck, and M. Stutzmann, Appl. Phys. Lett. 86 (2005) 3

[Gla00] H. J. Gläser, Large Area Glass Coating. Bd. 1. von Ardenne Anlagentechnik, 2000

[Gor07] I. Gordon, L. Carnel, D. Van Gestel, G. Beaucarne, and J. Poortmans, Progress in Photovoltaics: Research and Applications 15 (20077) 575

[Gre76] J. E. Greene, and L. Mei, Thin Solid Films 37 (1976) 429

[Gri06] V. Grigorov, O. Angelov, M. Sendova-Vassileva, and D. Dimova-Malinovska, Thin Solid Films 511-512 (2006) 381

[Gro01] R. Groenen, J. Loeffler, P.M. Sommeling, J.L. Linden, E.A.G. Hamers, R.E.I. Schroppand M.C.M. van de Sanden, Thin Solid Films 392 (2001) 226

[Har00] N. P. Harder, J. A. Xia, S. Oelting, O. Nast, P. Widenborg, and A. G. Aberle, Conference Record of the Twenty-Eighth IEEE Photovoltaic Specialists Conference (2000)

[Har77] J. M. Harris, R. J. Blattner, I. D. Ward, Jr C. A. Evans, H. L. Fraser, M. A. Nicolet, and C. L. Ramiller, J. App. Phys. 48 (1977) 2897

[Har91] G.L. Harding, B. Window, E.C. Horrigan, Sol. Energ. Mater. 22 (1991) 69

[Hau01] F.J. Haug, Z. Geller, H. Zogg, A.N. Tiwari, C. Vignali, J. Vac. Sci. Technol. A 19 (2001) 171

[Hel82] K.-H. Hellwege, Semiconductors. Bd. 17 b: Landolt-Börnstein Numerical Data and Functional Relationships. Springer-Verlag, 1982

[Hic73] F.S Hickernell, J. Appl. Phys 44 (1973) 1061

[Hsu03] C. M. Hsu, I.F. Chen, and M.C. Yu, Jpn. J. Appl. Phys. 42 (2003) 4928

[Hup06] J. Hüpkes, B. Rech, S. Calnan, O. Kluth, U. Zastrow, H. Siekmann and M. Wuttig, Thin Solid Films 502 (2006) 286

[Iba03] H. Ibach and H. Lüth, Solid State Physics. Bd. 3. Springer-Verlag, 2003

[Iga88] Y. Igasaki, M. Ishikawa, G. Shimaoka, Appl. Surf. Sci. 33/34 (1988) 926

[Iga91] Y. Igasaki, H. Saito, J. Appl. Phys. 29 (1991) 3613

[Ito03] T. Ito, H. Fukushima, and M. Yamaguchi, Jpn. J. Appl. Phys. 42 (2003) 1526

[Ito04] T. Ito, H. Fukushima, and M. Yamaguchi, Sol. Energy Mater. Sol. Cells, 83 (2004) 91

[Iza96] M. Izaki, T. Omi, J. Appl. Phys. 68 (1996) 2439

[Jae08] C. Jaeger, T. Antesberger, and M. Stutzmann, J. Non-Cryst. Solids 354 (2008) 2314

[Jin88] Z.C. Jin, I. Hamberg, C.G. Granqvist, Thin Solid Films 164 (1988) 381

[Kim02] H. Kim, D. Kim, G. Lee, D. Kim, and S. H. Lee, Sol. Energy Mater. Sol. Cells, 74 (2002) 323

[Kim96] J.H. Kim and J.Y. Lee, Jpn. J. Appl. Phys. 35 (1996) 2052

[Kis03] R. Kishore, C. Hotz, H. A. Naseem, and W. D. Brown, J. App. Crystal. 36 (2003) 1236

[Kle04] J. Klein, J. Schneider, M. Muske, S. Gall, and W. Fuhs, Thin Solid Films 451-452 (2004) 481

[Klu03] O. Kluth, G. Schöpe, J. Hüpkes, C. Agashe, J. Müller and B. Rech, Thin Solid Films 442 (2003) 80

[Kon03] M. Kon, P.K. Song, Y. Shigesato, P. Frach, S. Ohno, K. Suzuki, Jpn. J. Appl. Phys. 42 (2003) 263

[Kon92] T. J. Konno, and R. Sinclair, Philosophical Magazine B 66 (1992) 749

[Kon93] T. J. Konno, R. Sinclair, A. G. Cullis, A. E. Staton-Bevan, and J. L. Hutchison, Proceedings of the Royal Microscopical Society Conference (1993)

[Kon94] T. J. Konno, and R. Sinclair, Mater. Sci. Eng. A 179/180 (1994) 426

[Kub96] M. Kubon, E. Böhmer, F. Siebke, B. Rech, C. Beneking and H. Wagner, Sol. Energ. Mater. Sol. Cell. 41-42 (1996) 485

[Lor03] M. Lorenz, E.M. Kaidashev, H.von Wenckstern, V. Riede, C. Bundesmann, D. Spermann, G. Benndorf, H. Hochmuth, A.R. Semmelhack and M. Grundmann, Solid-State Electronics 47 (2003) 2205

[Maj77] G. Majni and G. Ottaviani, Appl. Phys. Lett. 31 (1977) 125

[Maj78] G. Majni and G. Ottaviani, Thin Solid Films 55 (1978) 235

[Maj79] G. Majni and G. Ottaviani, J. Cryst. Growth 46 (1979) 119

[Mal00] N. Malkomes, T. Yamamoto, T. Miyata, Thin Solid Films 366 (2000) 63

[Man81] J. C. Manifacier, J. P. Fillard and J. M. Bind, Thin Solid Films 77 (1981) 67

[Men98] R. Menner, R. Schäffler, B. Sprecher and B. Dimmler, in Proceedings of the 2nd World Conference on Photovoltaic Energy Conversion, Vienna, 1998

[Min84] T. Minami, H. Nanto and S. Takata, Jpn. J. Appl. Phys. 23 (1984) L280

[Min90] T. Minami, K. Oohashi, S. Takata, T. Mouri, and N. Ogawa, Thin Solid Films 193/194 (1990) 721

[Mor09] H. Morkoç and Ü. Özgür, Zinc Oxide: Fundamentals, Materials and Device Technology, 2009

[Mul01] J. Müller, O. Kluth, S. Wieder, H. Siekmann, G. Schöpe, W. Reetz, O. Vetterl, D. Lundszien, A Lambertz, F. Finger, B. Rech and H. Wagner, Sol. Energ. Mater. Sol. Cell. 66 (2001) 275

[Mul03] J. Müller, G. Schöpe, O. Kluth, B. Rech, V. Sittnger, B. Szyszka, R. Geyer, P. Lechner, H. Schade, M. Ruske, G. Dittmar and H.-P. Bochem, Thin Solid Films 442 (2003) 158

[Nas00] O. Nast and A. J. Hartmann, J. Appl. Phys., 88 (2000) 716

[Nas00S] O. Nast and S.R. Wenham, J. Appl. Phys. 88 (2000) 124

[Nas01] O. Nast, S. Brehme, S. Pritchard, A. G. Aberle, and S. R. Wenham, Sol. Energy Mater. Sol. Cells, 65 (2001) 385

[Nas98] O. Nast, T. L. M. Putter, Koschier, A. B. Sproul, and S. R.Wenham, App. Phys. Lett. 73 (1998) 3214

[Ott79] G. Ottaviani, and G. Majni, J. Appl. Phys. 50 (1979) 6865

[Par97] K.C. Park, D.Y. Ma, K.H. Kim, Thin Solid Films 305 (1997) 201

[Par99] D.F. Paraguay, L.W. Estrada, N.D. R. Acosta and E. Andrade, Thin Solid Films 350 (1999) 192

[Pen08] S. Peng, X. Shen, Z. Tang, and D. He, Thin Solid Films 516 (2008) 2276

[Pih04] E. Pihan, A. Slaoui, P. R. I. Cabarrocas, and A. Focsa, Thin Solid Films 451 /452 (2004) 328

[Pul84] H.K. Pulker, Coatings on Glass. Elsevier, 1984

[Qin82] H. Qingheng, E.S. Yang, and H. Izmirliyan, Solid-State Electronics 25 (1982) 1187

[Rau04] B. Rau, I. Sieber, J. Schneider, M. Muske, M. Stöger-Pollach, P. Schattschneider, S. Gall, and W. Fuhs, J. Cryst. Growth 270 (2004) 396

[Ree06] H.S. Reehal and G. Ekanayake, Vacuum 81 (2006) 272

[Rei02] P. Reinig, F. Fenske, W. Fuhs, and B. Selle, J. Non-Cryst. Solids, 299/302 (2002) 128

[Sch05] J. Schneider, PhD thesis (2005)

[Scr78] R. A. Scranton and J. O. McCaldin, J. Vac. Sci. Technol. 15 (1978) 1358

[Sie03] I. Sieber, R. Schneider, I. Doerfel, P. Schubert-Bischoff, S. Gall, and W. Fuhs, Thin Solid Films 427 (2003) 298

[Sla06] A. Slaoui, E. Pihan, A. Focsa, Sol. Energy Mater. Sol. Cells 90 (2006) 1542

[Sug05] Y. Sugimoto, N. Takata, T. Hirota, K. Ikeda, F. Yoshida, H. Nakashima and H. Nakashima, Jpn. J. Appl. Phys. 44 (2005) 4770

[Szy99] B. Szyszka, Thin Solid Films 351 (1999) 164

[Tho58] D.G. Thomas, J. Phys. Chem. Solids 9 (1958) 31

[Tsa81] B-Y. Tsaur, G.W. Turner and J.C.C Fan, Appl. Phys. Lett. 39 (1981) 749

[Tuz08] Ö. Tüzün, A. Slaoui, I. Gordon, A. Focsa, D. Ballutaud, G. Beaucarne and J. Poortmans, Thin Solid Films 516 (2008) 6892

[Vos76] J. L. Vossen, Transparent conducting films, J. Vac. Sci. and Tech. 13 (1976) 116

[Wal03] T. Wallendorf, S. Marke, C. May, J. Strümpfel, Surf. Coat. Technol. 174-175 (2003) 222

[Wid02] P. Widenborg and A. G. Aberle, J. Cryst. Growth 242 (2002) 270

[Wid03] P. Widenborg, A.G. Aberle, A. Straub, NP. Harder, DH. Neuhaus and O. Nast., International PCT patent application PCT/AU03/01313 (filed on 7 October 2003).

[Wid07] P. Widenborg and A.G. Aberle, J. Cryst. Growth 306 (2007) 177

[Wu00] H.Z. Wu, K.M. He, D.J. Qiu, D.M. Huang, J. Crys. Growth 217 (2000) 131

[Zou05] M. Zou, L. Cai, and W. Brown, Electrochemical and Solid-State Letters, 8 (2005) G103

[Zou07] M. Zou, S. Dorey, D. Cai, Y. Song, R. Premachandran-Nair, L. Cai, and W. Brown, Electrochemical and Solid-State Letters, 10 (2007) K7

[CHAPTER 3]

[Aga04] C. Agashe, O. Kluth, J. Hüpkes, U. Zastrow, B. Rech, and M. Wuttig, J. Appl. Phys. 95 (2004) 1911

[Blo92] P. Blood and J. W. Orton, The electrical characterization of Semiconductors: Majority Carriers and Electron States (1992)

[Bo02] X. Bo, N. Yao, S.R. Shieh, T.S. Duffy and J.C. Sturm, J. Appl. Phys. 91 (2002) 2910

[Cou00] T.J. Coutts, D.L. Young, and X. Li, MRS Bull. 25 (2000) 58

[Day01] A. P. Day et al., Channel 5 User Manual, HKL Technology A/S, Hobro, Denmark (2001)

[Gal02a] S. Gall, J. Schneider, M. Muske, I. Sieber, O. Nast, and W. Fuhs, Proc. of PV in Europe -From PV Technology to Energy Solutions (2002) 87

[Hul99] R. Hull, Properties of Crystalline Silicon, INSPEC, London (1999)

[Kam88] T. Kamins, Polycrystalline Silicon for Integrated Circuit Applications. Kluwer: Boston, 1988.

[Klu74] H.P. Klug and L.E. Alexander, X-ray diffraction procedures for polycrystalline and amorphous materials (2nd edition) (John Wiley & Sons, New York, 1974) 120

[Mar93] P. Marcus, C. Hinnen, and I. Olefjord, Surface and Interface Analysis 20(1993) 923

[Nas00] O. Nast and A. J. Hartmann, J.Appl. Phys. 88 (2000) 716

[Nic00] N. H. Nickel, P. Lengsfeld, and I. Sieber, Phys. rev. B 61 (2000) 15 558

[Nyl94] A. Nylund and I. Olefjord, Surface and interface analysis 21 (1994) 283

[Owe03] J. Owens, D. Han, B. Yan, J. Yang, K. Lord, and S. Guha, NCPV and Solar Program Review Meeting (2003) 776

[Pau58] L.J. Van der Pauw, Philips Research Reports 13 (1958) 1

[Sch02] J. Schneider, Master thesis, Technische Universität Berlin (2002)

[Sch05] J. Schneider, PhD thesis (2005)

[Sch90] D.K. Schroder, Semiconductor material and device characterization (John Wiley & Sons, New York, 1990)

[Sch96] M. Schuster and H. Göbel, Adv. X-Ray Anal. 39 (1996) 1

[Tro93] K.Z. Troost. P. van der Sluis, and D.J. Gravesteijn, Appl. Phys. Lett. 62 (1993) 1110

[Wat04] H. Watanabe, N. Yamada, and M. Okaji, International J.Thermophys., 25 (2004) 221

[Wu96] X.L. Wu, G.G. Siu, S. Tong, X.N. Liu, F. Yan, S.S. Jiang, X.K. Zhang, and D. Feng, Appl. Phys. Lett. 69 (1996) 22

[Zho07] W. Zhou and Z.L. Wang, Scanning Microscopy for Nanotechnology (2007)

[CHAPTER 4]

[Abe06] A.G. Aberle, J. Cryst. Growth 287 (2006) 386

[Aga04] C. Agashe, O. Kluth, J. Hüpkes, U. Zastrow, B. Rech, and M. Wuttig, J. Appl. Phys. 95 (2004) 1911

[Bae07] J. W. Bae, S. W. Lee, and G. Y. Yeom, J. Electro. Soc. 154 (2007) 34

[Bel92] J.R. Bellingham, W.A. Phillips, and C.J. Adkins, J. Mat. Sci. Lett. 11 (1992) 263

[Ber06] M. Berginski, B. Rech, J. Hüpkes, G. Schöpe, M.N. van den Donker, W. Reetz, T. Kilper, and M. Wuttig, 21st European Photovoltaic Solar Energy Conference (2006)

[Ber08] M. Berginski, PhD thesis (2008)

[Bre03] S. Brehme, F. Fenske,W. Fuhs, E. Neubauer,M. Poschenrieder, B. Selle, and I. Sieber, Thin Solid Films 342 (1999) 167

[Cha01] J.F. Chang, W.C. Lin, M.H. Hon, Applied Surface Science 183 18 (2001).

[Dim07] D. Dimova-Malinovska, O. Angelov, M. Kamenova, A. Vaseashta and J. C. Pivin, J. Optoelectronics and Advanced Materials 9 (2007) 355

[Due08] J.N. Duenow, T.A. Gessert, D.M. Wood, A.C. Dillon, and T.J. Coutts, J. Vac. Sci. Tech. A 26 (2008) 692

[Ell01] K. Ellmer, J. Phys. D : Appl. Phys. 34 (2001) 3097

[Ell05] K. Ellmer and G. Vollweiler, Thin Solid Films 496 (2006) 104

[Ell06] K. Ellmer and G. Vollweiler, Thin Solid Films 496 (2006) 104.

[Ell08] K. Ellmer, R. Mientus, Thin Solid Films 516 (2008) 4620

[Ham05] O. Hamad, G. Braunstein, H. Patil, and N. Dhere, Thin Solid Films 489 (2005) 303

[Iga88] Y. Igasaki, M. Ishikawa, G. Shimaoka, Applied Surface Science 33/34 (1988) 926

[Kaw03] T. Kawashima, H. Matsui, and N. Tanabe, Thin Solid Films 445 (2003) 241

[Kim05] K.-K. Kim, S. Niki, J.-Y. Oh, J.-O Song, T.-Y. Seong, S.-J. Park, S. Fujita, and S.-W. Kim, J. Appl. Phys. 97 (2005) 066103

[Kim05b] K.K. Kim, H. Tampo, J.O. Song, T.Y. Seong, S.J. Park, J.M. Lee, S.W. Kim, S. Fujita, and S. Niki, Jpn. J. Appl. Phys. 44 (2005) 4776

[Kon03] M. Kon, P.K. Song, Y. Shigesato, P. Frach, S. Ohno, and K. Suzuki, Jpn. J. Appl. Phys. 42 (2003) 263

[Lec03] R. Lechner, Master thesis (2003)

[Li05] X. Li, B. Keyes, S. Asher, S. B. Zhang, S.H. Wei, and T. J. Coutts, S. Limpijumnong, and C.G. Van de Walle, Appl. Phys. Lett. 86 (2005) 122107

[Lor03] M. Lorenz, E.M. Kaidashev, H. von Wenckstern, V. Riede, C. Bundesmann, D. Spemann, G. Benndorf, H. Hochmuth, A. Rahm, H.-C. Semmelhack, and M. Grundmann, Solid-State Electron. 47 (2003) 2205

[Mas83] G. Masetti, M. Severi and S. Solmi, IEEE Trans. Electron Devices 30 (1983) 764

[Min00] T. Minami, MRS Bulltin 25 (2000) 38

[Min89] T. Minami, H. Sato, H. Nanto, and S. Takata, Thin Solid Films 176 (1989) 277

[Min90] T. Minami, K. Oohashi, S. Takata, T. Mouri, and N. Ogawa, Thin Solid Films 193/194 (1990) 721

[Min92] T. Minami, H. Sato, K. Ohashi, T. Tomofuji, and S. Takata, J. Cryst. Growth 117 (1992) 370

[Min99] T. Minami, T. Miyata, and T. Yamamoto, J. Vac. Sci. Technol. A 17(4) (1999) 1822

[Mue04] J. Müller, B. Rech, J. Springer, and M. Vanecek, Solar Energy 77 (2004) 917

[Myo03] S.Y. Myong and K.S. Lim, Appl. Phys. Lett. 82 (2003) 3026

[Oh05] B. Oh, M. Jeong, D. Kim, W. Lee, and J. Myoung, J. Cryst. Growth 281 (2005) 475

[Rec06] B. Rech, T. Repmann, M.N. van den Donker, M. Berginski, T. Kilper, J. Hüpkes, S. Calnan, H. Stiebig, and S. Wieder, Thin Solid Films 511/512 (2006) 548

[Suz96] A. Suzuki, T. Matsushita, N. Wada, Y. Sakamoto, and M. Okuda, Jpn. J. Appl. Phys. 35 (1996) L56

[Tho56] D.G. Thomas and J.J. Lander, J. Chem. Phys. 25 (1956) 1136

[Wal03] C. G. Van de Walle and J. Neugebauer, Nature 423 (2003) 626–628

[Yu05] X. Yu, J. Ma, F. Ji, Y. Wang, X. Zhang, and H. Ma, Thin Solid Films 483 (2005) 296

[CHAPTER 5]

[Avr39] M. Avrami, J. Phys. Chem., 7 (1939) 1103.

[Avr40] M. Avrami, J. Phys. Chem.**,** 8 (1940) 212.

[Bro81] A. Brokman and R. Balluffi, Acta Metall. 29 (1981) 1703

[Cer72] F. Cerdeira, C. J. Buchenauer, F. H. Pollak and M. Cardona, Phys. Rev. B 5 (1972) 580.

[Cse75] L. Csepregi, J.W. Mayer and T.W. Sigmont, Physics Letter A 54 (1975) 157

[Cse78] L. Csepregi, E.F. Kennedy, J.W. Mayer and T.W. Sigmont, J. Appl. phys. 49 (1978) 3906

[Dim06] D. Dimova-Malinovska, V. Grigorov, M. Nikolaeva-Dimitrova, O. Angelov and N. Peev, Thin Solid Films 501(1-2) (2006) 358

[Dog08] P. Dogan, E. Rudigier, F. Fenske, K.Y. Lee, B. Gorka, B. Rau, E. Conrad and S. Gall, Thin Solid Films 516 (2008) 6989

[Gal02b] S. Gall, M. Muske, I. Sieber, O. Nast and W. Fuhs, J. Non-Crystal. Solids 299–302 (2002) 741

[Ges08b] D. Van Gestel, P. Dogan, I. Gordon, H. Bender, K. Y. Lee, G. Beaucarne, S. Gall and J. Poortmans, Material science & engineering B, in press (2008)

[Gor07] B. Gorka, B. Rau, K.Y. Lee, P. Dogan, F. Fenske, E. Conrad, S. Gall and B. Rech, 22nd European Photovoltaic Solar Energy Conference (2007) 2024

[Gri07] V. Grigorov, O. Angelov, M. Kamenova and D. Dimova-Malinovska, NATO Science Series II: Mathematics, Physics and Chemistry 223 (2007) 333

[Hir79] J. Hirvonen and A. Anttila, Appl. Phys. Lett. 35 (1979) 703

[Hsu03] C.M. HSU, I.F. CHEN and M.C. YU, Jpn. J. Appl. Phys. 42 (2003) 4928

[Hul98] R. Hull (Ed.), Properties of Crystalline Silicon—Technology, 1998, pp. 600

[Hwa80] J.C.M. Hwang, P.S. Ho, J.E. Lewis and D.R. Campbell, J. Appl. phys. 51 (1980) 1576

[ICDD] International Center for Diffraction Data (ICDD) database, PDF-card 00-027-1402

[Jen92] AK Jena,MC Chaturvedi (1992). *Phase Transformations in Materials*. Prentice Hall. p. 247.

[Joh39] W.A. Johnson and R.F. Mehl, Trans. Amer. Inst. Min. Metall. Eng. 135 (1939) 416.

[Kal79] L. Kalinovski and R. Seguin, Appl. Phys. Lett. 35 (1979) 211

[Kam98] T.I. Kamins, Polycrystalline Silicon for Integrated Circuit and Displays, 2nd ed., Kluwer Academic Publishers (1998)

[Kim02] H. Kim, G. Lee, D. Kim and S.-H. Lee, Curr. Appl. Phys. 2 (2002) 129

[Kis03] R. Kishore, C. Hotz, H. A. Naseem and W. D. Brown, Applied Crystallography 36(5) (2003) 1236

[Kit02] K. Kitahara, R. Yamazaki, T. Kurosawa, K. Nakajima, and A. Moritani, Jpn. J. Appl. Phys. 41 (2002) 5055

[Kon92] T. J. Konno and R. Sinclair, Philos Mag-B 66 (1992) 749

[Kon95] T.J. Konno and R. Sinclair, Philos. Mag. B 71 (1995) 163

[Lee97] J.N. Lee, B.J. Lee, D.G. Moon and B.T. Ahn, Jpn. J. Appl. phys. 36 (1997) 686

[Nas00b] O. Nast, Conference Record of the Twenty-Eighth IEEE Photovoltaic Specialists Conference (2000)

[Man78] G. Manjni and G. Ottaviani, J. Cryst. Growth 45 (1978) 132

[McC71] J. McCaldin and H. Sankur, Appl. Phys. Lett. 19 (1971) 524

[Nas00] O. Nast, PhD thesis, (2000)

[Nas00b] O. Nast and A. Hartmann, J. Appl. Phys. 88 (2000) 716

[Nas00S] O. Nast and S. R. Wenham, J. Appl. Phys. 88 (2000) 124

[Nas01] O. Nast, S. Brehme, S. Pritchard, A.G. Aberle and S.R. Wenham, Sol. Energy Mater. Sol. Cells 65 (2001) 385

[Pih07] E. Pihan, A. Slaoui and C. Maurice, J. Cryst. Growth 305 (2007) 88

[Rau06] B. Rau, E. Conrad and S. Gall, Twentyfirst European Photovoltaic Solar Energy Conference (2006)

[Rob04] J.D. Robson, Acta Mater. 52 (2004) 4669

[Sch04] J. Schneider, J. Klein, M. Muske, S. Gall and W. Fuhs, Journal of Non-Crystalline Solids 338–340 (2004) 127

[Sch05] J. Schneider, PhD thesis, (2005)

[Sch06] J. Schneider, A. Schneider, A. Sarikov, J. Klein, M. Muske, S. Gall and W. Fuhs, Journal of Non-Crystalline Solids 352 (2006) 972

[Sch98] R. E. I. Schropp and M. Zeman, Amorphous and Microcrystalline Silicon Solar Cells: Modelling, Materials and Device technology (Kluwer Acadamic, Boston, 1998)

[Sec72] F. Secco d'Aragona, J. Electrochem. Soc. 119 (1972) 948

[Spi98] C. Spinella, S. Lombardo and F. Priolo, J. Appl. phys. 84 (1998) 5383

[Str04] A. Straub, P.I. Widenborg, A.B. Sproul, Y. Huang, N.-P. Harder and A.G. Aberle, J. Cryst. Growth 265 (2004) 168

[Ter07] M.L. Terry, D. Inns and A.G. Aberle, Advances in OptoElectronics 2007 (2007) 11 Article ID 83657

[Vou95] A.T. Voutsas, M.K. Hatalis, J. Boyce and A. Chiang, J. Appl. Phys. 78 (12) (1995) 6999

[Wid02] P. Widenborg and A.G. Aberle, J. Cryst. Growth 242 (2002) 270

[Wid05] P.I. Widenborg, A. Straub and A.G. Aberle, J. Cryst. Growth 276 (2005) 19

[Wid07] P.I. Widenborg and A.G. Aberle, J. Cryst. Growth 306 (2007) 177

[Yu97] G. Yu, Y.K.L. Lai and W. Zhang, J. Appl. Phys. 82 (1997) 4270

[CHAPTER 6]

[Abe06] A.G. Aberle, J. Cryst. Growth 287 (2006) 386

[Ber06] M. Berginski, B. Rech, J. Hüpkes, G. Schöpe, M.N. van den Donker, W. Reetz, T. Kilper, and M. Wuttig, 21st European Photovoltaic Solar Energy Conference (2006)

[Gal08] S. Gall, C. Becker, E. Conrad, P. Dogan, F. Fenske, B. Gorka, K.Y. Lee, B. Rau, F. Ruske and B. Rech, Sol. Energy Mater. Sol. Cells, in press (2008)

[Gor07a] I. Gordon, D. Van Gestel, L. Carnel, G. Beaucarne, J. Poortmans, K.Y. Lee, P. Dogan, B. Gorka, C. Becker, F. Fenske, B. Rau, S. Gall, B. Rech, J. Plentz, F. Falk and D. Le Bellac, 22nd European Photovoltaic Solar Energy Conference (2007) 1890

[Gor07b] I. Gordon, L. Carnel, D. Van Gestel, G. Beaucarne and J. Poortmans, paper accepted for publication in Progress in Photovoltaics (2007) 765

[Kor07] L. Korte, E. Conrad, H. Angermann, R. Stangl and M. Schmidt, 22nd European Photovoltaic Solar Energy Conference (2007) 859

[Pih07] E. Pihan, A. Slaoui and C. Maurice, J. Cryst. Growth 305 (2007) 88

[Rau08] B. Rau, T. Weber, B. Gorka, P. Dogan, F. Fenske, K.Y. Lee, S. Gall and B. Rech, Material science & engineering B, in press (2008)

[Rec06] B. Rech, T. Repmann, M.N. van den Donker, M. Berginski, T. Kilper, J. Hüpkes, S. Calnan, H. Stiebig, and S. Wieder, Thin Solid Films 511/512 (2006) 548

LIST OF PUBLICATIONS

- **K.Y. Lee**, P. Dogan, F. Ruske, B. Gorka, J. Hüpkes, S. Gall and B. Rech; "The properties of poly-Si films grown on ZnO:Al coated borofloat glass by aluminium-induced layer exchange (ALILE) process", Proceeding of 23rd European Photovoltaic Solar Energy Conference: 2008 p. 2261-2265

- **K.Y. Lee**, M. Muske, I. Gordon, M. Berginski, J. D'Haen, J. Hüpkes, S. Gall, B. Rech: "Large-grained poly-Si films on ZnO:Al coated glass substrates". **Thin Solid Films** 516 (20) (2008), p. 6869-6872

- P. Dogan, E. Rudigier, F. Fenske, **K.Y. Lee**, B. Gorka, B. Rau, E. Conrad, S. Gall: "Structural and electrical properties of epitaxial Si layers prepared by E-beam evaporation". in press, **Thin Solid Films** 516 (20) (2008), p. 6989-6993

- B. Rau, T. Weber, B. Gorka, P. Dogan, F. Fenske, **K.Y. Lee**, S. Gall, B. Rech ; "Development of a rapid thermal annealing process for polycrystalline silicon thin-film solar cells on glass" : in press, **Materials Science and Engineering: B** (2008)

- D. Van Gestel, P. Dogan, I. Gordon, H. Bender, **K.Y. Lee**, G. Beaucarne, S. Gall, J. Poortmans ; "Investigation of intragrain defects in pc-Si layers obtained by aluminum-induced crystallization: comparison of layers made by low and high temperature epitaxy", in press, **Thin Solid Film** (2008)

- **K.Y. Lee,** C. Becker, M. Muske, F. Ruske, S. Gall, B. Rech, M. Berginski, and J. Hüpkes: "Temperature stability of ZnO:Al film properties for poly-Si thin-film devices". **Applied Physics Letter** 91 (2007), p. 241911/1-3

- S. Gall, C. Becker, E. Conrad, P. Dogan, F. Fenske, B. Gorka, **K.Y. Lee,** B. Rau, F. Ruske, and B. Rech: "Polycrystalline silicon thin-film solar cells on glass". Technical digest / 17th International Photovoltaic Science and Engineering Conference (PVSEC-17) : 2007, p. 343-344

- C. Becker, T. Hänel, B. Gorka, **K.Y. Lee**, P. Dogan, F. Fenske, M. Berginski, J. Hüpkes, S. Gall, and B. Rech: "Solid phase crystallization of amorphous silicon on ZnO:Al for thin film solar cells". Technical digest / 17th International Photovoltaic Science and Engineering Conference (PVSEC-17) : 2007, p. 1122-1123

- **K.Y. Lee,** C. Becker, M. Muske, S. Gall, B. Rech, I. Gordon, J. D'Haen, M. Berginski, and J. Hüpkes: "Poly-Si films grown on ZnO:Al coated glass by aluminum-induced layer exchange process". Proceedings of 22nd European Photovoltaic Solar Energy Conference : 2007, p. 2028-2031
- S. Gall, **K.Y. Lee,** P. Dogan, B. Gorka, C. Becker, F. Fenske, B. Rau, E. Conrad, B. Rech,: "Large-grained polycrystalline silicon thin-film solar cells on glass". Proceedings of 22nd European Photovoltaic Solar Energy Conference : 2007, p. 2005-2009

- I. Gordon, D. Van Gestel, L. Carnel, G. Beaucarne, J. Poortmans, **K.Y. Lee,** P. Dogan, B. Gorka, C. Becker, F. Fenske, B. Rau, S. Gall, B. Rech, J. Plentz, F. Falk, and D. Le Bellac: "Advanced concepts for thin-film polycrystalline-silicon solar cells". Proceedings of 22nd European Photovoltaic Solar Energy Conference : 2007, p. 1890-1894

- B. Gorka, B. Rau, **K.Y. Lee,** P. Dogan, F. Fenske, E. Conrad, S. Gall, and B. Rech: "Hydrogen passivation of polycrystalline Si thin films by plasma treatment". Proceedings of 22nd European Photovoltaic Solar Energy Conference : 2007, p. 2024-2027

- P. Dogan, F. Fenske, L.-P. Scheller, **K.Y. Lee,** B. Gorka, B. Rau, E. Conrad, S. Gall, and B. Rech: "Structural and electrical properties of epitaxial Si layers prepared by e-beam evaporation". Proceedings of 22nd European Photovoltaic Solar Energy Conference : 2007, p. 2019-2023

- B. Rau, **K.Y. Lee,** P. Dogan, F. Fenske, E. Conrad, and S. Gall: "Improvement of epitaxially grown poly-Si thin-film solar cells on glass by rapid thermal annealing". Proceedings of 22nd European Photovoltaic Solar Energy Conference : 2007, p. 2010-2014

CONFERENCES

- **K.Y. Lee**, P. Dogan, F. Ruske, B. Gorka, J. Hüpkes, S. Gall and B. Rech; "The properties of poly-Si films grown on ZnO:Al coated borofloat glass by aluminium-induced layer exchange (ALILE) process", 23rd European Photovoltaic Solar Energy Conference , Valencia, Spain, 1-5 September (2008)

- **K.Y. Lee,** C. Becker, M. Muske, S. Gall, B. Rech, I. Gordon, J. D'Haen, M. Berginski, and J. Hüpkes: "Poly-Si films grown on ZnO:Al coated glass by aluminum-induced layer exchange process". 22nd European Photovoltaic Solar Energy Conference Milan, Italy, 03.09.2007 - 07.09.2007 (2007)

- **K.Y. Lee,** M. Muske, I. Gordon, M. Berginski, D'Haen, J. Hüpkes, S. Gall, and B. Rech: "Large-grained poly-Si films on ZnO:Al coated glass substrates". E-MRS SPRING MEETING 2007 Strasbourg, France, 28.05.2007 - 01.06.2007 (2007)

ACKNOWLEDGEMENT

I would like to thank Prof. Dr. B. Rech for his fantastic support of my study from idea to finish.

I would like to thank Dr. Stefan Gall for supervising my work and being supportive and giving me all these opportunities to present my results to the scientific community and also accepting my application which I could start this work at HZB on an almost blind date.

I would like to thank Dr. Florian Ruske as a TCO professionalist for all the on and off topic discussions and for being the first proof reader of this thesis.

I would like to thank Dr. Christiane Becker for discussion of results and being the first proof reader of this thesis.

I would like to thank Dr. Björn Rau for the RTA treatments.

I would like to thank Pinar Dogan for growing absorber layers.

I would like to thank Benjamin Gorka for working on hydrogen passivation treatments.

I would like to thank Martin Muske as a room mate and a best friend for working together in order to make tons of samples.

I would like to thank Stefan Common for all the hilarious times, especially coffee time on afternoon.

I would like to thank Kerstin Jacob and Anja Scheu for tons of sample and substrate treatments.

I would like to thank Carola Klimm for performing SEM measurements.

I would like to thank Marion Krusche and Dr. Gabriele Lampert for helping me with administrative matters, which allowed me to focus on my scientific work.

I would like to thank all the other members of silicon thin film solar cell group for a pleasant work atmosphere.

I would like to thank all the other members of E-I1 in HZB for a pleasant work atmosphere.

I would like to thank Dr. Ivan Gordon for EBSD measurements and discussions.

I would like to thank Dr. Jürgen Hüpkes and Dr. Michael Berginski for preparing lots of ZnO:Al samples.

I would like to thank my wife and my children for filling with joy and happiness.